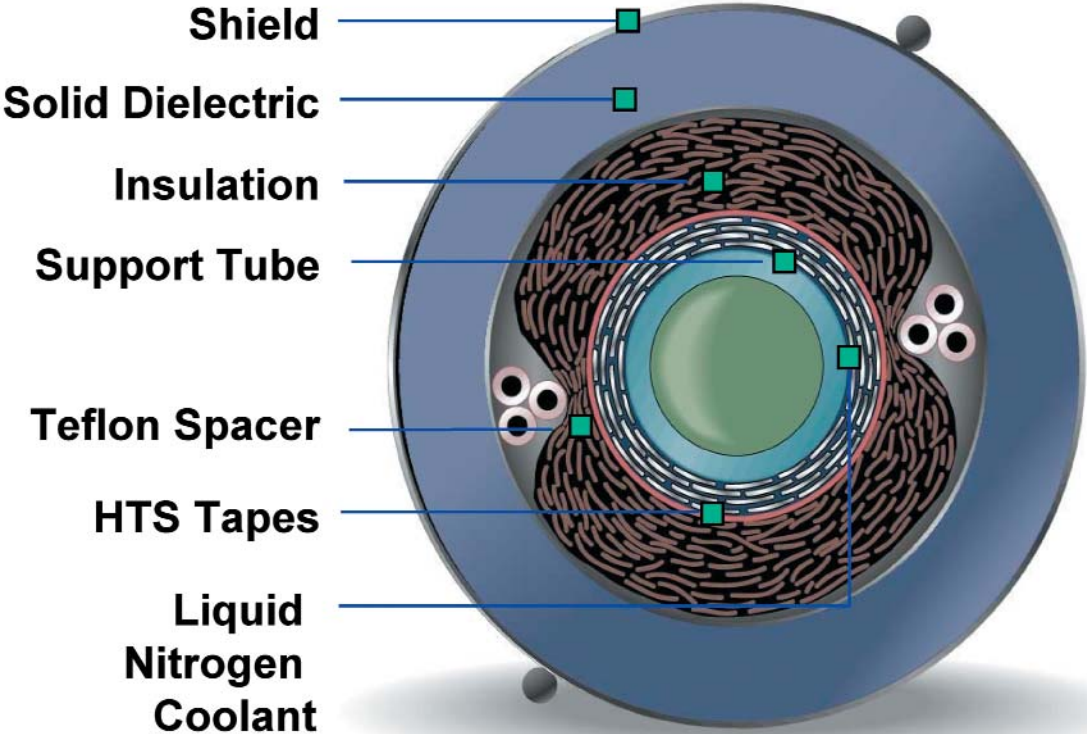


Superconducting Cable Construction and Testing

Technical Report



Superconducting Cable Construction and Testing

1000160

Final Report, November 2000

Cosponsor
U.S. Department of Energy
Forrestal Building, OE142
Washington, D.C. 20585

Project Manager
J. Daley

EPRI Project Manager
D. Von Dollen

DISCLAIMER OF WARRANTIES AND LIMITATION OF LIABILITIES

THIS DOCUMENT WAS PREPARED BY THE ORGANIZATION(S) NAMED BELOW AS AN ACCOUNT OF WORK SPONSORED OR COSPONSORED BY THE ELECTRIC POWER RESEARCH INSTITUTE, INC. (EPRI). NEITHER EPRI, ANY MEMBER OF EPRI, ANY COSPONSOR, THE ORGANIZATION(S) BELOW, NOR ANY PERSON ACTING ON BEHALF OF ANY OF THEM:

(A) MAKES ANY WARRANTY OR REPRESENTATION WHATSOEVER, EXPRESS OR IMPLIED, (I) WITH RESPECT TO THE USE OF ANY INFORMATION, APPARATUS, METHOD, PROCESS, OR SIMILAR ITEM DISCLOSED IN THIS DOCUMENT, INCLUDING MERCHANTABILITY AND FITNESS FOR A PARTICULAR PURPOSE, OR (II) THAT SUCH USE DOES NOT INFRINGE ON OR INTERFERE WITH PRIVATELY OWNED RIGHTS, INCLUDING ANY PARTY'S INTELLECTUAL PROPERTY, OR (III) THAT THIS DOCUMENT IS SUITABLE TO ANY PARTICULAR USER'S CIRCUMSTANCE; OR

(B) ASSUMES RESPONSIBILITY FOR ANY DAMAGES OR OTHER LIABILITY WHATSOEVER (INCLUDING ANY CONSEQUENTIAL DAMAGES, EVEN IF EPRI OR ANY EPRI REPRESENTATIVE HAS BEEN ADVISED OF THE POSSIBILITY OF SUCH DAMAGES) RESULTING FROM YOUR SELECTION OR USE OF THIS DOCUMENT OR ANY INFORMATION, APPARATUS, METHOD, PROCESS, OR SIMILAR ITEM DISCLOSED IN THIS DOCUMENT.

ORGANIZATION(S) THAT PREPARED THIS DOCUMENT

Pirelli Cables and Systems

ORDERING INFORMATION

Requests for copies of this report should be directed to the EPRI Distribution Center, 207 Coggins Drive, P.O. Box 23205, Pleasant Hill, CA 94523, (800) 313-3774.

Electric Power Research Institute and EPRI are registered service marks of the Electric Power Research Institute, Inc. EPRI. ELECTRIFY THE WORLD is a service mark of the Electric Power Research Institute, Inc.

Copyright © 2000 Electric Power Research Institute, Inc. All rights reserved.

CITATIONS

This report was prepared by

Pirelli Cables and Systems
710 Industrial Drive
Lexington, South Carolina 29072

Principal Investigator
M. Nassi

This report describes research sponsored by EPRI and U.S. Department of Energy.

The report is a corporate document that should be cited in the literature in the following manner:

Superconducting Cable Construction and Testing, EPRI, Palo Alto, CA, and U.S. Department of Energy, Washington, D.C.: 2000. 1000160.

REPORT SUMMARY

Superconducting cables, carrying three to five times more power than conventional cables, can meet increasing power demands in urban areas via retrofit applications. These high capacity cables will allow utilities to greatly enhance capacity, thereby giving the grid more flexibility and reliability. This report describes the development, construction, and testing of a superconducting cable system.

Background

In the late eighties, a new class of ceramic oxides was discovered with superconducting properties above the boiling point of liquid nitrogen. This discovery sparked international efforts to improve the properties of the new high temperature superconductors, as well as a race to develop systems to capitalize on the new technology. Since 1989, EPRI has been involved with the development of superconducting cable technology. In 1992, EPRI performed a design analysis to retrofit a conventional 115 kV, 200 MVA pipe-type cable system with an ampacity increase of 100%. Based on the conclusions of this design study, EPRI, with partial funding from the U.S. Department of Energy, undertook a program to develop this cable design into a prototype system including joints, terminations and cryogenic refrigerator. This program focused on the challenges of designing and building a cable system at liquid nitrogen temperatures.

Objective

To develop, construct, and test a commercially viable room temperature dielectric superconducting cable system using industrial equipment and techniques suited for the manufacture of long-length commercial systems.

Approach

The project team established specifications for robust, high performance superconducting wire. They developed a process for stranding a multi-layer conductor with a very high superconducting property retention during manufacturing and a critical current value of 3300 A. Using a factory-based manufacturing technology process, the team produced a cable system including two outdoor terminations and an in-line joint. They performed qualification tests on the system in a high voltage laboratory.

Results

The project demonstrated a factory-based manufacturing technology and complete system design for a 115kV-400MVA high temperature superconducting (HTS) cable. At each stage of development, tests were conducted to assess the performance and identify areas for improvement. These tests ranged from measuring the DC critical current of each spool of superconducting tape prior to stranding the multi-tape conductor to installing a complete cable

system mock-up to verify the performance of the complete system including cryogenic and dielectric systems, terminations, and joint.

The conductor assembly was fabricated by stranding the HTS tapes in eight layers; each applied with alternating pitch. The selection of the stranding equipment and configuration minimized the additional strain applied to the HTS tapes during application. Several prototype conductor assemblies were fabricated and tested to verify the design to be used for the final conductor. A continuously applied cryostat, designed to operate at a high vacuum with little maintenance, was constructed around the completed conductor, using concentric stainless steel corrugated tubes with multi-layer insulation. The dielectric designs for the accessories, consistent in principle with the Warm Dielectric cable design, separated the dielectric and thermal functions. The dielectric designs leveraged conventional techniques, minimizing the need for special techniques and materials. The application included a special technique to smooth the electric field disturbance caused by the cryostat corrugations. The cable accessories also incorporated a novel component, known as the Feed-Through-Bushing (FTB) that served as a thermally insulated transfer bushing for the liquid nitrogen.

EPRI Perspective

EPRI has identified superconducting cables as an essential technology for the electric utility industry in its Electricity Technology Roadmap. High capacity superconducting cables can transmit two to five times more power through existing rights of way. This new cable offers a powerful tool to improve the capacity and flexibility of power grids while reducing their environmental footprint. One possibly application for superconducting cables will be to provide a high capacity electrical highway solution to over-stressed transmission networks. With more power supply markets opening up due to utility deregulation, coupled with an ever-increasing demand for electricity, better electrical highways can be built to streamline the transportation of electricity from low cost generation suppliers to densely populated cities using smaller, higher capacity cables. Another promising future application for superconducting cables will be high power distribution. Today, to increase the power supply to an urban area, utilities have to install transmission level voltage cables and utilize transformers at new substations. With stringent siting requirements and the unfavorable view of new substations in urban areas, superconducting cable will be able to transmit the same amount of power at distribution level voltages and eliminate the need for new substations.

Keywords

Superconducting Cables
Cables
Superconductivity

ABSTRACT

High Temperature Superconducting (HTS) power cable technology provides a means to extend the range of technical and economic feasibility of underground electric transmission and distribution systems. This project demonstrated a factory-based manufacturing technology and complete system design for a 115kV-400MVA high temperature superconducting (HTS) cable system including joints, terminations, and cryogenic refrigerator. The project was divided into several tasks. These tasks included establishing the specifications for robust, high performance superconducting wire; developing a process for stranding a multi-layer conductor with a very high superconducting property retention during manufacturing and having a critical current value of 3300 A; creating a process for applying a cryostat with a continuous process directly over the conductor; completing the cable manufacturing with a lapped Paper Polypropylene Laminate insulation impregnated with dielectric fluid; and designing High Voltage and cryogenic accessories. The cable system, including two outdoor terminations and an in-line joint, was installed in a high voltage laboratory where cable system high voltage qualification tests were performed successfully.

EXECUTIVE SUMMARY

In 1992 Pirelli Cable Corporation (PCC) completed a design feasibility study examining a High Temperature Superconducting (HTS) power cable for the Electric Power Research Institute (EPRI). The study focused on designing a cable that could be used to retrofit existing 115kV High Pressure Fluid-Filled (HPFF) underground cable systems. The results of this study indicated that a cable system could be designed and manufactured to provide a 100% improvement in power transmission capacity, upgrading a 200MVA circuit to 400MVA without altering the existing installed pipe. Based on these conclusions, EPRI and PCC initiated a program to manufacture and test a complete HTS cable system.

While different cable configurations were considered for the retrofit application, a “Warm Dielectric (WD)” cable was selected as the most attractive. The WD design is so called, because the dielectric insulation is applied outside the thermal insulation and therefore operates near ambient temperatures, as opposed to a “Cold Dielectric Coaxial “(CDC) configuration, where the dielectric is used at the cable operating temperature, around 77 K. The WD design has unique features that make it optimal for the retrofit application: it uses dielectric materials and accessories that are derived from well-established conventional materials and components; it has a lower initial cost that makes it more attractive for the near-term system retrofit market; and it enables the use of a compact, flexible cryostat within the cable core, thereby eliminating the need for an external cryostat, as needed for CDC designs.

The primary parameters for the HTS retrofit cable system prototype were defined as follows:

- 115kV System Voltage ($1.7U_0$),
- 400MVA (3-phase) (representing 100% improvement in power capacity),
- overall dimension of the 3-phase circuit that allow its installation in an 8.0” IPS Oil Pipe (standard size for 200MVA/115kV conventional system),
- 30m length (to verify “scale-up” of laboratory results and manufacturing processes for long length cables). The cable length was increased during the course of the program to 50m + 13m, for a total length of 63m,
- Warm Dielectric (WD) cable construction,
- Outdoor terminations and one in-line joint.

The program built upon the separately-funded development contract for HTS materials between Pirelli Cavi and American Superconductor Corporation (ASC), which had begun three years prior to award of this program and had resulted in the availability of HTS tapes having lengths and performances suitable for cable applications.

Ultimately, the goal of this program is to construct a HTS cable system prototype designed to provide a high power capacity option for the HPPF retrofit market. The system demonstrated a factory-based manufacturing technology and the complete system design (cable, terminations, joint, refrigeration plant, and monitoring system) for a 115kV-400MVA (three-phase rating) cable. At each stage of development, tests were conducted to assess the performance and identify areas for improvement. These tests ranged from measuring the DC critical current I_c of each spool of HTS tape prior to stranding the multi-tape conductor, to installing a complete cable system mock-up to verify the performance of the complete system including cryogenic and dielectric systems, terminations and joint.

In addition to the incremental testing performed, a formal testing program was identified both to qualify the cable parameters and to advance the understanding of the mechanisms involved with high temperature superconductivity. The testing programs involved the following tasks:

- Testing DC critical currents and AC losses on 1-meter long PMCs (Prototype Multistranded Conductors) and MCAs (Multistranded Conductor Assembly) and 13 and 50 meter long MCAs .
- A short section of pipe, typical of that used for 115kV-200MVA HPPF cable systems, was installed in a manner which simulates a future HTS cable installation. High currents were passed through a conventional three-phase conductor lying inside the pipe to verify calculations of the inductive losses due to the pipe. It has been considered that the inductive losses in the pipe might become the limiting factor in WD cable design.
- The performance of the MCAs were measured under normal handling and operating conditions. Included in the test program were: Thermo-mechanical Tests - bending, tensile loading, and thermal fatigue tests; Electrical Tests - DC critical current measurement and AC losses at the rated operating conditions and at the maximum expected level of current; and Abnormal/Fault Conditions – electrical overload and cooling/thermal insulation system malfunction.
- The electrical tests, mainly DC critical current measurements, were repeated after the cabling procedures were completed (thermal and electrical insulation application).
- The cable system, including two outdoor terminations and an in-line joint, was installed in a high voltage laboratory where the final cable system high voltage qualification tests were performed successfully (shown in Figure E-1).



Figure E-1
HTS Cable System in HV Testing Facility

The testing program proved the feasibility of both the Warm Dielectric approach to electrical insulation and the technology and materials to manufacture long cables using processes compatible with established cable-making practices.

Main results

It is worthwhile to summarize the main results achieved in the following areas:

- HTS tape
- AC loss measurement system development
- Cable system design, technology development and manufacturing
- I_c performance of the 50 m long cable system prototype
- AC loss performance and understanding
- HV test of the 50 m long cable system prototype
- Cryogenic cooling system performance
- Pipe loss verification

HTS tape

The conductor design was based on BSCCO-2223 HTS tapes supplied by American Superconductor Corporation, and comprised an 8-layer conductor design in which the key performance specifications of the individual tapes set by Pirelli were as summarized in Figure E-2.

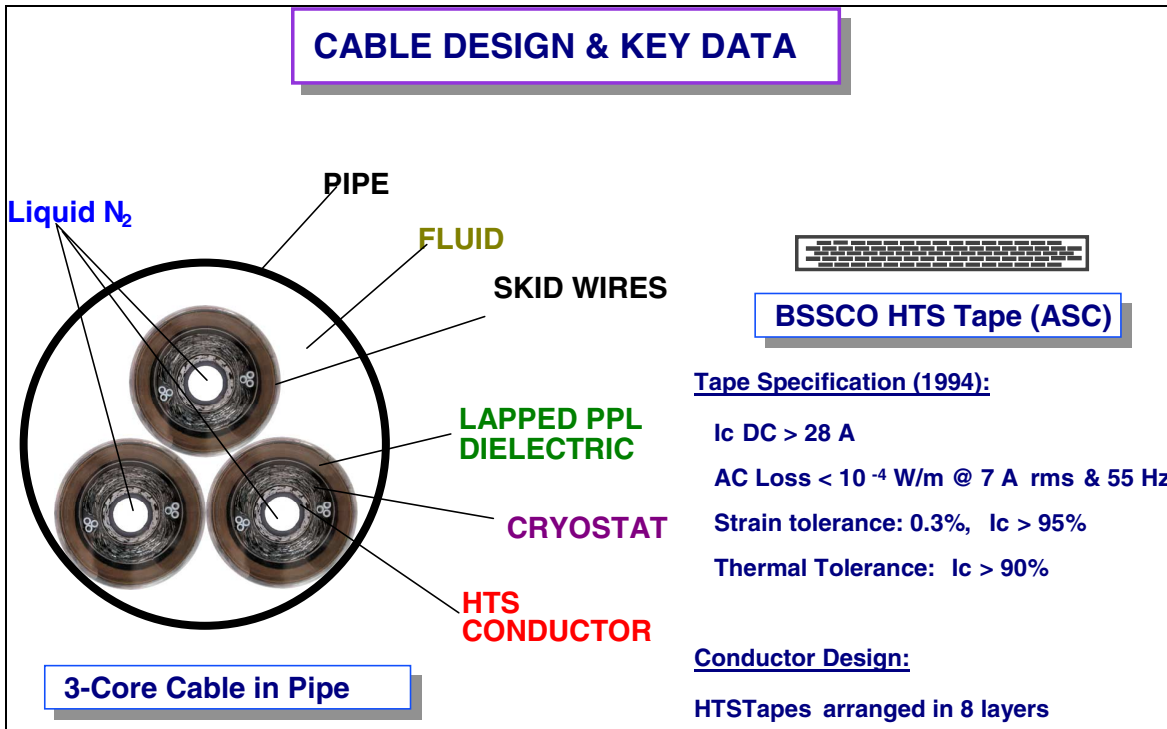


Figure E-2
115kV Warm Dielectric cable for pipe-type retrofit application and key performance specification for tapes

The actual HTS tape performances, compared to the specified limits, are reported in Table E-1.

Table E-1
Specifications and actual performances for HTS Tape for Prototype Cable

Type	Requirements	Average results
I_c	> 28 A	33 A
I_c uniformity	Standard deviation $Sd \leq 20\%$	$Sd = 6\%$
Thermal stability + tightness	I_c retention > 90%	I_c retention > 99%
Dimensions	width (w)= 4.1 ± 0.1 mm, thickness (th) = 0.267 ± 0.025 mm, straightness = 2mm/200 mm	w= 4.1 ± 0.09 mm, th= 0.267 ± 0.01 mm, straightness 1.4/200
Length	> 95 m	96 m
Strain tolerance at 8° twist test (0.3% strain)	I_c retention > 95 %	I_c retention > 99 %
Stress tolerance at 45 Mpa	I_c retention > 95 %	I_c retention = 100 %
AC loss	$< 1.4 \cdot 10^{-4}$ W/m at 7 A rms at 55 Hz	$9 \cdot 10^{-5}$ W/m at 7 A rms at 55 Hz
Defects = blisters th>0.5 mm	< 0.4/m	< 0.2/m

This program required the manufacturing of almost 12 km of HTS tape and proved ASC's capability to guarantee a high and uniform level of performance throughout the production campaign.

AC loss measurement system development

The evaluation of AC losses in HTS cables is necessary to adequately design commercial HTS cable systems. Several factors have to be assessed, including the effect of cable length and of the other conductors in the circuit.

No single technique has been developed so far which permits all necessary evaluations to be conducted at the same time. Subsequently, the results obtained with different measurement techniques have been compared for this project. These techniques include:

- an electrical method developed by Pirelli,
- a temperature measurement technique developed by Los Alamos National Lab (in conjunction with EPRI and the DOE Office of Energy Technology),
- a boil-off calorimeter developed by ENEL, the national Italian electrical utility, in the framework of the SMT 4-CT95-2008 contract of the European Community.

Each measurement method has its limits and merits. If we consider the development of a measurement method not only as a tool but also as a result, it is worth summarizing here the main advantages and drawbacks of each of them.

The range of the electrical data is, as expected, much wider than that of the “calorimetric” ones. It must be noticed, however, that the sensitivity reached in the “temperature-difference” measurements was also remarkable, allowing reliable detection at a power dissipation of less than 20 mW. A peculiarity of this method, on the other hand, is that the current flowing along the cable must be not only large enough to produce detectable ΔT , but also not too large, so that the temperature along the cable can be considered “almost” constant. This limited the maximum current to slightly below the critical current, and even in this case a temperature correction of losses due to the non-uniform temperature in the cable is required. For exactly the same reason the sample must be neither too long nor too short, practically about one meter.

The “boil-off” system, although being the most penalized in term of sensitivity, being restricted to losses above about 200 mW, doesn’t suffer any limitation in respect of high currents

Both calorimetric methods have advantage with respect to the electrical one substantially because of their independence from the environmental electromagnetic condition, which makes them potentially advantageous in a wide range of applications (*e.g.* 3-phase cables) and usable as reference for improving electrical measurements in complex configurations.

Both these methods suffer limitations concerning the range of applicability, either for current and sample length, while the electrical method is not limited in current if not by the required high quality of the signal, and is in principle applicable for every sample length. Other elements that can be taken into account are:

- the time required to perform a measurement, which is quite long for the boil-off technique (at least 15 minutes for each point in the curve), even more long in temperature difference calorimetry (about one hour to get steady state conditions) and very short in the electrical case
- the complexity of the experimental assembly, which is certainly greater in the case of the temperature difference technique, due to the vacuum thermal insulation and the fine temperature control.

Regardless of the particular limit of each technique, it is remarkable that all of them proved to be perfectly suitable to perform reliable measurements of AC losses on cable conductors as shown in Figure E-3 where the results of the three methods are compared. The losses are expressed as losses per cycle (mJ/m) to allow the comparison of measurements at different frequencies. The agreement is remarkably good taking into account the complexity of some experimental set-up.

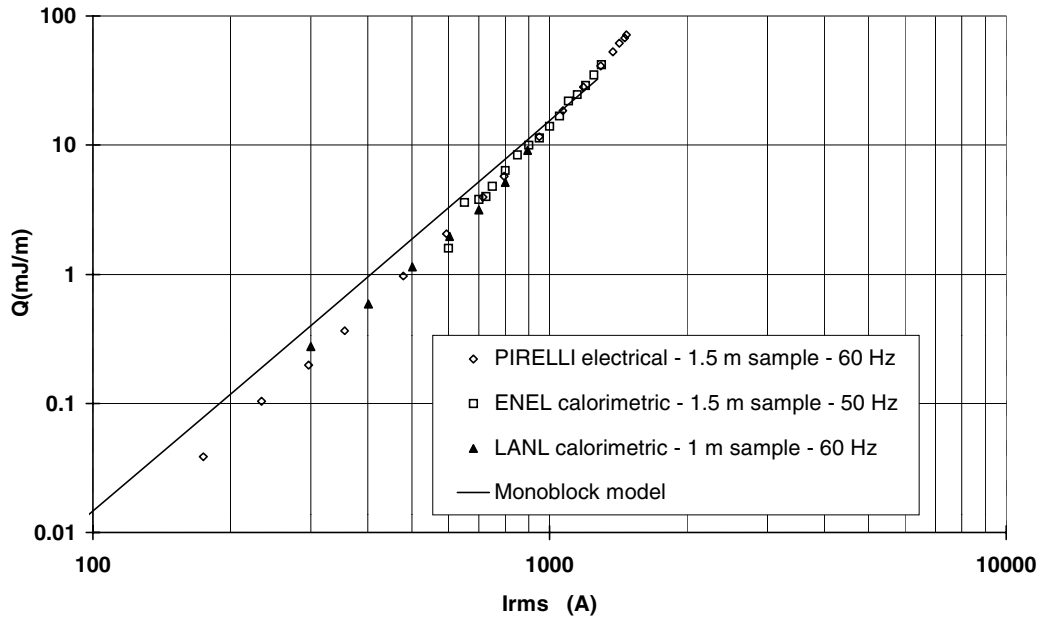


Figure E-3
AC Loss per cycle on a MCA-1 Sample measured with Electric and Calorimetric Techniques

Cable system design, technology development and manufacturing

The design of all the HTS cable system components was carried out in Pirelli. The design of the “retrofit” cable is of the so-called “warm-dielectric” concept (see Figure E-2), where the cryostat is incorporated as an integral part of the cable core, and the electrical insulation and external protection of the cable are applied over the cryostat, and therefore operate at the external ambient temperature.

This design, as already mentioned, has several advantages compared to the cold dielectric design, because it requires installation procedures similar to those used for a conventional pipe-type cable and it uses existing, well-proven dielectric materials.

The manufacture of the cable was undertaken using conventional manufacturing lines that were slightly modified to handle the HTS tapes without exceeding their mechanical strain limits (<0.3% tensile strain). Novel technologies for the application of the thermal “superinsulation”, between the inner and outer cryostat walls, were developed.

In order to prove the technical feasibility of incorporating the HTS cable into a transmission system, in-line splicing techniques for jointing consecutive cable lengths and also outdoor terminations were developed by Pirelli.

The design of the termination must take into account the need for a copper “current lead” to bring the transmitted power up from the HTS conductor core at about 77K to a “normal ambient” exit temperature. This is achieved by use of a special thermal gradient design in which liquid

nitrogen (LN₂) is allowed to boil off from a chamber within the termination, to balance out the Joule heating and the heat conduction losses in the copper current lead.

In regard to the in-line joint, which must also fit within the volume of a conventional pipe-type joint, the concept for the jointing technology was to adopt a short copper ferrule at the center of the joint, with large conductive cross-section, and to solder bond the HTS tapes to the ferrule on each side. Current flow thus passes through the ferrule at the joint position, but the resultant Joule heating losses are sufficiently small to be removed by the LN₂ flow through the conductor core without significantly increasing the LN₂ temperature. A vacuum-insulated cryostat tube is applied over the central part of the joint, and is hermetically welded to the cable cryostat on each side of the joint. The electrical insulation is reconstituted over the outside of the cryostat using conventional joint materials and techniques.

Ic performance of the 50 m long cable system prototype

The Multistranded Conductor Assemblies (MCA) MCA-1 and MCA-2 represented the culmination of long-length conductor development which evolved from laboratory samples to factory manufactured prototypes. This evolution is illustrated in Figure E-4.

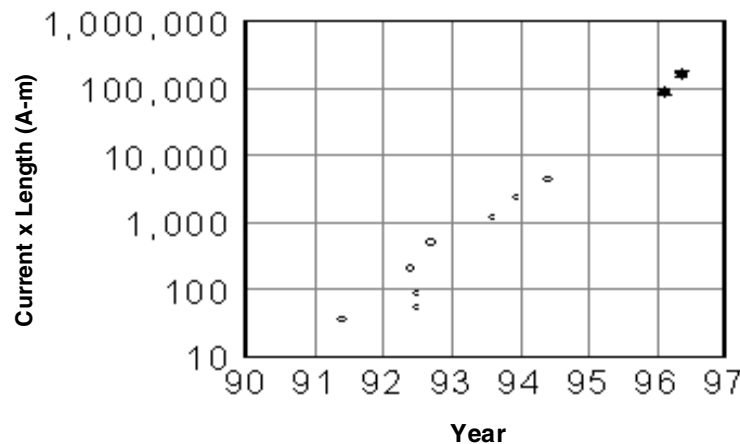


Figure E-4
Evolution of Conductor Length and Ampacity between 1991 and 1997

The conductor configuration for MCA-1 and MCA-2 and the achieved critical current (I_c) are reported in the following Table E-2.

Table E-2
Critical Current Results on MCA-1 and MCA-2

Conductor Configuration	Final MCA Length (m)	Average and Maximum I_c (A) @ standard criteria
MCA-1 (4 layers)	50	1800 – 1850
MCA-2 (8 layers)	50	3300 – 3510

Maintaining property uniformity can be achieved reliably in short samples (~ 1 m). However, the ability to attain the same level of uniformity in long-length, machine wound conductors had not been proven until these prototypes were developed and tested. Figure E-5, below, illustrates the critical current at various positions along the conductor. These results validate the reliability and reproducibility of the stranding process developed.

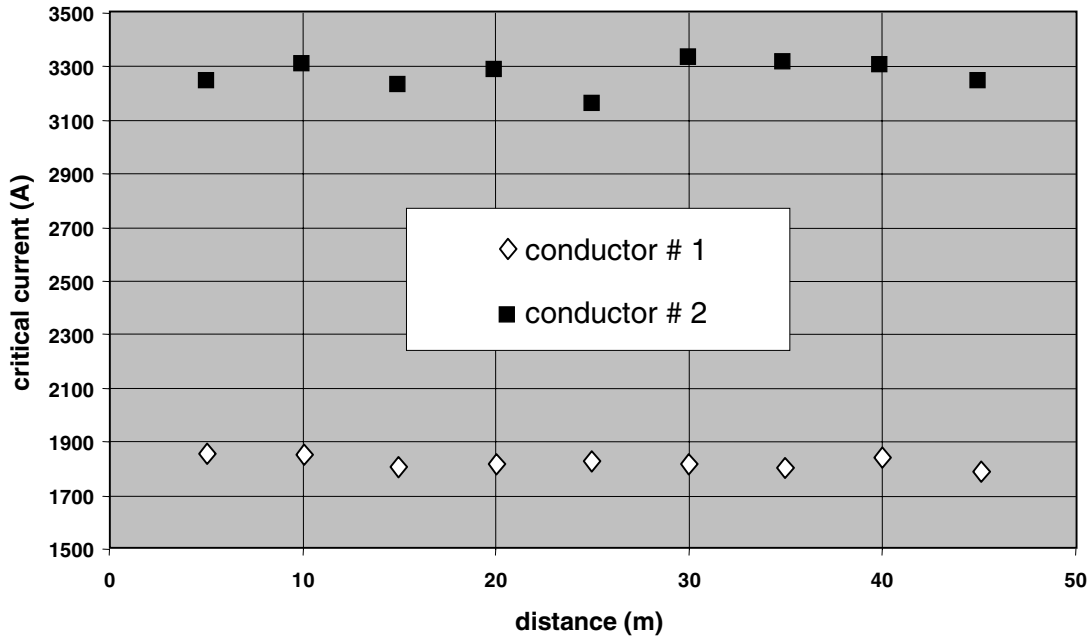


Figure E-5
Critical Current Measured over the Length of the Prototype Conductor

Ampacity tests were undertaken on each tape before cabling, on the completed “bare” conductor, on the cable after completion of all manufacturing stages, and on the finished cable system assembly comprising cable, terminations and one in-line joint. Before installing the joint and the terminations DC measurements were performed varying the operating temperature. The cable showed the same scaling law of I_c against temperature already determined for tapes. The I_c measurement confirmed that the degradation of the BSCCO tape performance through all the steps of the cable manufacturing was very small. Figure E-6 shows results for the ampacity at 77 K for the conductor, cable, and system respectively and in Figure E-7 the n value of the HTS transition is shown to highlight the retention of the superconducting behavior during the

manufacturing and testing phases. It can be seen that the performance of the conductor in the complete system exceeded the targeted minimum performance of $I_c > 2800A$ DC. Subsequently 2000Arms AC were successfully passed through the completed assembly, using inductive transformers to induce a current through the HTS core.

Effect of cabling and jointing

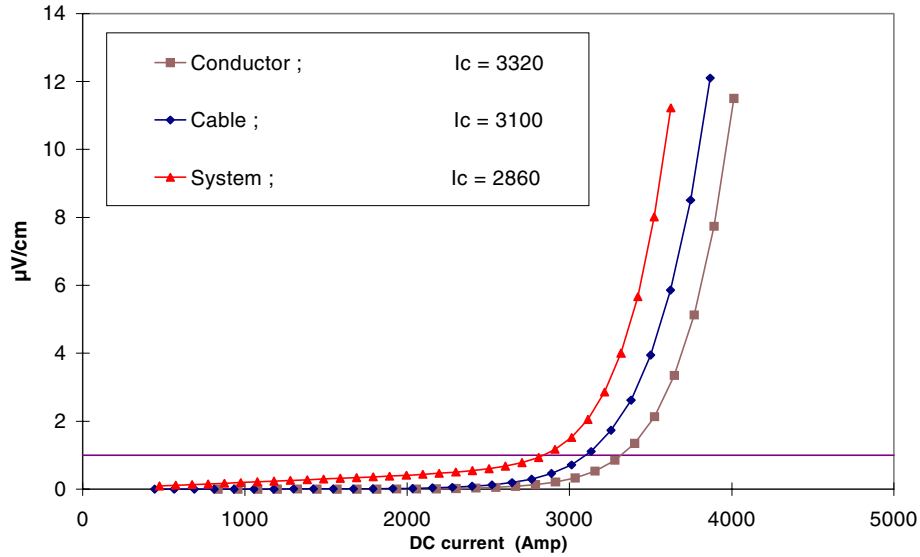


Figure E-6
Effect of cabling and jointing on HTS conductor performance. In the system case the joint losses are included.

Effect of cabling and jointing

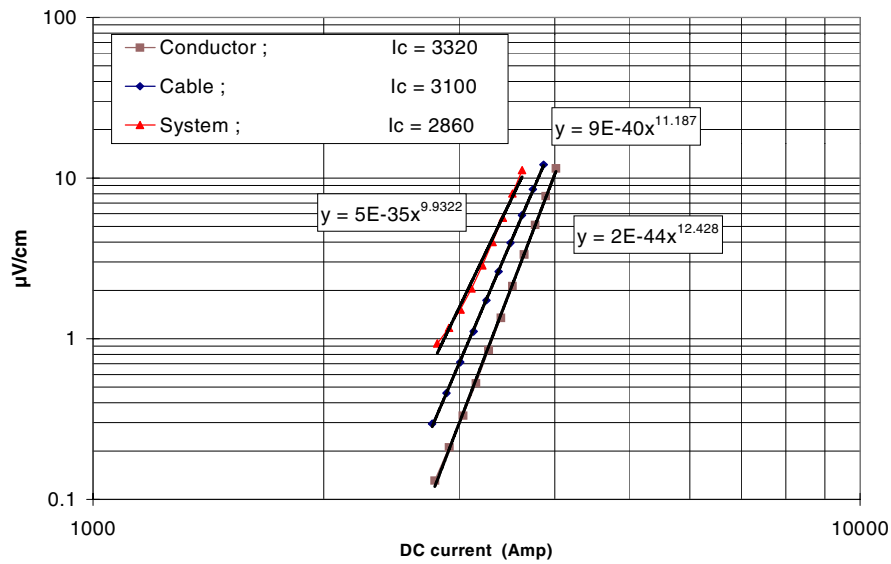


Figure E-7
Effect of cabling and jointing on HTS conductor performance. The n value of the HTS transition are highlighted

AC loss performance and understanding

In order to address the understanding of some features of the AC loss behavior of an HTS cable, a comprehensive testing program was conducted as described in Table E-3.

Table E-3
Summary of Conductor and Cable Samples and Tests Performed

Task	Sample	Length(m)	Number of HTS layers	I _c (A) 77 K	Tests
1	MCA-2	1	8	3300 measured	PIRELLI I _c , electrical AC loss
2	MCA-2	3	8	3300 measured	PIRELLI I _c , electrical AC loss
3	MCA-2	13	8	3300 measured	PIRELLI I _c , electrical AC loss at 40, 60, 90 Hz
4	MCA-2 with cryostat	13	8	3300 measured	PIRELLI I _c , electrical AC loss
5	MCA-2	1	8	3300 expected	LANL calorimetric AC loss x1-Ø - 76, 70 K
6	MCA-2	1	reduced from 8 to 4 layers	1800 expected	LANL calorimetric AC loss 1-Ø - 76, 70 K
7	MCA-2	1	reduced from 4 to 3 layers	1350 expected	LANL calorimetric AC loss 1-Ø - 76, 70 K
8	MCA-1	1.5	4	1800 measured	PIRELLI I _c , electrical AC loss 40, 52, 60 Hz ENEL Boil off calorimetric AC loss 50 Hz
9	PMC-1	1	2	1290 measured	PIRELLI I _c , electric AC loss LANL Calorimetric AC loss 1-Ø - 76 K 3-Ø - 76, 64 K 2-Ø - 76 K
10	PMC-2	1	2 layers electrically insulated	1250 measured	LANL calorimetric AC loss 1-Ø - 75, 69, 64 K 3-Ø - 75, 69, 64 K 3-Ø - 76, 70 K with 20 cm spacing
11	MCA-2 Conductor only, straight configuration	50	8	3320 measured	PIRELLI I _c
12	MCA-2 With cryostat and electrical insulation Straight configuration	50	8	3100 measured	PIRELLI I _c 73, 76, 81 K Electrical AC loss 50 Hz, 73, 76, 81 K
13	MCA-2 Set up for HV tests termination comprised U configuration	50	8	2860 measured	PIRELLI I _c

In summary, the results achieved in the above testing programs are as follows:

1. The cabling processes (application of cryostat, dielectric, etc.), if properly performed, do not greatly affect conductor performance (task 4, 13,14)
2. Superconducting properties are not significantly affected by the strains imposed during manufacturing, handling, transport and installation (task 3, 11, 12, 13)
3. The critical current of the conductors varies with changing temperature following approximately the same empirical law followed by tapes (task 12)
4. The AC losses measured in cable conductors samples are independent of the length of the sample (tasks 1, 2, 3, 13)
5. The main contribution to AC losses in BSCCO tapes conductors in single phase configuration is due to hysteretic losses (task 3, 8)
6. The AC losses dependence on temperature is mainly due to the variation of the critical current (task 5, 6, 7, 11, 12)
7. The AC loss for 2-layer conductors in trefoil configuration with 10 cm distance among the phases are approximately 2 to 3 times higher than the same losses in single-phase(task 9, 10)
8. The AC losses for conductors in trefoil configuration are approximately inversely proportional to the square of the distance among the conductors (task 10)
9. The eddy losses produced in the stainless steel cryostat tubes are negligible provided the two corrugated tubes are electrically disconnected. Significant losses may arise in the cryostat if there is current circulating between the two corrugated cryostat tubes or between the conductor and the corrugated tubes.
10. The cross check of three different and independent measurement methods indicates that all of them are suitable to perform reliable AC loss measurement in the suitable current range (tasks 1- 5, 6 - 8, 9)
11. The presence of an insulating interlayer between superconducting layers doesn't affect the AC losses of the 2-layer conductor (task 9,10)

Furthermore, the 50m long cable's AC performance was tested in a suitably designed experimental installation, not requiring a cable joint nor high voltage terminations. The cable was laid in straight configuration, using a couple of copper braids symmetrically disposed at about half a meter away from the cable for current return, as already experimented in a previous measurement on a 13 m cable conductor. More than 4000 Amps DC and up to 2200 Arms AC 50 Hz were available for power feeds. Circulating LN₂ at 5 bar pressure and different temperature (72 – 83 K) at the cable's inlet was provided by an open cycle refrigerator, fed by a 12.000 litre LN₂ tank. Voltage taps were disposed along the conductor before the cryostat and electric insulation construction to allow voltage detection on several different cable sections.

The voltage drop due to AC losses was measured using a lock-in amplifier for the measurement of the signal amplitude and an accurate phase meter for the phase angle with respect to a signal in phase with the current.

The AC loss measurements revealed two different contributions to the total dissipation: hysteretic losses, due to the intrinsic dissipation in the superconducting tapes, and ohmic losses, due to the current circulating in the cryostat.

The hysteretic losses confirmed substantially that the same level of losses found in the 13 m cable conductor section; an additional effect due to the presence of the cryostat was found in this cable installation because the cryostat tubes were electrically connected between themselves and with the terminations at the cable ends. The loading current is inductively pushed towards the cryostat, especially the outer tube, due to its larger diameter, thus producing small but detectable losses. The resulting voltage drop measured along the cable is higher than in the presence of the conductor alone and the intrinsic superconductor losses has to be extrapolated by the calculation and subtraction of this additional contribution (Figure E-8).

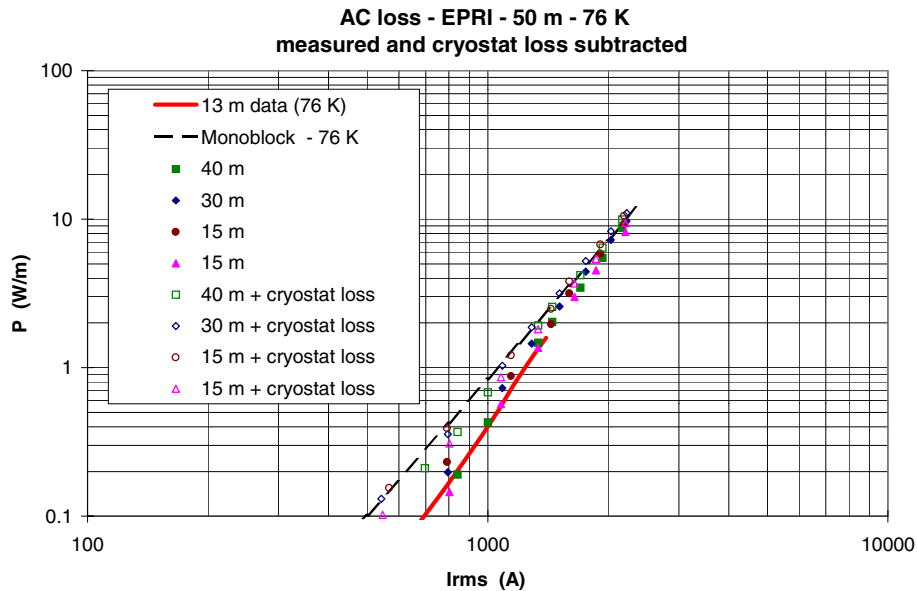


Figure E-8
AC losses at 76 K in the EPRI 50-m cable prototype. The unfilled markers represent the measured losses, while the filled ones the hysteretic superconductor losses once the cryostat contribution has been subtracted.

AC losses measured at different temperatures have been reported in Figure E-9 (The cryostat contribution here has been subtracted); the indicated temperature is the average value along the cable length.

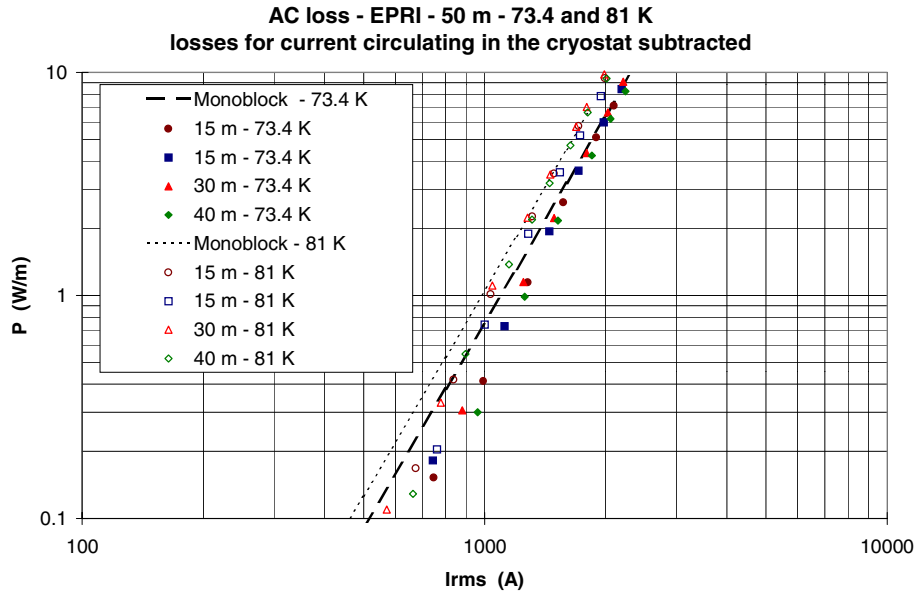


Figure E-9
Hysteretic AC losses in the EPRI 50 m cable prototype at 81 and 73.4 K

HV test of the 50 m long cable system prototype

The electrical performances of the insulation system, joint, and terminations were checked with a complete range of Type Tests, generally in accordance with AEIC CS2-90, and IEEE standards, including AC withstand tests to 165kV AC for 24 hrs, 205 kV for 1 minute, and lightning impulse tests at +/-550kV (10 pulses each).

The dielectric system (cable and accessories) was shown to perform beyond the criteria established for phase to phase or phase to ground voltages as reported in the following Table E-4.

**Table E-4
High Voltage Testing Summary on Prototype Cable**

Test	Test Parameter	Test Result
Ionization factor test	Voltage level: (8, 10, 20, 30, 40, 50, 60, 70, 80) kV r.m.s.	Satisfactory (1.37 – 1.64)X10E-3
Power factor measurement vs. temperature	Voltage level: 115 kV r.m.s. Oil temperature (pipe): 16 °C, 55 °C, 75 °C)	Satisfactory (1.36X10E-3, 1.09X10E-3, 1.04X10E-3)
HVAC test	Voltage level: 165 kV (r.m.s.) Voltage applied for: 24 hours	NO BREAKDOWN
HVAC test (sealing end investigation)	Voltage level: 205 kV (r.m.s.) Voltage applied for: 1 min.	NO BREAKDOWN
HVDC test (joint investigation)	Voltage level: 275 kV Voltage applied for: 15 min.	NO BREAKDOWN
HOT LIGHTNING IMPULSE WITHSTAND TEST	Oil temperature (pipe): 75 °C Starting Voltage: 450 kV Final Voltage: 550 kV Step Voltage: 25 kV Shots per step: 10 shots both polarity Polarity sequence: +,-/+,+/-,+/-,-	NO BREAKDOWN
HVAC TEST AFTER LIGHTNING IMPULSE	Voltage level: 120 kV r.m.s. Voltage applied for 15 min.	NO BREAKDOWN

Furthermore, one of the newest system components, i.e. Feed Through Bushing, was shown to exhibit at least an impulse breakdown strength that was 50% greater than the required design BIL as reported in Table E-5.

**Table E-5
Hot Lightning Impulse Test on the Feed Through Bushing**

Hot lightning impulse test up to breakdown	Starting Voltage: 450 kV Final Voltage: breakdown or flash over Step Voltage: 25 kV Shots per step: 10 shots both polarity Polarity sequence: +,-/+,+/-,+/-,-.....	BREAKDOWN AT + 828 kV (withstood 10 shots at – 850 kV)
--	--	--

Cryogenic cooling system performance

The cryogenic cooling system demonstrated its suitability to control the average cable temperature in the range from 73 K up to 81 K at full load conditions. This temperature range was sufficient, as described later in section 3.2, to carry out the superconducting testing programs.

The refrigeration system operated reliably for a total duration of 27 weeks. The problems experienced were minimal, and related either to the quality of the air supply to the control valves or vacuum degradation of components.

The cooling plant, because of its design based on a sub-cooled bath of LN₂, has an ideal minimum operating temperature of 63.2 K (triple point of nitrogen). Before installation in the cable system its capacity to remove heat loads up to 2 kW was successfully verified. Loss of Cooling and Loss of Pumping tests were performed. Resuming of cooling and pumping demonstrated the cooling plant capability to recovery normal operating limits in few minutes, without any damage.

Pipe loss verification

The experimental system indicated that the current pipe loss calculation techniques over-state the pipe losses when applied to a 12 in. pipe enclosure operating at near ambient temperatures. Taking the losses at 3090 A, the standard equations predict losses of 275.8 W/m, while the Aron technique and the calorimetric technique measured 187.7 W/m and 158.3 W/m respectively. Because the standard equations have been developed and refined using experimental studies and practical experience, the linear extrapolation of these models beyond the range (both for the pipe dimensions and the cable ampacity) from which they have been derived must be considered when analyzing the results. Though these results do not provide conclusive evidence that the Neher-McGrath equations for pipe loss are not applicable to very high current levels, it does indicate that there are limits of applicability, i.e. larger pipe diameter and lower operation temperature. In order to develop a method for calculating pipe losses for conditions that deviate from the current practices, further empirical and analytical evaluation should be necessary.

Project partners and their role

- Energy Power Research Institute - project manager
- Pirelli Cable Corporation - prime contractor: system manufacturer
- American Superconductor Corporation- sub-contractor: HTS tape and PMCs manufacturer
- Los Alamos National Laboratory -sub-contractor: calorimetric AC loss measurements and understanding

Conclusions

Thus as early as 1992, Pirelli and EPRI commenced their first feasibility evaluation of an HTS pipe-type retrofit cable that was subsequently finalized in 1995, under the US Department of Energy Superconductivity Partnership Initiative (SPI), for the development of a complete prototype cable system.

This project was concluded in January 1999 with the successful demonstration of a 50m 400MVA 115kV pipe-type HTS cable system (comprising a single phase HTS cable, joint, outdoor terminations and LN₂ cooling plant) capable of carrying 2kA_{rms}.

This project was the first development and test program in the world to target and achieve the qualification of a complete single-phase HTS cable system. These results are to be considered as the first step in the demonstration of the technical feasibility of HTS cable system based on the WD design.

Several improvements and future tests are needed before proving all the technical, reliability, operational, and maintenance aspects of this new technology as well as its overall economical attractiveness.

The large number of special benefits of the HTS cable system, in terms of their high current carrying capacity, reduced electrical losses, compact overall dimensions, low weight, minimal environmental impact and overall economical competitiveness, are the driving factors for this development. This program was a first positive step in the assessment of such potential benefits.

The next step has already started, building on the success of the 115kV development with EPRI, in 1998 Pirelli and EPRI initiated the Detroit Edison Project, which will involve the world's first HTS cable system installation in an utility site at Detroit Edison's Frisbie Station. The participants in the project are Pirelli, Detroit Edison, ASC, EPRI Lotepro and LANL, and the project is being partially supported under the US DoE's SPI initiative.

This project will involve design, engineering, installation, test and routine operation of a 24kV 3-phase Warm Dielectric cable system which will replace existing conventional cables in the Frisbie station. The three HTS cables will replace nine existing cables, which together carry a total power of 100 MVA. Thus at 24 kV, each HTS cable will carry 2400Arms AC, a level which would be inconceivable in a conventional cable of this voltage rating. The system design and engineering will be completed in 1999, with cable manufacture commencing in early 2000, installation at the end of the 2000, and « go-live » in the year 2001. The cable design for the Detroit project will be based on the 115kV EPRI cable concept using a warm dielectric construction, which in this instance will be extruded solid insulation designed for operation at the 24kV voltage level.

The cables will be installed in existing "fibre" ducts of 4 inch (~100mm) internal diameter, and will have five 90° bends in the 120m route between the 120kV/24kV transformer and the 24kV switchgear which they will interconnect.

Preliminary AC loss measurements on short conductor samples have already been performed (see fig 10). These results already showed more than one order of magnitude reduction in AC loss, compared to the value presented in this report for the EPRI cable, due to the improvements on HTS tape performances as well as cable design.

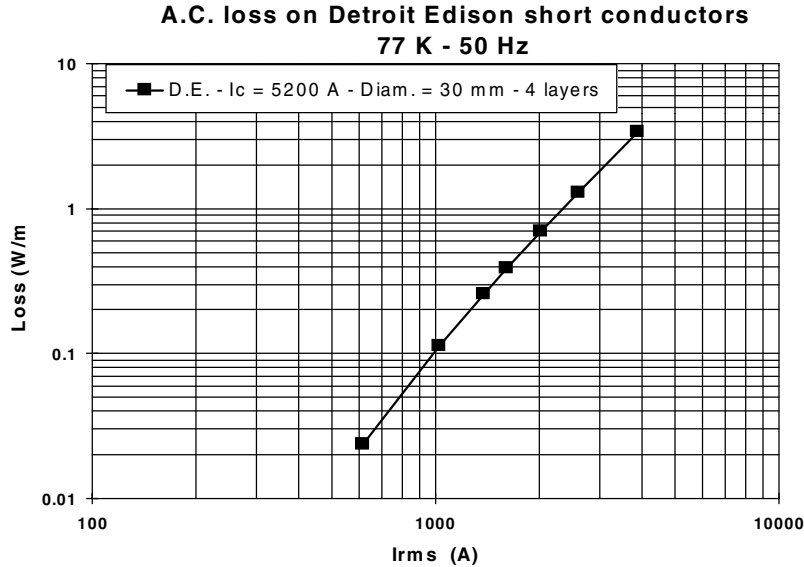


Figure E-10
AC loss measurements on short conductors carried out within the Detroit Edison project

Acknowledgements

This project was partially supported by the U.S. Department of Energy's Office of Energy Technology under their Superconducting Partnership Initiative. The remaining cost was shared between EPRI, Pirelli Cable and ASC.

The authors would like to thank the many without whom this project would not have been such a success:

- The assistance of EPRI who provided not only funding, but also valuable guidance through the life of this project;
- Los Alamos National Labs that made available world-class resources, both scientists as well as equipment, to carry out AC loss measurements and to understand the physics of these phenomena;
- American Superconductor Corporation research and manufacturing teams that made a wonderful job in delivering HTS tapes that comply with and exceed all the specifications set by Pirelli;
- the Pirelli resources outside the HTS team who supported the design, manufacturing and testing of the complete system;

CONTENTS

1 INTRODUCTION	1-1
1.1 Background.....	1-2
1.2 HTS Materials	1-3
1.2.1 Superconducting Characteristics - T_c , I_c , H_c	1-3
1.3 Applications.....	1-4
1.3.1 Impact of HTS on Superconducting Cable Development	1-5
2 PROJECT ACTIVITIES	2-1
2.1 Bismuth Compounds - Structure and Composition	2-1
2.1.1 Physical Features (T_c , J_c , H_c).....	2-2
2.2 HTS Material Development	2-4
2.2.1 Processability	2-5
2.2.2 Tape Conductor - Fabrication Process	2-5
2.2.3 Transport Electrical Properties.....	2-6
2.2.4 Mechanical Properties	2-8
2.3 Superconducting Tapes for the Prototype Cable	2-9
2.3.1 Specifications	2-11
2.4 Cable Design	2-12
2.4.1 Design Process and Parameters	2-15
2.4.2 Conductor Design.....	2-16
2.4.3 Former Design.....	2-17
2.4.4 Conductor Assembly and Manufacturing	2-19
Stranded Configuration	2-19
Stranding Process Development	2-20
Conductor Testing.....	2-21
2.4.5 Cryostat.....	2-23
Cryostat Design.....	2-24
Cryostat Tests.....	2-25

Cryostat Manufacture.....	2-26
2.4.6 Dielectric	2-27
2.5 Cable System Design.....	2-27
2.5.1 Terminations.....	2-27
Cryogenic Termination (CT)	2-28
2.5.2 Joint.....	2-29
2.5.3 Feed-Through-Bushing.....	2-29
2.6 Refrigeration Plant	2-31
2.6.1 Specification	2-31
2.6.2 Description	2-32
2.6.3 Engineering and Test	2-33
2.6.4 Monitoring System.....	2-34
2.7 Oil Pumping Plant	2-35
3 EXPERIMENTAL RESULTS	3-1
3.1 Superconductor Testing Program.....	3-1
3.1.1 Conductor Samples	3-2
3.2 AC loss tests on cable conductors	3-4
3.2.1 Electrical Measurement Technique (Pirelli).....	3-6
Electrical measurement at different frequencies	3-8
Electrical measurement on samples of different length – MCA-2.....	3-10
3.2.2 Temperature Difference Calorimetric Technique (LANL)	3-11
Comparison of Pirelli and LANL methods.....	3-12
3.2.3 Boil-off Calorimetric Technique (ENEL)	3-14
Pirelli, LANL and ENEL measurements comparison.....	3-14
3.3 Cryostat Effect on AC Losses.....	3-16
3.4 Single phase AC Losses: Comparison with Theoretical Models	3-20
3.5 LANL Three-Phase Measurements	3-26
3.6 Interlayer Insulation.....	3-29
3.7 8, 4, 3-Layer conductors: LANL AC loss Measurements	3-30
3.8 Testing of the 50 m Prototype Cable	3-33
3.8.1 Mechanical History of Prototype Cable: Cabling Processes.....	3-33
3.8.2 Superconducting Properties Testing: Straight Configuration.....	3-34
Critical Current	3-34
AC Losses.....	3-35

Cryostat Effect	3-37
3.8.3 Thermal and Mechanical History of the Prototype Cable: “Straight” Tests and High Voltage Installation	3-40
3.8.4 Superconducting Property Testing: HV Installation Configuration	3-41
Critical Current	3-41
3.9 High Voltage System Testing	3-42
3.9.1 HV Testing on Mock-Up Cable without Liquid Nitrogen.....	3-43
Test Assembly Description.....	3-43
Ionization Factor.....	3-44
Power Factor / Dielectric Power Factor	3-44
HV AC Time Test	3-44
HV AC Termination Test	3-44
HV DC Joint Test	3-44
Lightning Impulse Test	3-44
HV AC Proof Test.....	3-45
3.9.2 High Voltage Mock-Up System Tests – with Liquid Nitrogen	3-45
Test Assembly Description.....	3-46
Ionization Factor.....	3-47
Power Factor / Dielectric Power Factor	3-47
HV AC Time Test	3-47
HV AC Termination Test	3-47
HV DC Joint Test	3-47
Lightning Impulse Test	3-47
3.9.3 High Voltage Test of the 50 m Prototype Cable System	3-48
Test Assembly Description.....	3-50
Ionization Factor.....	3-51
Power Factor / Dielectric Power Factor	3-51
HV AC Time Test	3-51
HV AC Termination Test	3-51
HV DC Joint Test	3-51
Lightning Impulse Test	3-51
HV AC Proof Test.....	3-52
3.9.4 Impulse Testing of the Feed Through Bushing	3-52
3.9.5 Conclusions.....	3-53
3.10 Test of the cryogenic cooling system.....	3-53

Description of the test loop.....	3-53
Cool down.....	3-54
3.10.1 Functional evaluation.....	3-54
Loss of Cooling	3-55
Loss of Pumping	3-56
Conclusions	3-56
3.11 Pipe Loss Verification.....	3-57
3.11.1 Experimental Installation.....	3-58
3.11.2 Measurement Methods	3-59
Aron Method	3-59
Calorimetric Technique	3-59
3.11.3 Experimental Description.....	3-60
Aron Method	3-60
Calorimetric Method.....	3-61
Standard Equations.....	3-63
3.11.4 Comparison of measured and calculated losses.....	3-64
3.11.5 Results and Conclusions	3-65
A THEORETICAL BASIS FOR AC LOSS CALCULATION.....	A-1
AC loss in Ag/2223 tapes	A-1
AC loss in HTS cable conductors	A-7
Monoblock model.....	A-8
Uniform Current Distribution (UCD) model.....	A-9
Clem model	A-10
B REFERENCES.....	B-1
Section 1	B-1
Section 2	B-1
Section 3.....	B-2
Appendix A.....	B-3

LIST OF FIGURES

Figure 2-1 Resistivity vs Temperature Curve for BSCCO Tapes	2-3
Figure 2-2 Irreversibility Line for BSCCO Tapes, Parallel and Perpendicular to the Copper Oxide Plane	2-4
Figure 2-3 Cross-Section Photograph of HTS Multi-Filament Tape	2-5
Figure 2-4 Typical Load/Elongation Response for Metals and Ceramics.....	2-8
Figure 2-5 Strain Patterns for Thin Tapes under Various Loading Conditions	2-9
Figure 2-6a Model of Warm Dielectric Cable Design	2-14
Figure 2-6b Schematic of Warm Dielectric Cable Design	2-14
Figure 2-7 Stranding Machine Winding HTS Conductor	2-19
Figure 2-8 Critical Current of the MCA-0 Conductor for each Layer Applied.....	2-21
Figure 2-9 Evolution of Conductor Length and Ampacity between 1991 and 1997	2-22
Figure 2-10 Critical Current Measured over the Length of the Prototype Conductor.....	2-23
Figure 2-11 MLI Application	2-26
Figure 2-12 Schematic drawing of the HTS Cable Termination Assembly.....	2-28
Figure 2-13 Feed-Through-Bushing, Transfer Lines and Termination	2-30
Figure 2-14 Schematic of the Body of the FTB.....	2-31
Figure 2-15 Refrigeration System Set-up for Mock-up Cable Testing.....	2-32
Figure 2-16 Refrigerator System Proof Tests at Various Power Levels and Flow Rates.....	2-33
Figure 2-17 Monitoring System at High Voltage Potential.	2-34
Figure 2-18 Data Display from Data Acquisition System	2-35
Figure 3-1 AC Loss Measurements on the MCA2-13 m Conductor.....	3-8
Figure 3-2 AC loss measurement at different frequencies: voltage taps on the current terminations.....	3-9
Figure 3-3 AC Loss Measurement at Different Frequencies: Low Resistance Ring Voltage Contacts.....	3-9
Figure 3-4 AC Loss Measurements on Samples of Different Length.	3-10
Figure 3-5 AC Losses on MCA -2 13 m Sample - Comparison of Electric and Calorimetric Techniques.....	3-13
Figure 3-6 AC Losses on PMC-1 Sample - Comparison of Electric and Calorimetric Techniques.....	3-13
Figure 3-7 AC Loss on a MCA-1 Sample measured with Electric and Calorimetric Techniques.....	3-15

Figure 3-8 Alternating current I_{ac} flowing along the axis of a metallic tube, which is characterized by the radius R and the wall thickness d	3-18
Figure 3-9 Contour used to derive the induced electrical field	3-18
Figure 3-10 Comparison of losses determined experimentally on conductor with and without the cryostat.	3-20
Figure 3-11 AC loss Vs F measured at 76 K in LANL with difference temperature calorimeter	3-21
Figure 3-12 AC loss Vs F measured at 70 K in LANL with difference temperature calorimeter'.....	3-22
Figure 3-13 AC loss Vs F measured at 64 K in LANL with difference temperature calorimeter	3-22
Figure 3-14 Reduced loss $\pi W/\mu v l_c^2$ Vs F for the PMC samples at different temperatures.....	3-24
Figure 3-15 AC loss per unit length Vs I for the MCA2 sample at 76/77K compared with the theoretical model	3-25
Figure 3-16 Reduced loss $\pi W/\mu v l_c^2$ Vs F for the MCA2 sample at different temperatures	3-25
Figure 3-17 AC loss per unit length Vs I for the MCA-1 sample at 76K measured in different laboratories.....	3-26
Figure 3-18 Comparison of 1 phase, 2–phase and 3-phase AC Losses on the PMC 1 Conductor.....	3-27
Figure 3-19 Three-Phase Loss for 10 and 20 cm distance between Phases Compared to Single-Phase Losses.....	3-28
Figure 3-20 3-Phase / 1-Phase Loss Ratio Vs $1/d^2$	3-29
Figure 3-21 AC Losses on Samples with (PMC2) and without (PMC1) Electrical Insulation Between Layers.	3-30
Figure 3-22 AC loss Vs Irms in 8,4 and 3-layer samples at 76K.....	3-31
Figure 3-23 AC loss Vs Irms in 8,4 and 3-layer samples at 70K.....	3-32
Figure 3-24 Reduced loss Vs F for 8,4 and 3-layer samples at 76K and 70 K.....	3-32
Figure 3-25 Scheme of the Voltage Taps Location along the Cable	3-34
Figure 3-26 V-I Characteristics of the 50 m Prototype at Different Temperatures.....	3-35
Figure 3-27 50 m cable AC Loss Measurements Vs I at 73.4K	3-36
Figure 3-28 50 m Cable AC Loss Vs I at 76 K and the 13 m Sample AC Loss Vs I at 77 K.....	3-36
Figure 3-29 50 m Cable AC loss Vs I at 81 K.....	3-37
Figure 3-30 Scheme of the Circuit Model to Estimate the Additional Losses in the Cryostat.....	3-38
Figure 3-31 Estimation of the Additional Losses Due to Current Circulating in the Cryostat.....	3-39
Figure 3-32 Asymmetrical U disposition for the HV test installation and voltage taps disposition. In parenthesis are reported the distances of each Vtap from termination 1.	3-41

Figure 3-33 V-I Characteristic as Measured on the Conductor just After Construction, on the Cable during the AC Loss Measurement, and on the Final Complete System Comprising the Joint.....	3-41
Figure 3-34 n-Value Determination for the Bare Conductor, Cable and System Configurations.Effect of cabling and jointing	3-42
Figure 3-35 50 m Prototype Cable Installation in High Voltage Testing Facility	3-49
Figure 3-36 Cool-Down of Subcooler Bath	3-54
Figure 3-37 Temperature Rise through Test Loop at Different Powers and Flow Rates	3-55
Figure 3-38 Pressure Response of Cable System to Loss of Cooling	3-56
Figure 3-39 Experimental Setup.....	3-58
Figure 3-40 Cable Configuration Inside the Pipe	3-59
Figure 3-41 Position of Thermocouples around Pipe Enclosure	3-60
Figure 3-42 Mean Total Dissipated Power as a Function of Current.....	3-61
Figure 3-43 Pipe Temperature Increase with a Current of 3090 A.....	3-62
Figure 3-44 Calculated Pipe Losses using Standard Equations	3-64
Figure 3-45 Comparison of Total Pipe Losses Determined with the Three Different Methods	3-65
Figure A-1 AC loss Vs the reduced current F for the tape OP1433 at different values of frequency	A-1
Figure A-2a Cross section micrograph of the multifilamentary sample	A-4
Figure A-2b Measured loss per cycle and per unit length as a function of the peak reduced current i compared with the theoretical curves for the ellipse and thin strip core geometry	A-4
Figure A-3 Reduced loss per cycle and per unit length as a function of F	A-6
Figure A-4 Sketch of the cross section of the two layers conductor: 1- inner layer; 2 - outer layer.....	A-11
Figure A-5 Plots of S2, S4, S6, and S8 versus the pitch angle θ (in degrees).	A-14

LIST OF TABLES

Table 2-1 Specifications for HTS Tape for Prototype Cable	2-11
Table 2-2 System Parameters for HTS Prototype	2-12
Table 2-3 Cable Dimensions	2-16
Table 2-4 Critical Current Results on MCA-1 and MCA-2.....	2-22
Table 3-1 Summary of Conductor and Cable Samples and Tests Performed.....	3-3
Table 3-2 Mechanical history of EPRI 50 m before HV Installation.....	3-33
Table 3-3 Mechanical history of EPRI 50 m cable [Straight Tests → High Voltage Installation]	3-40
Table 3-4 Thermal history of EPRI 50 m cable [Straight Tests → High Voltage Installation]	3-40
Table 3-5 Mock-up Cable High Voltage Testing Summary (without LN ²)	3-43
Table 3-6 Mock-up Cable High Voltage Testing Summary (with LN ²)	3-46
Table 3-7 High Voltage Testing Summary on Prototype Cable.....	3-50
Table 3-8 Hot lightning Impulse Test on FTB	3-53
Table 3-9 Pipe Characteristics and Measured Power.....	3-62

1

INTRODUCTION

High Temperature Superconducting (HTS) power cable technology provides a means to extend the range of technical and economic feasibility of underground systems. Improving underground cable performance has several implications, particularly in areas where installing overhead lines is restricted. The Electric Power Research Institute (EPRI) recognized the advantages that HTS cables promise and has worked to accelerate the availability of this technology to their membership. In 1989, they initiated a project with Underground Systems, Inc. (USi) to investigate the potential for HTS cable for power transmission. This project developed several concepts for cable design and identified some potential applications for HTS power cables in the electric system [1.1].

Pirelli Cable Corporation (PCC) began an internal program investigating the potential of HTS cables in 1989, focusing on the material requirements necessary for cable manufacture. To this end, they formed a partnership with American Superconductor Corporation (ASC) to develop conductor materials that possessed the necessary electrical and mechanical properties.

In 1992, EPRI established a program with PCC to perform a detailed design analysis of the cable construction concepts from the USi study. Using PCC's existing experience in HTS materials and cable manufacturing, the study determined that a "Room-Temperature" or "Warm" dielectric cable could be manufactured and have the necessary handling characteristics, dimensions, and performance attributes "to increase the capacity of existing pipe-type circuit" beyond any retrofitting method currently known [1.2]. Based on the conclusions from this study, EPRI and PCC formed a partnership to develop, construct, and test an HTS cable system prototype. The major milestones for this partnership included:

- Manufacture 12 km of high performance HTS tapes;
- Manufacture a 30m length of full-scale Warm Dielectric cable using Pirelli's existing cabling equipment;
- Design and construction of a flexible, vacuum insulated cryostat;
- Design and construction of a joint and terminations;
- Develop testing methods for AC loss measurements;
- Engineer cryogenic cooling and control system;
- Define a complete High Voltage test protocol for the HTS cable system;
- Carry out the qualification and characterization of the system and all its sub-systems.

The final design targets were determined by focusing on a retrofit system for the conventional 115kV/200MVA High Pressure Fluid Filled (HPFF) system that would provide a 100% increase in power capacity and maintain the same specific losses (kW/MVA·km). The length of the cable prototype was increased during the program to 50m.

The present work reports the efforts under this partnership, culminating in the qualification testing of a 115kV/400MVA warm dielectric (WD) HTS cable system.

1.1 Background

Several factors differentiate power cables as being particularly applicable for HTS technology. Primary among these is the low magnetic field intensity experienced by the conductor. This is significant because HTS materials have an inherently limited magnetic field tolerance. Another major factor is the extensive experience available from previous low temperature superconductor cable projects. These programs were technically successful, but could not provide economic suitability. The operating conditions of the HTS materials relieve many of the economic issues experienced with LTS cables, and offer comparable performance expectations.

The USi report identified room temperature dielectric cables as a strong candidate for initial development of the HTS technology. Beyond the conductor and the cryostat assemblies, the cable (dielectric, shielding, and pipe enclosure) is conventional in every respect. Making the cryostat assembly the same diameter range of normal copper conductors (30 to 60mm), the physical size and appearance of the cable will be identical to conventional cables. As such, they can be assimilated into the existing cable industry/utility infrastructure. The physical similarities will permit the new cables to be used as retrofit upgrades of conventional cables, significantly improving the power capacity without requiring the civil construction required to install new pipes [1.1].

A “typical” underground cable system was selected to provide the constraints, around which the HTS cable would be designed. The circuit selected for retrofit was a 115kV high pressure fluid filled cable installed in a 8-5/8” diameter pipe. Typically, this would be a 2500 kcmil paper insulated cable with a nominal capacity of 200MVA, or a nominal current of 1000Arms. The WD HTS cable can provide 400MVA using the same pipe, representing a power increase of 100%.

A HTS power cable system is comprised of several components and sub-components, each of which required detailed engineering and development to produce the prototype. The cable itself is one of the most important components in the system, and its construction and design benefited significantly from PCC’s experience and know-how within the fields of High Voltage cable engineering.

Fundamental to the cable system’s performance are the superconducting tapes. Under a separately Pirelli funded program, Pirelli Cavi and American Superconductor have worked since 1989 in the development of HTS wires, which have the engineering properties required for cable applications. High temperature superconducting materials were first discovered in 1986, which renewed interest in the development of revolutionary devices for the power industry.

1.2 HTS Materials

It is very well known that several materials, cooled below a certain material-specific temperature, called “critical temperature” (T_c), undergoes a phase transition into the superconducting state. This thermodynamic state is characterized by two extremely interesting properties, namely, perfect diamagnetism and zero electrical resistivity.

Both of these characteristics, but especially the absence of electrical resistivity, offer significant benefits to practical applications. Though the discovery of superconducting materials occurred in 1911, the early materials required very low temperatures (typically on the order of a few Kelvin degrees) to attain a superconductive state. Cooling objects down to these temperatures typically has been achieved by the use of liquid helium, which is particularly costly and difficult to handle. Historically, this restriction has hampered the widespread introduction of superconducting technologies in industrial applications.

A revolutionary event in the field of superconductivity was the 1986 discovery [1.3] of a new class of materials called “High Temperature Superconductors” (HTS) with T_c 's higher than 77K (-320°F). The ability to operate at higher temperatures presents a variety of advantages, both for simplifying the design and increasing the overall efficiency of the system. However, the most significant impact that these new materials offer is that they can be cooled with liquid nitrogen (LN_2), as opposed to liquid helium. LN_2 is used in many industries and is inexpensive and readily available throughout the United States and most industrialized countries throughout the world.

The availability of these new materials offers a significant impact on almost all the applications, particularly those where the expense and complexity of very low temperature cooling systems represented the most significant obstacle to exploitation.

1.2.1 Superconducting Characteristics - T_c , I_c , H_c

The superconducting state represents the thermodynamic equilibrium condition in a suitable range of the thermodynamic variables. Transition to the normal state can be driven by an increase in the overall energy of the system due to the increase of the material temperature, the external magnetic field, and the circulating electrical current. Actually, the thermodynamic boundaries above which a material loses its superconductivity can be represented by a three-dimensional surface in the temperature, magnetic field, and transport current space. The three points representing the intersection between that surface and the frame axes are defined as the critical values: Critical Temperature or T_c , Critical Current or I_c and Critical Field or H_c .

In particular, T_c is referred as the transition temperature above which, under zero external magnetic field and no current flow, superconductivity disappears. At the same time I_c represents the maximum current that a superconductor can carry in absence of magnetic field and at zero temperature, that value decreases as temperature and field increase.

In the HTS materials, which are type II superconductors, the thermodynamic H_c is generally lower than the high upper critical H_{c2} that represents the limit for the coexistence of magnetic

field and superconductivity. When the temperature is decreased further than T_c the critical field increases and it is maximum at the lowest temperature.

Therefore, T_c is extremely important for qualifying a superconductor not only directly, in that superconductivity cannot exist above T_c , but also indirectly, since assuming a certain working temperature according, for example, to the availability of suitable cooling fluids, the maximum working current and the maximum critical field will depend upon the ratio of such working temperature to the critical temperature T_c . In order for a cable to work in liquid nitrogen, at temperatures around 77K, it is therefore necessary to have a superconducting material with a significantly higher T_c .

The transport parameters are commonly referred as the critical current, I_c , or the critical current density, J_c , which is determined by the critical current of a sample divided by the superconducting cross-section. Another common term when discussing critical current is the engineering critical current density J_e , which is the critical current of a sample divided by the total material cross section. Of course these are nominal critical current densities, because we assume an overall uniformity of the superconductor material across the cross section.

While T_c and H_c are intrinsic properties of the materials, J_c can be altered by processing procedures. HTS materials are generally polycrystalline materials and the microstructure of the material such as the presence of defects, grains dimension, or small amounts of secondary (non primary phase or non superconducting) phases at the grain boundaries can affect the critical current density.

Among the many peculiarities which HTS materials show compared to Low T_c ones, quite a number are due to the above mentioned polycrystalline structure, which causes anisotropy in many of their physical, electrical, mechanical, and thermal properties. In particular, I_c is increased if the current flows along the CuO planes rather than perpendicular to them, and also the dependence of I_c upon an applied magnetic field is much stronger if such field is applied perpendicularly to the CuO planes than in the other directions.

1.3 Applications

The main commercial applications of superconductivity realized to date have used the low temperature superconductor (LTS) materials and have been limited to highly specialized applications. They are most frequently used in the production of very high magnetic fields, such as those used in the field of high-energy physics in accelerators designed for the study of elementary particles or in reactors for nuclear fusion. The most common application of superconductors is in nuclear magnetic resonance (NMR) imaging for medical diagnosis. Recently, superconductors have achieved commercial deployment in the electric power industry in power quality devices called superconducting magnetic energy storage (SMES or microSMES). This technology uses a solenoid to store high levels of energy and discharges this when the line voltage dips to maintain a constant flow of power. These devices have been applied to manufacturing facilities where power sags create significant disturbances in automated systems.

The HTS materials have reinitiated development efforts in a variety of fields where the cooling expense required for LTS blocked commercial viability. Among these applications are several designed for the electric power industry. Extensive worldwide efforts have been initiated to develop superconducting corollaries to conventional power system equipment, including cables, transformers, motors, generators, magnets and fault current limiters.

1.3.1 Impact of HTS on Superconducting Cable Development

The geometry of power cables, characterized by long length and having a high surface-to-volume ratio, makes them unfavorable to cool. As a result, HTS cables enjoy a significant improvement in economic and technical viability compared to LTS cables due to the increased refrigeration temperatures. Actually, most other power applications still use very low operating temperatures to improve the magnetic field resistance of the materials.

In fact, a thorough investigation carried out in the 1970's and 1980's culminated with the construction of a LTS cable prototype at Brookhaven National Labs; showing that helium cooled (Low Tc) superconducting cables were technically attractive, but (in general) economically unacceptable, due to the high cost of refrigeration at liquid helium temperature [1.4].

The new HTS materials are considered particularly attractive for electrical power transmission cables for a variety of reasons. One important reason, as mentioned before, is the use of LN₂ as coolant. LN₂ strongly increases the efficiency of the refrigeration system compared to Low Temperature Superconductor (LTS) cable, reducing the minimum level of transmitted power needed for achieving an economical advantage of HTS cable systems compared to conventional copper cable systems. Furthermore, the low magnetic field intensities associated with cables, compared to other high current applications, makes HTS materials possible candidates in spite of their intrinsically limited magnetic field tolerance at LN₂ temperatures (as detailed in the following sections). In fact, of the early prototype efforts, only the power cables and some transformer designs are cooled directly by liquid nitrogen. All of the other power applications use lower temperatures to maximize the magnetic field resistance. Another significant reason for the expectations surrounding HTS power cable development is the availability of a LTS cable experience, as mentioned above, as a positive technical background.

2

PROJECT ACTIVITIES

Though the development of the HTS wires was performed under separately funded activities, a description of the material used and how its mechanical and electrical properties affect the cable design has been included in the first three paragraphs of this chapter. An understanding of these properties is useful when considering the complex series of optimizations necessary in a cable design, as well as providing some insight into the nature of the technology and the considerations.

Once the basic building blocks (the HTS tapes) were properly specified, the remaining project activity was dedicated to the design, construction, and evaluation of the cable system:

- Different solutions were considered for the conductor, which was designed to work in blocked end configuration. The project activity on this element was aimed to avoid any degradation of the HTS tapes transport ampacity.
- Cryostat requirements were primarily focused on its thermal efficiency, flexibility and to the production of long-lengths of this component.
- Pirelli's experience on dielectric materials was fundamental in the development of the dielectric system.
- Other parallel activities concentrated on the definition and development of a joint and terminations able to match both the electrical, mechanical and thermal requirements imposed by the cable installation and handling, as well as the cryogenic cooling system and the monitoring and control system requirements.

2.1 Bismuth Compounds - Structure and Composition

In the last twelve years a large number of new superconductors, with T_c higher than that of previously known (intermetallic) materials (maximum T_c of 23 K) have been synthesized.

All superconductors with a T_c higher than the temperature of boiling nitrogen (77.3 K at ambient pressure) belong to the cuprate class, that is, they are all mixed copper oxides, including also a number of other cations. Most cuprate superconductors may be viewed as intercalation of perovskite and rock-salt blocks. The rock-salt block is composed of AO (A=Bi, Tl) layers and the perovskite block of CuO_2 and M (e.g. M=Ca, Y) layers. The intercalation region in common is the BO (e.g. B= La, Sr, Ba) layer, being structurally related to both the rocksalt and perovskite blocks. The CuO_2 layers represent the electronically active part of the structure, responsible for the transport of the superconducting charge carriers, whereas the adjacent "blocks" act as charge "reservoirs", by providing the necessary doping with free charges. Such charges have been recognized to be constituted by holes (not electrons) for the most common HTS cuprate compounds.

The family of cuprates includes quite a number of different materials, that can be further grouped into different sub-families. The highest critical temperature achieved up to now amounts to 164 K, and has been obtained with a material called Hg-1223, of the mercury-based compounds, by processing under special conditions (high pressure). This material, however, does not seem to be compatible with processing in the form of long wires or tapes, as is strictly required for most power applications.

The material that has been selected for prototypes and demonstrators in almost all electrotechnical applications presently under study belongs to the class of materials called “BSCCO” from the initials of the cations that they contain. The general formula of the BSCCO family is $\text{Bi}_2\text{Sr}_2\text{Ca}_{n-1}\text{Cu}_n\text{O}_{4+2n+\delta}$. This includes a homologous series of compounds that differ from each other for the number, n , of CuO_2 layers in the unit crystalline cell, and have correspondingly different critical temperatures. In particular, for n up to 3, the highest T_c (about 107 K) is found in the compound with the higher number of CuO_2 layers. Therefore the material that is typically adopted for use in liquid nitrogen is the one called BSCCO 2223, which is chemically defined by the formula $(\text{BiPb})_2\text{Sr}_2\text{Ca}_2\text{Cu}_3\text{O}_{10+x}$, and in which bismuth is partially substituted by lead.

2.1.1 Physical Features (T_c , J_c , H_c)

The critical temperature of the BSCCO-2223 phase is about 107 K, the highest measured among the isolated phases of the bismuth family. The critical temperature of BSCCO-2223 is less affected by oxygen stoichiometry than most of the other cuprates, but it can assume slightly different values if it is magnetically or electrically measured, and whether it is referred to the onset value or the zero resistance one. In Figure 2-1, the typical resistivity Vs temperature curve for BSCCO tapes is reported.

BSCCO-2223 phase, because of its layered structure, is characterized by very anisotropic behavior, not only in the intrinsic properties, such as coherence length and London penetration depth, but also for the macroscopic characteristics, such as upper critical field, critical current and pinning properties. Nevertheless by means of special techniques, it has been possible to form conductors with an optimally aligned grain structure, best exploiting these anisotropies.

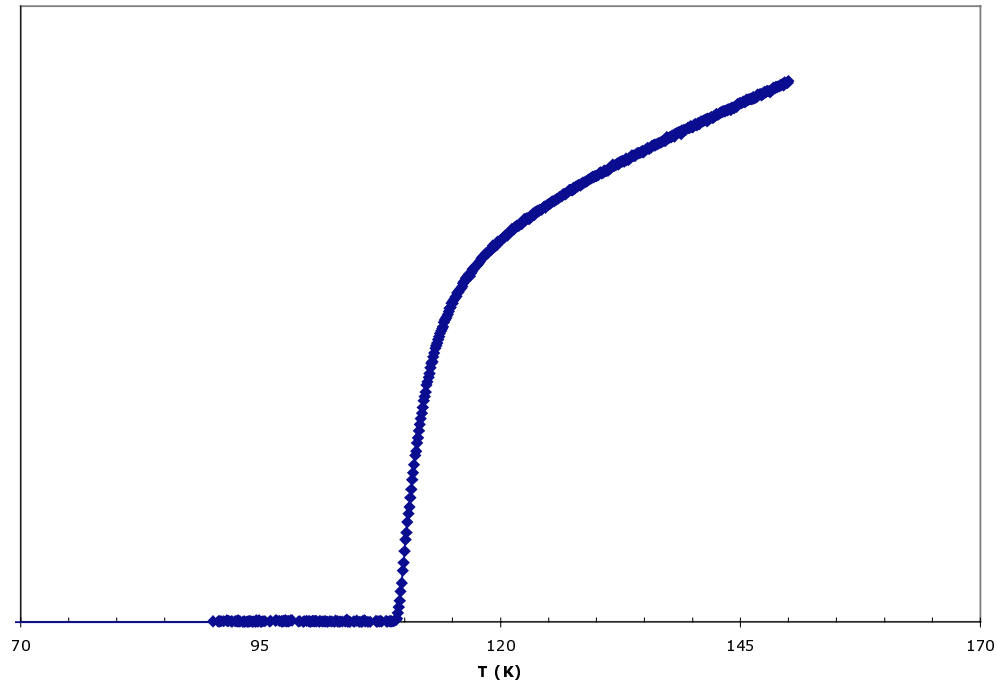


Figure 2-1
Resistivity vs Temperature Curve for BSCCO Tapes

It must also be considered that in granular materials, such as BSCCO-2223, the presence of both inter- and intra-granular circulating currents combine for the transport current, as well as contributing to its limiting factors. The relative effect of the inter- or intra-granular currents will depend on the operating conditions (H , T). While the intra-granular properties are strongly affected by the material structure and composition, inter-granular performance can be largely improved by the manufacturing process and by the grain texturing.

Potentially, BSCCO-2223 material with its high T_c and H_{c2} is a valid candidate to achieve high critical current density. However, the transport capacity of this material is limited by the dependence of J_c on the magnetic field and the temperature. This dependence can be improved by increasing the density of flux pinning centers. On the field/temperature graph shown in Fig. (2-2), the typical irreversibility line (IL) for BSCCO tapes, representing the borderline between the useful superconducting regime ($J_c > 0$) and the useless one ($J_c = 0$), is reported.

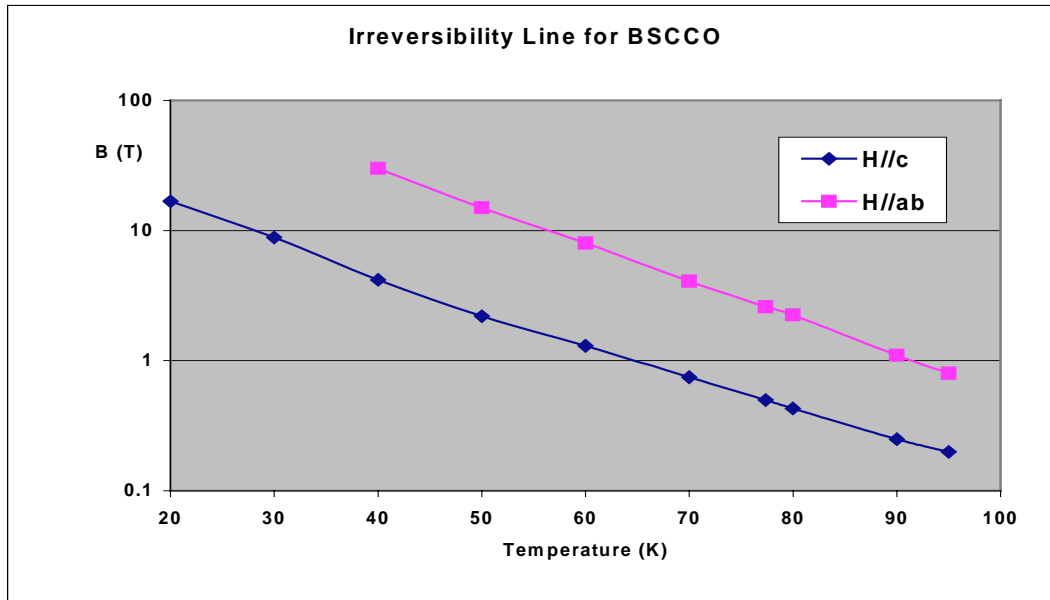


Figure 2-2
Irreversibility Line for BSCCO Tapes, Parallel and Perpendicular to the Copper Oxide Plane

2.2 HTS Material Development

High temperature superconducting (HTS) tapes with proper electrical and thermo-mechanical performances are fundamental to the feasibility of the HTS cable system. In particular, practical HTS cable systems require conductor elements with sufficient mechanical performances that enable manufacturing long lengths of cable with appropriate stranding equipment. Pirelli started early in the identification of the principal performance requirements imposed by cable manufacturing and operation. Then, Pirelli and ASC cooperated in the development of a tape architecture and manufacturing process capable to providing the necessary physical characteristics and mechanical and electrical performances.

Figure (2-3) is a cross-sectional photograph of a tape developed by Pirelli and ASC. Its architecture represents an optimization of the mechanical and electrical properties with a design that can be manufactured consistently and in long continuous lengths. Examining the photograph, the dominant physical features of the tape are obvious. There is a continuous silver sheath which envelopes several superconductor filament bundles. The filament bundles have been flattened by the mechanical rolling processes used in fabrication (as discussed below in Section 2.2.2).

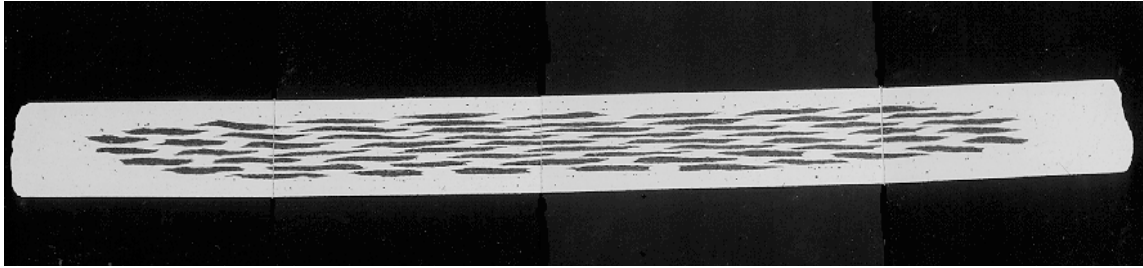


Figure 2-3
Cross-Section Photograph of HTS Multi-Filament Tape

The efforts between Pirelli and ASC have resulted in world-leading current capacities in long lengths of BSCCO-2223 based superconducting tape. These efforts have been well documented in the available literature [2.1].

2.2.1 Processability

Cable manufacturing requires that the superconducting materials be made into long, flexible tapes that can be incorporated into cable structures without loss of performance. Because of their ceramic nature HTS materials are typically brittle. This imposes constraints not only to handling or fabrication operations, but also requires a different approach for processing than is typically adopted in the case of low T_c metallic superconductors.

Whereas other oxides like silica can be melt and drawn under controllable conditions (this is the way optical fibers are fabricated), BSCCO-2223 undergoes phase separation upon melting, making it impossible to draw it into very thin, flexible fibers. The almost “natural” choice is therefore a sintering process, where the polycrystalline behavior of the material is preserved, which in turn almost implies the necessity of a ductile matrix in order to be able to comply with both the fabrication and handling constraints.

On the other hand, the structural anisotropy, and consequently anisotropic I_c of BSCCO make a “ribbon” shape potentially more suitable for optimizing the current transport capacity of the wire itself. In fact, the possibility to texture the material in such a way that the conducting copper-oxygen planes are predominantly parallel to the conductor length is more realistic with tapes with high aspect ratio rather than with a round wire.

2.2.2 Tape Conductor - Fabrication Process

BSCCO-2223 tapes for power applications are fabricated by the so-called Powder in Tube technique [2.2]. This represents a successful approach to achieve the necessary grain texturing. Schematically, this consists in filling a silver tube with a precursor powder having appropriate nominal and phase compositions, which is sealed and then reduced in diameter by repeated cold-drawing steps.

For the optimization of the overall electrical and mechanical performances of the tape, a “multifilamentary” structure is desirable. To fabricate multifilamentary conductors, many mono-wires are packed into one tube or billet, which will be further drawn down to the required diameter. The number of filaments in a typical multifilamentary wire can be from a few tens to over one hundred.

Single core or multifilamentary wires are then turned into thin tapes by repeated rolling steps. Rolling is one of the most critical of all the cold-deformation procedures, since it should promote the alignment of platelet-like powder particles parallel to the tape surface, as well as a further increase of ceramic-green density, and should be as homogeneous as possible to avoid or reduce the risk of “sausaging” (irregular, occasionally reduced thickness).

Annealings at high temperature, generally in a controlled atmosphere with suitable oxygen content, are then to be given the “green” tapes in order for the precursor powder to transform into the desired Bi-2223 phase and form a sintered body.

Silver is one of the very few materials suitable for use as the sheath of HTS conductors, being chemically inert during such thermal treatments at high temperature, ductile to mechanical deformation and permeable to oxygen; moreover, has been experimentally verified the improvement of the superconductor texturing close to the silver surface.

To strongly improve the superconducting properties of Ag/BSCCO-2223 tapes, at least one more cycle including intermediate deformation (rolling) step followed by annealing is usually performed after the first one. It is worth remarking that the long length required for a wire to be used in cable technology imposes constraints in terms of performance uniformity, which in turn requires very close control of the processing parameters (mechanical, “chemical” and thermal) throughout the entire wire fabrication process.

The primary functional properties of such tapes depend upon their composite nature. The presence of a metallic matrix in which the ceramic filaments are embedded, makes their mechanical and thermal behavior the result of an equilibrium between two materials which have different elastic moduli, yield behavior, thermal expansion coefficients. Even in the determination of the critical current specific care should be given to precisely separate the contribution to the total current by the small amount of current flowing in the silver matrix. Furthermore, the presence of the silver matrix may generate eddy current losses which will contribute to the overall AC losses.

2.2.3 Transport Electrical Properties

All the HTS cuprates are Type II superconductors. Without going into the detail of the physical meaning of this, let us remind that the classification as “Type I” applies to those superconductors where the current cannot flow *inside* the material, and is confined to flow only on the *surface* of the material by perfect diamagnetism. Type I materials are not useful for power applications. Type II materials are those for which a so-called “mixed state” can exist, where the diamagnetism is no more “perfect”. In fact, in this “mixed” state the material is partially penetrated by quanta of magnetic flux, called “fluxons”, often represented also as “vortices” of supercurrents, including a “normal” (non

superconducting) core. This is still not enough for the transport of large macroscopic currents through such materials to be possible. In fact, if such fluxons were free to move, any transport current would cause them to drift across the material as a consequence of the associated Lorentz force, creating energy dissipation. However, if another condition is verified, namely, the presence of microscopic defects or impurities with suitable dimension, it will be energetically favorable for the fluxons to localize at such sites. In other terms, these sites, called “pinning centers”, will tend to prevent the motion of the fluxons as if each exerts a certain “binding” force, called “pinning force” on the associated fluxon. Such “pinning force” counteracts the Lorentz force, making the transport of non-negligible, macroscopic, currents possible. In practice, this also means that, given a certain material, with uniform properties, the whole cross-section can actively carry the current, making the total transportable current scale approximately with its cross-sectional area. This is the reason why Type II materials are the only candidates for power applications.

In a polycrystalline material, such as BSCCO-2223, the transport current represents the current that can be transferred between adjacent grains. That current is generally lower (by one or two orders of magnitude) with respect to the material critical current at the same T and H conditions and is strongly affected by the grain boundary quality.

For most applications, the superconducting property sought is the amount of current that can be carried without appreciable electrical resistance. This characteristic, typically referenced at a specific temperature and external magnetic field, is called the critical current, or $I_c(T, H)$. The determination of the critical current of a real sample, however, must confront the non-infinite sensitivity of instrumentation as well as with the non-ideality of the systems themselves. No sample, in fact, appears to undergo a perfectly abrupt transition from zero to finite, constant resistivity, but rather they show, on measuring voltage V for increasing current, I, a gradual onset of a non-linearly increasing V, which takes quite a while to reach its asymptotic (constant) V-I slope.

That effect is observed mostly on superconductor tapes where the superconductor is in presence of a metallic material and during the transition the amount of current carried by the metallic sheath is not negligible. As a result of this, the critical current of a real sample of HTS material or assembly must be defined according to some conventional criterion. A commonly accepted criterion to define the transition out of the superconductive state is the one that defines the critical DC current (I_c) as the transport current that produces an electric field of $1\mu\text{V}/\text{cm}$.

In the Type II materials unlike the DC condition, the dissipation in AC conditions is always non-zero. In fact, an alternating current (let's assume it a periodic one, for example) implies that the associated magnetic “self”-field is also alternating. As a consequence, fluxons will enter, and exit, the material at each cycle and due to the presence of pinning, this motion will experience a kind of “friction”. The result is a non-zero energy dissipation, which is “hysteretic”, in a qualitatively similar way as happens with ferromagnetic materials. The prediction of such dissipation in practical wires and cables for AC transmission, as well as its experimental determination, represent a very important issue in any techno-economic analysis of a superconducting power link. Analytical modeling is generally based on a phenomenological description developed a few decades ago, called the Critical State Model (CSM), with reference to existing Low Tc superconductors, and which has been proved recently to apply very well to HTS materials [2.3].

2.2.4 Mechanical Properties

As discussed earlier in Section 2.2, BSCCO tapes are composite materials consisting of a ceramic material, the superconductor, embedded in a metallic matrix, typically silver or silver alloy. The mechanical properties resulting from this configuration depend on the geometric and compositional properties of the system, as well as the mechanical characteristics of the constituent materials [2.4, 2.5].

The resulting superconducting wire, or tape, has mechanical characteristics that are dominated by its geometric dimensions, superconductor filaments architecture, fill factor (ratio between the superconductor and the total cross section), and mechanical properties (strength and stiffness) of the matrix. The mechanical performance of the individual tapes results in the fundamental limitation of certain cable parameters, such as the winding angle and the former radius. These characteristics have been optimized through the tape architecture and production processes to realize the mechanical and electrical properties necessary for a practical HTS cable.

The elastic strain characteristics of typical ceramic materials exhibit brittle response to tensile loading where the strain response is elastic and proportional to the load only for very small linear elongations. Beyond the elastic strain limit, the materials undergo catastrophic, irreversible fracture. This is different from metals that continue to deform without breaking even after exceeding their elastic limit. The typical elongation response for both typical ceramics and metals is illustrated in Figure 2-4.

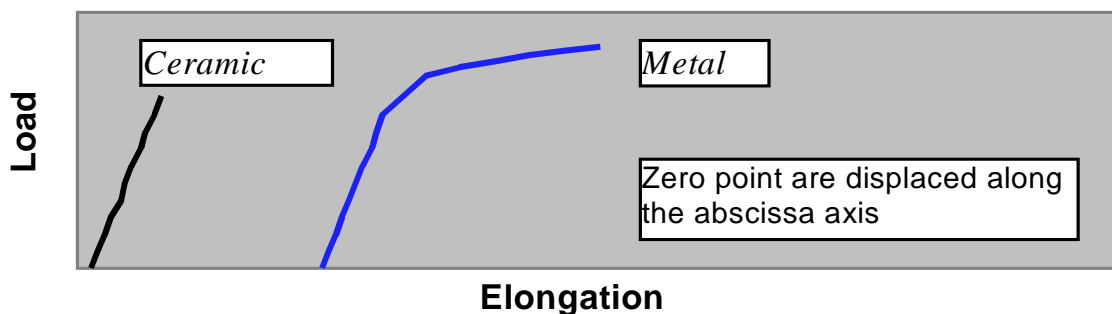


Figure 2-4
Typical Load/Elongation Response for Metals and Ceramics

Both the BSCCO ceramic and the metallic matrix are polycrystalline with a high degree of grain texture imparted during the rolling steps in the manufacturing process, creating anisotropic mechanical properties in the final tapes. The ultimate mechanical behavior of the composite system is a function of the relative fraction of ceramic superconductor to matrix material and improves with increasing matrix to ceramic ratio and matrix strength. Recent efforts to exploit the latter characteristic use high strength matrix alloys and have produced tapes with much superior mechanical properties.

The stresses to which the conductor elements will be exposed during the various stages of manufacturing, handling, cable installation and operation impose severe mechanical requirements on the conductor elements. The analysis of these stresses, and the design of an

HTS tape, which can survive them, has been the focus of the Pirelli Cavi/ASC wire development program. The results from that program have revealed that the HTS wires exhibit strain resistance, which is dependent on both temperature and the nature of the strain, i.e. bending, twisting, or tension. As can be seen in Figure 2-5, the area of the HTS wire experiences different strain profiles for the different strain modes.

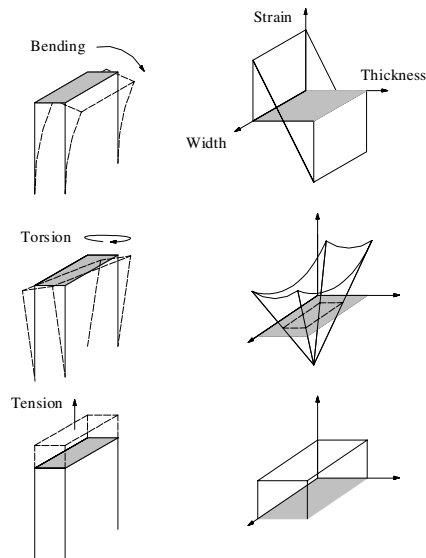


Figure 2-5
Strain Patterns for Thin Tapes under Various Loading Conditions

The recognition of these dependencies highlighted the importance of characterizing the tapes under bending and torsion, as well as tensile conditions, and at room and liquid nitrogen temperature. The mechanical response of the tapes is important in many obvious instances: for example, it is necessary to know the elastic modulus of the composite in order to be able to correctly calculate the stresses that are to be applied to the tapes during all the above conditions.

2.3 Superconducting Tapes for the Prototype Cable

The essential property that must always be guaranteed, however, is the current carrying capacity of the tapes. The I_c retention under stress and strain is therefore the very qualifying feature that must be thoroughly determined and understood. In fact, although different conditions are associated with the different steps of a superconducting cable “life”, some of which involve the application of a given stress, generally the most critical variable for a tape turns out to be strain. Imposed strains are, for example, those associated to the winding of the tapes on the conductor former, and those possibly arising from cooling the cable with fixed ends (due to restricted thermal contraction).

The performance specifications developed use these criteria to evaluate the tape’s suitability for use in a cable. Two physical parameters included in the tape specification, dimensional tolerance

and surface blisters, relate to the quality of the tape manufacture and can be strongly affected by the conductor manufacturing processes.

As defined earlier in Section 1.6.2, the DC critical current (I_c) represents the maximum current the superconductor can carry and exhibit an electric field that is less than an empirical criterion, defined as $1\mu\text{V}/\text{cm}$ for this program. The I_c value is highly dependent on test conditions, such as temperature and magnetic field [2.6]. For example, samples measured while wound around a spool experience a higher magnetic field, and their measured critical current is reduced with respect to the same sample measured flat. Uniformity of critical current between different tapes affects the multi-tape conductor uniformity and can have an impact on the shape of the I-V transition for the conductor. Furthermore, the uniformity of critical current along the length of a single tape is critical to avoid localized energy dissipation effects.

AC losses represent another specification for tapes in this project. Their experimental evaluation on BSCCO-2223 superconducting tapes has been fully achieved in recent years [2.7, 2.8]. The value of AC losses on single tape cannot be directly extended to calculate cable losses, but they can give a first indication of the overall conductor losses assuming that the tapes remain magnetically independent. The obvious necessity of maintaining low AC losses is that these losses must be removed from the cable system through the cooling system; and though the total AC losses are not the sum of the individual tape losses, the total losses will be dependent on the losses of each individual tape.

The mechanical performance specifications use the measurement of the tape critical current degradation as the metric to evaluate the tape's performance. For test specimens, the critical current is characterized in an unloaded condition. Mechanical tests are then performed and the critical current re-measured. The comparison of the critical current values provides an indication of any changes within the material. Tests were specified [2.5] to emulate the strains experienced by the HTS wire during its life, to which samples from the production batch were subjected. These results were used to ensure the high quality required for the prototype cable.

Because of the ceramic nature of the HTS materials, they require more attention in their handling than conventional conductors. Degradation of superconducting properties typically is caused by crack formation in the thin filaments. With these mechanical limitations understood, Pirelli's past experience and know-how was applied to minimize additional stresses on the tapes. However, practical application of tapes implies that mechanical stresses and strains cannot be eliminated. Therefore, the HTS tapes must be able to endure tensile loading, bending, and torsion without experiencing a significant reduction in critical current.

The environmental stability has a broad impact on the use of the conductor in a practical cable system. Environmental stability includes the effect of thermal cycles (both high temperature and low temperature) and the ingress of penetrants (humidity, nitrogen, etc.). The thermal history of a cable during and after manufacturing involves several conditions beyond the obvious cryogenic to ambient temperature cycle. The tapes must also be designed to survive cryostat baking processes as well as soldering temperatures for connection to normal current leads and couplings.

A condition known as “tightness” must be verified for the tape to protect against the ingress of penetrants that can result in deterioration of the superconducting properties. Degradation is generally expected to occur when there is penetration or diffusion of external agents into the superconducting tapes which have a chemical or physical affect on the superconductor. Atmospheric components can directly attack the superconducting compounds, as the presence of alkaline metals (such as calcium and strontium) makes the compound very reactive in the presence of water and carbon dioxide.

Dimensional uniformity has both a direct and indirect impact on the cable manufacturing process. Tape straightness, width, and thickness have a significant effect on the mechanical and electrical properties of the tapes. Broad variations in these physical parameters will also affect the tape performance in other specification tests.

2.3.1 Specifications

To evaluate the suitability of individual tapes, a list of specifications for sampling, test procedures, requirements and acceptance tests for HTS tapes was developed. The specification limits are summarized below in Table 2-1.

Table 2-1
Specifications for HTS Tape for Prototype Cable

Type	Requirements	Average results
I_c	> 28 A	33 A
I_c uniformity	Standard deviation $Sd \leq 20\%$	$Sd = 6\%$
Thermal stability + tightness	I_c retention > 90%	I_c retention > 99%
Dimensions	WIDTH (w)= 4.1 ± 0.1 mm, thickness (th) = 0.267 ± 0.025 mm, straightness = 2mm/200 mm	w= 4.1 ± 0.09 mm, th= 0.267 ± 0.01 mm, straightness 1.4/200
Length	> 95 m	96 m
Strain tolerance at 8° twist test (0.3% strain)	I_c retention > 95 %	I_c retention > 99 %
Stress tolerance at 45 Mpa	I_c retention > 95 %	I_c retention = 100 %
AC loss	$< 1.4 \cdot 10^{-4}$ W/m at 7 A rms at 55 Hz	$9 \cdot 10^{-5}$ W/m at 7 A rms at 55 Hz
Defects = blisters th>0.5 mm	< 0.4/m	< 0.2/m

2.4 Cable Design

The final cable design was achieved following the design method and preliminary results described in [2.5]. Some modifications to the cable construction and design parameters have been introduced in the actual design to alleviate problems encountered during cable construction, as well as to include some practices common in the field of high voltage cable engineering.

The cable design study was based on the following system requirements summarized in Tab. 2-2.

Table 2-2
System Parameters for HTS Prototype

System Voltage	115kV
BIL	550kV
Current Rating	2000Arms
Installation	Retrofit, 8 5/8" Steel Pipes
Section Length	0.6miles

On the basis of these requirements, preliminary design studies were conducted examining alternative solutions. The systems considered were:

- Warm Dielectric, three-phase conductor configuration;
- Cryogenic Dielectric, common cryostat design;
- Cryogenic Dielectric, individual cryostats design.

The Warm Dielectric cable design offers some operational advantages particularly for retrofit applications, which have been recognized as a potential market entry point of the technology. Furthermore the design can use conventional dielectric systems, limiting the technical challenges to the conductor, cryostat and accessory development. Subsequently, this construction was selected as the most appropriate design for the first prototype system. The detailed results leading to this conclusion are presented in [2.1].

In the Warm Dielectric (WD) design (see Figures 2-6a and 2-6b), the HTS conductor, made up of one or more layers of current carrying HTS tapes, is housed in a thermally insulating element (called the cryostat), which in turn is covered by conventional dielectric materials. This design has several advantages, such as:

- has similar aspect and similar installation procedures when compared to a conventional pipe type cable;
- can carry, at the same level of losses, more than twice the power of a conventional cable;
- uses already developed dielectric materials;
- needs accessories, both termination and joint, that can be easily derived from conventional accessories;

- requires fewer HTS tapes than the cold dielectric coaxial design where two concentric HTS conductors, separated by a dielectric at LN temperature, are enclosed in the cryogenic environment;
- it is generally suitable for pipe retrofit application because it reduces the radial space requirement, (compared to a cold dielectric cable) this is one of the most demanding issues in cable design for retrofit;
- the cable can be factory tested for HV performance, as with any conventional cable, before shipping and installing while a cold dielectric cable will be impregnated and tested after installation;
- The ampacity of the WD cable (as well as in the cold dielectric design) is independent of the thermal conditions of the surrounding soil.



Figure 2-6 a
Model of Warm Dielectric Cable Design

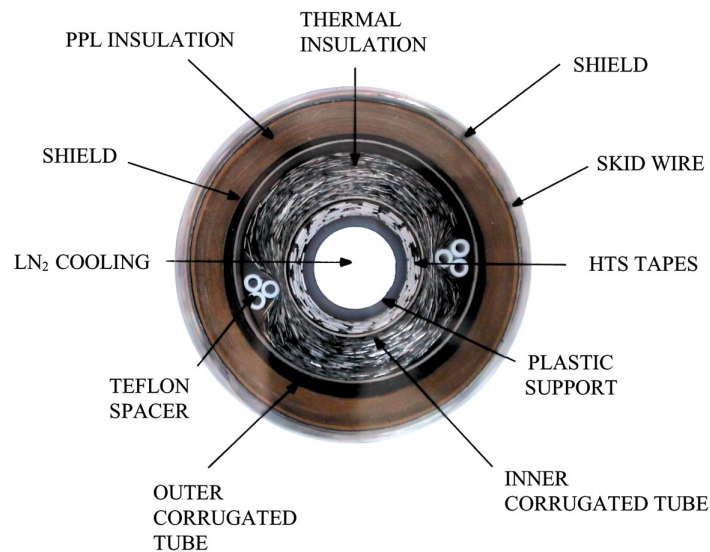


Figure 2-6 b
Schematic of Warm Dielectric Cable Design

The design of a HTS cable, suitable for retrofitting, must begin by assessing the critical parameters of the application. By definition, the cable must be capable of conveying significantly higher levels of current through a fixed cable size. The challenge is to optimize the available design variables, in order to achieve the best cable performance characteristics, while satisfying the necessary physical and dimensional requirements.

2.4.1 Design Process and Parameters

The design process begins by using the available duct diameter to determine the maximum possible cable diameter. The upgrade targeted by this prototype system requires fitting the three-phases into a 8.0 IPS Sch.40 carbon steel pipe with a nominal internal diameter of 8 5/8-inches. Considering standard clearance requirements, an overall outer diameter of 3.47-inches per phase was calculated.

With the maximum outer diameter fixed by the clearances necessary for installation, the cable was designed considering the geometric constraints imposed by the necessary cable components.

The dielectric system design was based on available industry specifications and standard techniques used in High Voltage cable engineering. The thickness, including dielectric system, shields and the external skid wires, was 0.47 in. (11.87mm), which provided a maximum outer diameter for the cryostat of 2.53 in. (64.4mm).

The primary variables in the cryostat design are the maximum permissible thermal losses. Though the actual calculation of losses through a super-insulated system is very complex, the total thermal resistivity can be correlated to the total width of the insulation space. Therefore, it can be said generally that the cryostat efficiency depends directly, but not linearly, on the radial space between the inner and outer cryostat walls.

Although it is imperative to have a very efficient cryostat design, the performance requirements for the cable were considered to be the primary design variables. The final geometry of the cryostat, including inner tube diameter and corrugation depths were determined after the conductor assembly. The final cryostat overall thickness was fixed to be 0.53 in. (13.4mm). The inner diameter of the inner cryostat wall's corrugations was 1.48 in. (37.5mm).

The ampacity required for the cable design dictates the number of HTS tapes that are required. The number of layers required for a given number of tapes depends directly on the diameter of the former. Therefore, the actual conductor layout was completed after the mechanical requirements of the former were met. The thickness of the former is determined by its handling characteristics and the maximum channel diameter required to provide long flow lengths between cooling stations. The final dimensions for the former were determined to be an outer diameter of 1.18 in. (30mm) and an inner diameter of 0.94 in. (24mm). This geometry provides low flow resistance permitting cooling lengths of 0.8 mile and the strength required for manufacturing and handling.

Using the outer diameter of the former and the conductor assembly, the necessary number of HTS layers can be determined. The overall thickness of the superconducting layer is nearly equal to the thickness of the tapes multiplied by the number of layers.

The final cable dimensions are summarized in Table 2-3.

**Table 2-3
Cable Dimensions**

Component	Material	Outer Diameter (in / mm)
LN ₂ Duct	/	0.944 / 24.0
Former	Plastic	1.181 / 30.0
HTS Conductor	BSCCO-2223	1.46 / 37.1
Cold Pipe	Corrugated SS	1.64 / 41.8
Super-Insulation	Vacuum / MLI	2.272 / 57.7
Warm Pipe	Corrugated SS	2.535 / 64.4
Dielectric System	HPFF PPL	3.47 / 88.1

2.4.2 Conductor Design

Once the minimum number of tapes and the former outer diameter were determined, the configuration of the tapes around the former had to be considered. The variables for tape application are the lay angle and the number of layers. The lay angle of the tapes was chosen based on the material selected for the former and the other data already available such as the minimum bending radius, the maximum pulling tension, as well as the mechanical performance of the HTS tape. The final lay angle was selected to ensure that there would be minimal electrical or mechanical degradation due to manufacturing, handling, and testing. The number of layers used was determined by the number of tapes that could be wound for each layer. A minimum gap between tapes was maintained to compensate for slight deviations in straightness and width of the tapes. The final design used 120 tapes, arranged in eight layers.

HTS cables have some characteristics, both constructional and operational, that distinguishes them from conventional systems and require additional care in the design of the conductor element.

The most obvious difference between conventional and WD superconducting cables is the conductor material and the operating temperature. This difference affects not only the electrical function of the cable, but also its mechanical characteristics. Conventional conductors are rugged materials that have inherently good ductility and reasonably high strength. Furthermore, a conventional cable cross-section is dominated by the conductor, providing large areas across which mechanical loads are distributed.

As discussed in Section 2.2.4, the superconducting material is considerably more delicate with finite stress and strain levels above which the conductor performance decreases. Consequently, the conductor assembly must be designed considering the eventual mechanical loads that will be

experienced by the HTS tapes. A particular difficulty is to avoid the imposition of excessive stress on the HTS tapes after cooling the cable in a locked configuration.

The mechanical and thermal constraints to the conductor design were solved by adopting a multi-layer stranded structure around the suitable thermoplastic former. Computational tools were applied to optimize the conductor design considering the primary dimensional, performance, and material constraints. In particular, the level of strain applied to the HTS tapes during the cable assembly, installation, cooling and energizing phases were evaluated. Several parameters were adjusted to minimize strain levels.

In order to ensure that the mechanical performance of the cable allows it to be bent for transportation and handling, the strain applied to each single filament of the HTS tapes was modeled for every manufacturing stage. These strains were compared to the critical strain of the HTS tape. The critical strain is defined as the tensile strain below which the tape will retain 95% of its initial critical current. In order to ensure constant cable capacity, the maximum strain was kept below the critical strain during each stage of the cable's life. This requirement is shown in the expression below.

$$\varepsilon(\text{nominal strain}) < \varepsilon_{cr},$$

where,

ε_{cr} = the critical strain for the HTS tape

2.4.3 Former Design

Two primary functions can be identified for the former: it is a support around which the HTS tapes are wound and it provides a channel through which the liquid nitrogen flows.

The mechanical function of the former is to provide mechanical support to the HTS tapes, to maintain the shape of the conductor layers and to give the conductor assembly mechanical properties required for manufacturing, installation, and operation

Several material and design configurations were considered, such as:

1. Stainless steel in a spiral cylindrical configuration realized with a large and thick tape (8 mm x 2 mm) wound on a cylindrical mandrel;
2. Copper in corrugated pipe shape;
3. Plastic tube with and without reinforcing elements;
4. Combinations of the various configurations.

Once the material was selected, the dimensions for the former were determined. The outer diameter of the core is established by the necessary cryostat inner diameter and the required

thickness of HTS conductor (it was also verified that applying the HTS tapes at the selected lay angle around this diameter would not cause any excessive strain). The major parameters used to determine the inner diameter evolve from the manufacturing processes. As noted earlier, the cable must have an axial stiffness to limit elongation when pulled through the winding process, and the compressive strength sufficient to resist the compressive load applied by the tensioner grips. Obviously, both of these characteristics improve with increasing wall thickness.

However, other parameters must be considered that are optimized by reducing the wall thickness, such as contraction loads and hydraulic resistance. As the cable cools, the force required to restrain the ends increases with the cross-sectional area. This force must be supported by the connections between the former and the terminations and the joint. Also, this force can be transferred as a lateral load against the inner cryostat wall where the cable bends. The corrugated surface of the cryostat wall could cause very high local pressures where the peaks of the corrugations and tapes are in contact.

The cooling duct, which is bordered by the inner diameter of the former, has a strong effect on the flow of LN₂. The most significant factor affecting the hydraulic losses through the cable is the diameter of its flow channel, as seen in the formula below:

$$\Delta P = 32f \frac{L}{D^5} \left(\frac{m^2}{\rho \pi^2} \right)$$

where:

ΔP = pressure loss [Pa]

f = Fanning frictional coefficient [-]

L = Length of the duct [m]

m = Mass flow rate [kg/s]

ρ = fluid density [kg/m³]

D = duct diameter [m]

Besides the duct diameter, “ f ” in the above equation can have a significant effect on the overall hydraulic loss. The variable “ f ” is known as the frictional coefficient for fluid flow. For fully developed turbulent flow along a very smooth surface, the friction coefficient approaches a value of 0.003. However, the same flow along a rough surface can have friction coefficient as high as 0.02.

The final dimensions of the former were determined to be:

- Inner radius 24 mm,
- Outer radius 30 mm,
- Thickness 3 mm.

These dimensions are suitable for both commercial lengths of a three phase system, as well as a prototype installation. Calculations of a three phase system with a single-ended cooling configuration show that the overall pressure drop would be 155 psi (10 bar) for a section length of 0.8 miles.

2.4.4 Conductor Assembly and Manufacturing

Stranded Configuration

The conductor was stranded using an existing fiber optic stranding line that was slightly modified. Figure 2-7 shows the stranding head during conductor manufacturing. The stranding line is described below:

- a standard self centering pay-off with dancer able to handle reels with a drum diameter up to 3 m
- a small tensioner able to apply a controlled force on the conductor. The pressure applied by the tensioner on the conductor was adjustable by means of a hydraulic circuit.
- a stranding head for HTS tapes.
- two standard lapping heads for applying tapes,
- a large pulling device. The pressure applied on the conductor was adjustable by means of a hydraulic circuit.
- a standard take-up with dancer able to handle reels with a drum diameter up to 3 m

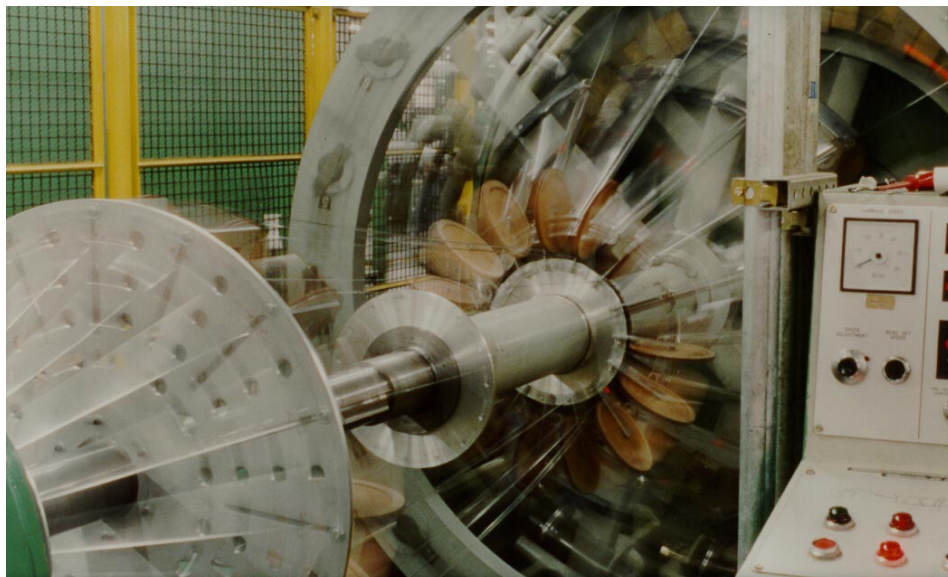


Figure 2-7
Stranding Machine Winding HTS Conductor

Stranding Process Development

To prevent damage to the HTS tapes, a series of stranding trials was employed to establish the necessary manufacturing parameters. The trials were designed to establish the necessary settings and techniques, as well as to identify any unforeseen difficulties with the process.

The main modification to the original optical ribbon-stranding head concerned the locking system for the HTS bobbins and a set of pulleys for guiding the tape onto the conductor.

The tape lay angle was set for each layer. Its control was achieved by adjusting the angular velocity of the stranding head with respect to the longitudinal velocity of the conductor through the line. Typical line speeds during the stranding trials were in the range of 3 to 5 m/min.

The stranding machine was set up, modified and calibrated using dummy tapes. Afterwards a set of trials was carried out to verify the I_c retention of a single HTS tape at different positions along the stranding line: from the stranding head to the take-up reel. The results of these trials resulted in a few alterations in the machine configuration to reduce the strain applied. The results achieved showed a final I_c retention of around $100\% \pm 2\%$, which lies inside the statistical error and fluctuations of the I_c measurement.

Several stranding trials were performed to optimize the overall process, to demonstrate its reproducibility and to guarantee its applicability to long length conductors realized with several layers of HTS tape.

An optimization of the mechanical performance of the conductor in terms of flexibility, interaction between layers and consistent gap sizes between tapes was carried out. Furthermore, the possible onset of long length issues related to incremental errors was investigated.

After sufficient experience had been gained in stranding mock-up conductors, several full size conductor samples, called MCA's (Multi-strand Conductor Assemblies) were manufactured and tested.

Conductor Testing

The results from the first 3 m conductor assembly, MCA-0, are summarized in the following section. Figure 2-8, below, shows the I_c values measured at two locations of the conductor for all of the different combinations of the four layers of the MCA-0. The results show the uniformity achieved with the stranding process

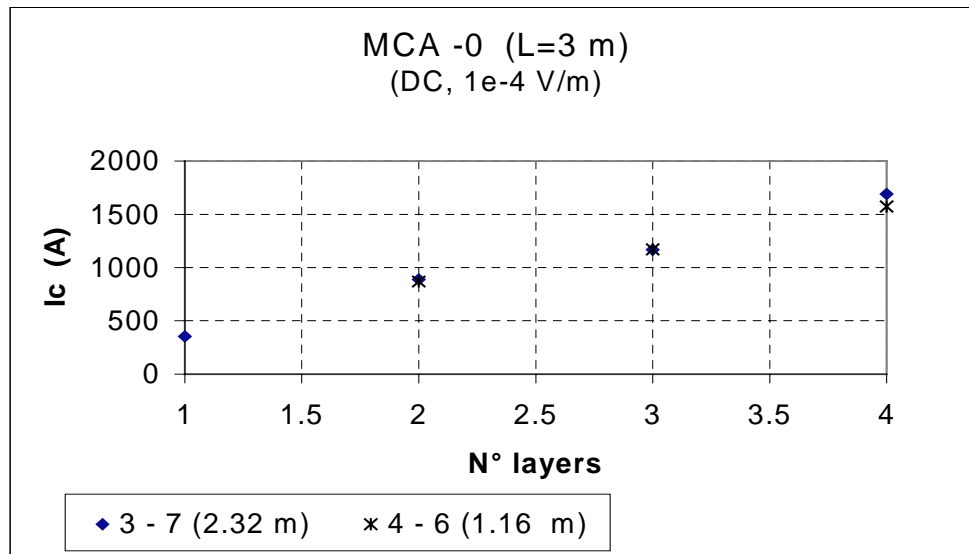


Figure 2-8
Critical Current of the MCA-0 Conductor for each Layer Applied

The final cable was designed taking into account the appropriate corrections to compensate for degradation of critical current due to mechanical stress and self-induced magnetic fields. The measured results agree very closely with the expectations. The slight differences between the two values could be due to the approximations included in the model, as well as degradation beyond that considered in the conductor design.

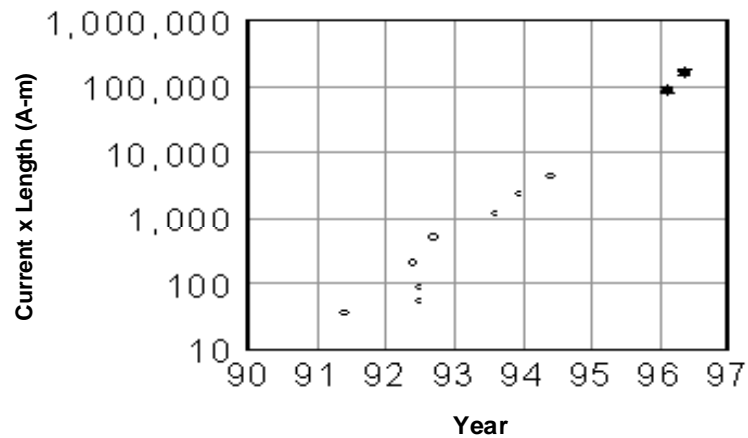


Figure 2-9
Evolution of Conductor Length and Ampacity between 1991 and 1997

The MCA-1 and MCA-2 conductors represented the culmination of long-length conductor development which evolved from laboratory samples to factory manufactured prototypes. This evolution is illustrated above in Figure 2-9.

The conductor configuration for MCA-1 and MCA-2 and the achieved critical current are reported in the following table

Table 2-4
Critical Current Results on MCA-1 and MCA-2

Conductor Configuration	Final MCA Length (m)	Average and Maximum I_c (A) @ standard criteria
MCA-1 (4 layers)	50	1800 – 1850
MCA-2 (8 layers)	50	3300 – 3510

Maintaining property uniformity can be achieved reliably in short samples, as has been shown in the multiple hand-assembled conductors. However, the ability to attain the same level of uniformity in long-length, machine wound conductors had not been proven until these prototypes. Figure 2-10, below, illustrates the critical current at various positions along the conductor. These results validate the reliability and reproducibility of the stranding process developed.

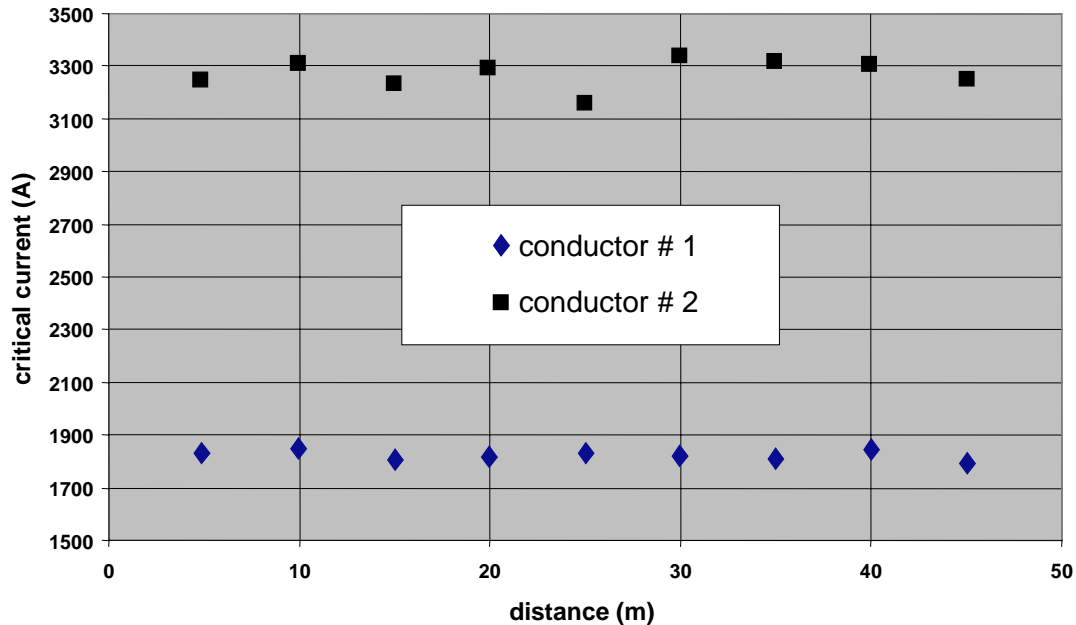


Figure 2-10
Critical Current Measured over the Length of the Prototype Conductor

2.4.5 Cryostat

The thermal insulation for the cable is provided by means of a flexible cryostat.

The cryostat is one of the primary features of an HTS cable. Its efficiency has a dramatic effect on the cable system's maximum cooling length and refrigeration requirements (affecting both initial and life cost). Furthermore, its stability over the life of the cable strongly affects the reliability and performance of the entire cable system.

The typical cryostat construction elements for a warm dielectric cable are:

- internal pipe (cold pipe – which directly surrounds the conductor core);
- thermal insulation;
- spacers;
- pumping elements such as getters and/or zeolites;
- external pipe (warm tube – around which the dielectric insulation is applied).

A vacuum exists between the internal and external pipes, with the spacers serving to maintain the concentricity of the system.

Cryostat Design

The cryostat has several physical, mechanical, thermal and electrical design constraints around which it must be designed.

Despite its importance to the overall cable performance, the cryostat has the greatest degree of physical limitation to its design. Its outer diameter is dictated by the maximum cable diameter and necessary electrical insulation, while the inner diameter is limited by the necessary cooling channel diameter, conductor support thickness, and conductor layers. The final inner and outer diameters were established as 37.1mm and 64.4mm respectively.

The cryostat has the contradictory requirement that it must withstand high pressures, but also remain flexible. The inner tube of the cryostat contains the pressurized liquid nitrogen conductor coolant. The outer tube of the cryostat must resist the pressure of the dielectric fluid and lateral pressures generated during installation. As mentioned earlier, a vacuum exists between the inner and outer pipes, so the acting pressures do not counteract each other.

The minimum cryostat flexibility must be such that it can be wound around a reel and installed in systems with bends and offsets. The minimum bending radius considered for the cryostat design was 1 m.

To meet the mechanical requirements, stainless steel corrugated tubes were selected as the cryostat material. The corrugations permit a more flexible structure of a thickness necessary to resist the mechanical loading conditions. This type of solution is commonly employed in cable sheath manufacturing, as well as commercial flexible liquid nitrogen transfer lines.

Cryostats limit the transfer of heat energy from ambient sources to the cryogenic environment by minimizing the three mechanisms for heat transfer – conduction, convection, and radiation. To combat these effects, typical cryostat designs separate the inner and outer walls with a spacer designed to minimize thermal conduction. Convection is reduced by creating a vacuum space between the cryostat walls. A vacuum below $10^{-3} \div 10^{-4}$ mbar reaches a regime known as *free molecular conduction* where the overall heat transfer becomes dominated by radiation [2.6]. To further limit heat transfer by radiation, *Multi-Layer Insulation* (MLI) was used.

Because the cryostat is placed directly around the conductor, the losses due to electromagnetic interactions had to be considered. Any losses occurring in the inner wall have to be removed through the cryogenic system, and therefore increase the cooling power requirement. Losses through the outer wall will combine with the dielectric losses and raise the ambient temperature surrounding the cryostat. This will affect the temperature of the surrounding soil. Though this increases the temperature gradient over which the cryostat insulates, the effect of this additional heat is minimal.

The requirements for the cryostat material were that it had relatively high strength, could be efficiently and effectively welded, did not embrittle at cryogenic temperatures, had a low electrical conductivity (to limit eddy current losses), and was non-magnetic. The material that best encompassed these traits was AISI 304 stainless steel.

A spacer was used to maintain the separation of the inner and outer walls of the cryostat. The objective was to find a material that has a low thermal conductivity and retains some flexibility at cryogenic temperatures. The design of the spacer must provide a low cross-section for thermal conduction, but also have sufficient strength to resist crushing during cable bending.

Furthermore, the geometry of the spacer must be such that it limits the compression on the MLI insulating layers. In the real configuration, the cryostat bending, the conductor assembly and liquid nitrogen weight, and cold pipe contraction apply a load on the spacer used to keep the two pipes coaxial. The load compresses the MLI thereby reducing its local efficiency. Furthermore, the material had to have low out-gassing characteristics to avoid reducing the cryostat vacuum life.

An optimum configuration for the MLI was sought to provide the low thermal conductivity and permit reasonable vacuum maintenance.

Cryostat Tests

Different cryostat configurations were manufactured and characterized for their thermal insulation properties. To perform these tests, a standard length, 33 ft (10 m), of cryostat was fabricated. A boil-off measurement was used to evaluate each design's thermal performance.

The boil-off method is based on an enthalpy balance. All the heat transferred through the cryostat will cause LN₂ to boil. The rate of evaporation will be directly dependent on the rate of heat transfer into the system. By measuring the mass flow rate of the evaporating LN₂, the thermal losses can be calculated using the equation:

$$\dot{Q}_{Therm.losses} = \dot{m}_{boil-off} \cdot \Delta H$$

Where, ΔH is the change in enthalpy per unit mass of the boiled off nitrogen.

$$\Delta H = h_{fg}$$

where, h_{fg} = the latent heat of vaporization for nitrogen at ambient pressure
= 198.8 J/g

$$\dot{Q}_{Therm.losses} = \dot{m}_{boil-off} \cdot h_{fg}$$

where:

$\dot{Q}_{Therm.losses}$ = Thermal losses rate due to heat inlet through thermal insulation [W or J/s];

$\dot{m}_{boil-off}$ = Mass flow rate of evaporating liquid nitrogen, due to heat inlet through thermal insulation [g/s];

Cryostat Manufacture

Manufacturing the cryostat requires separate steps to apply the different components (i.e. inner tube, MLI/spacer/outer tube). In the first step, the conductor assembly passes through the manufacturing line for corrugated pipe. In this process, a stainless steel ribbon is cleaned, formed and welded axially around the conductor. Then, the tube is corrugated and the new assembly wound on a reel

After the inner cryostat tube has been installed, the multi-layer insulation and spacer are applied. For this process, the conductor and inner tube assembly goes through a three-headed lapping line: two heads apply MLI and the third applies the spacer. Figure 2-11 shows the MLI applicator in motion.

The manufacturing line for corrugated pipe machine is used again to complete the cryostat by applying the outer cryostat tube.

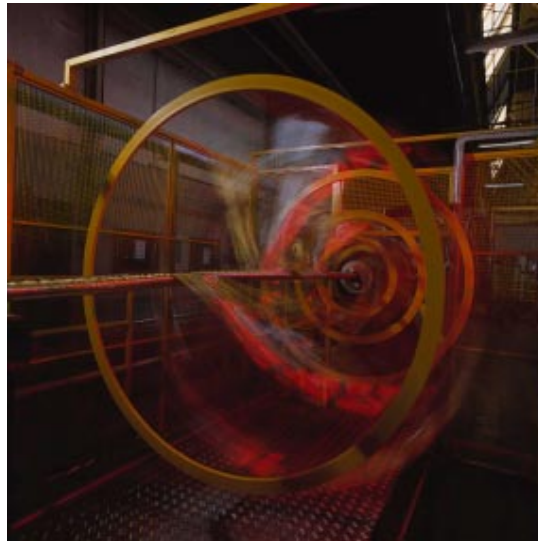


Figure 2-11
MLI Application

The cryostat manufacturing process was developed following from main phases:

- Inner tube manufacturing trials on dummy cable with few HTS tapes;
- Complete cryostat assembly on long dummy cable;
- Complete cryostat assembly, on a 13 m fully populated HTS conductor;
- Final cryostat manufacturing on the 50 m prototype.

2.4.6 Dielectric

Impregnated oil PPLP (Polypropylene Laminated Paper) was used as dielectric material outside the cryostat. It works, as in the copper conventional cables, at room temperature. The same procedure of the conventional copper cables was used, in terms of lapping and oil impregnation. The only technology issue was the application of the shield outside the outer corrugated tube.

A 50 m long mock-up cable, which used a conductor made with aluminum tapes instead of HTS tapes, complete with cryostat and dielectric was assembled in order to test different processes and verify the performance of the single elements. In particular this dummy cable was used for testing the dielectric, as described in the section 3.9.

2.5 Cable System Design

The HTS cable system encompassed all of the components that will be necessary for deployment into the utility structure:

- To emulate a true cable installation, two 138kV conventional outdoor terminations were modified to integrate the liquid nitrogen coolant.
- An additional “Feed Through Bushing” (FTB) was required to transfer the LN₂ from ground potential voltage to high voltage.
- A joint was included to complete the necessary cable accessories.
- An oil pressurization plant controlled the pressure of the dielectric fluid.
- The system used a 2kW rated closed loop cooling flow (cooled by an evaporative bath) as cryocooler. This technique requires more attention than a mechanical refrigerator, but provides greater flexibility with respect to operating conditions.
- The system parameters were monitored and recorded using a Control and Monitoring system. This system was designed to measure temperatures, pressure, and electrical signals from the high voltage system and transmit them to a data acquisition system.

2.5.1 Terminations

Following the design philosophy applied to the Warm Dielectric cable, the terminations were designed to isolate the electrical insulation requirements from the thermal. To accomplish this separation, modifications were made to a conventional high voltage termination. The new termination assembly provided control of the electrical fields, as well as accommodating the transfer of LN₂ into- and out of- the cable and providing a controlled thermal field for the transition from HTS conductor to normal current leads.

The terminology adopted for describing the terminations was ‘termination’ for the conventional aspect and ‘cryogenic termination’ for the new part. The complete termination assembly, shown schematically in Figure 2-12, is made by the addition of a separate vacuum insulated vessel that affixes above the conventional termination.

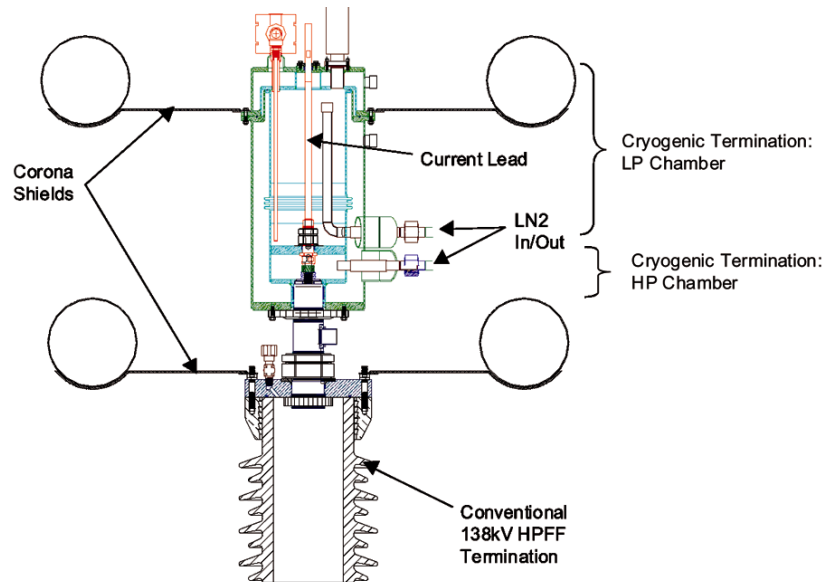


Figure 2-12
Schematic drawing of the HTS Cable Termination Assembly

The conventional termination was based on a standard 138kV insulating pothead.

Cryogenic Termination (CT)

To perform its dual function (accommodating the liquid transfer and managing the thermal transition for the normal current lead), the cryogenic termination is separated into two functionally different parts – the High-Pressure (HP) chamber, and Low Pressure (LP) chamber.

The HP chamber is an integral part of the HP LN₂ cable flow loop. It provides the transition for the LN₂ flow between the inlet and outlet transfer lines and the cable, as well as providing cooling at the HTS/Cu current lead transition zone. The LP chamber is designed to reduce the amount of heat transferred through the current lead into the primary cable loop.

The transition between the HTS conductor and the copper current lead begins in the HP chamber. The connection is made by soldering the HTS tapes to the bottom of the connector piece. This portion of the piece is completely submerged in the high pressure LN₂ and has holes through its sides for the passage of LN₂ to remove any resistive heating in the connector.

The copper connector mechanically fixes the end of the conductor former to the termination, creating a locked-end configuration.

The copper connector passes between the HP and LP chambers. The portion in the LP chamber extends to exit from the top of the CT to connect with the electrical circuit. The LP chamber serves to limit the amount of heat transferred through the connector piece into the cable circuit loop by providing an evaporative LN₂ bath around the current lead.

To cool the current lead, saturated liquid nitrogen in the low-pressure chamber boils to remove the heat inleak down the current lead and joule heating from current flow. The dimensions of the lead were optimized to minimize the amount of cooling required in this region. The minimum heat flux into the system (at design current) occurs when the resistive heat generated in the lead causes the warm end temperature to be equal to the ambient temperature. When this condition is met, there is no ambient temperature contribution to the heat transferred into the system.

Because of the thermal intercept design, the additional heat load due to the current lead should be negligible. Therefore, the energy inleak will be due to thermal transfer from the enclosure. The terminations were anticipated to experience approximately 100W of loss. In the absence of the lead coolant, the heat load due to thermal inleak and resistive loss will be an additional 150 W for each termination.

2.5.2 Joint

The warm dielectric joint is very similar to a conventional joint - it provides continuity for the various cable components. The WD HTS cable has three main components that must be addressed in the joint construction; the conductor, the cryostat, and the dielectric.

The conductor joint provides conductive continuity, as well as permitting the free flow of liquid nitrogen. For this purpose a copper connector was designed. Because a normal conductor is used, the amount of energy generated by joule heating must be considered. To limit the amount of heat generated, a large cross-sectional area of copper was used. However, the connector has size restrictions from the cryostat for the outer diameter and the LN₂ flow for the inner diameter. The transition between copper and HTS tapes required the HTS tapes to be soldered to the joint.

The cryostat joint was made using welding sleeves that were positioned after the conductor joint was completed. MLI was wrapped between the welding sleeves to minimize heat transfer through the joint. After each welding sleeve was applied, a helium leak check was performed to ensure that there were no leaks that would affect the life of the cryostat vacuum.

The dielectric insulation system applied over the cryostat is based on experience with conventional cables. The outer cryostat and welding sleeve area is wrapped with lead tape to smooth any irregularities that might cause localization of electrical stress. The joint is then applied using design tools and techniques developed for conventional cable systems.

2.5.3 Feed-Through-Bushing

In the warm dielectric cable design the dielectric system is separated from the cryogenic environment and therefore the liquid nitrogen coolant must provide cooling at the system operating voltage. One difficulty is that traditional transfer lines are made of continuous metallic pieces and in order to transfer the coolant from the refrigerator to the cable (and back), a specialized bushing was designed called the Feed Through Bushing (FTB). This bushing must provide both an insulating break in the predominantly metallic LN₂ transfer system, protection from external breakdown due to electrical conduction or “flashover”, and thermal insulation of the LN₂ transfer lines.

The Feed-Through-Bushing can be seen connecting the cryogenic terminations in Figure 2-13.



Figure 2-13
Feed-Through-Bushing, Transfer Lines and Termination

The FTB is a component unique to the WD cable application. Its design used a 115kV/550kV BIL bushing to provide protection from external discharge during impulse conditions.

Internally, fiberglass/epoxy laminate tubes were used to convey the liquid nitrogen. Designated tubes provided the feed and return channel for the high pressure nitrogen coolant for the cable and feed low pressure nitrogen to the Low Pressure chamber in the cryogenic terminations. The low pressure feed line operated in a saturated condition (meaning that both nitrogen gas and liquid were present in the line). Because of the nature of the low pressure cooling technique (described earlier in the Termination section), the return line carries only nitrogen gas. A schematic of the body of the FTB is shown in Figure 2-14.

Tests were conducted on individual components and on the completed assembly to ensure that the bushing maintained the desired thermal, mechanical, and electrical characteristics.

After the completion of the cable system test program, experiments were conducted to evaluate the margin of safety offered in the FTB design. The other components in the dielectric system use designs and materials with years of operational experience.

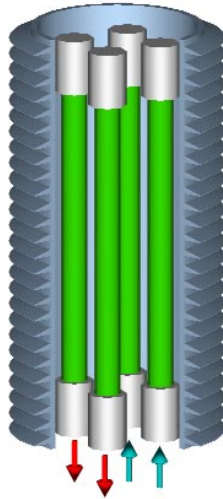


Figure 2-14
Schematic of the Body of the FTB

So, it was necessary to determine whether the FTB introduces a preferred breakdown element.

In summary, the cable system components were dismantled and moved away from the FTB. A U-bend was used to connect the HP LN₂ streams to complete the closed loop flow. To emulate the conditions in the LP lines, saturated nitrogen filled the inlet line while gas nitrogen filled the outlet line. The lightning impulse test was conducted until a breakdown occurred at +850kV – which verified a design margin of 50% over the cable system BIL rating of 550kV.

2.6 Refrigeration Plant

2.6.1 Specification

To maintain the superconductor below its critical temperature, it is necessary to use specialized refrigeration techniques. The refrigeration system must remove any form of energy that enters the system. The primary sources of energy loss are the AC loss of the superconducting material, the thermal inleak through the cryostat and terminations, and hydraulic losses of the fluid flow. The loss mechanisms do not include dielectric losses, which would have to be included for a Cold Dielectric cable design. Each of these loss mechanisms must be considered to specify the necessary capacity of the refrigeration plant. Other considerations also factor into the refrigerator design. These include the desired mass flow rate of the coolant, the hydraulic drop through the cable circuit, and the desired temperature range; determined during the cable design stage. The resulting system specifications are summarized as follows:

- 2kW of refrigeration power,
- variable coolant outlet temperature,
- variable flow rates with an optimum value of 0.7L/s.

The prototype refrigerator as set-up for the mock-up system tests is shown in Figure 2-15.

2.6.2 Description

Fundamentally all cooling systems are identical, in that energy must be transferred from a system of low temperature to a system of higher temperature. Because this contradicts the normal flow of thermal energy, multiple steps must be employed. There are various techniques for accomplishing those steps, and the method used varies depending on the application. For the prototype system, an evaporative bath refrigerator system was employed. This type of system uses the latent heat of vaporization of a saturated liquid refrigerant to provide the heat removal from the cable coolant loop, as opposed to a system which uses expansion of gas to absorb energy as in a common household refrigerator or air conditioner.

The main component of this refrigerator is a copper tube heat exchanger immersed in a bath of saturated refrigerant. The cable coolant flow passes through the heat exchanger and transfers heat into the bath. The pressure within the evaporative bath controls the saturation temperature, and subsequently the temperature at the exit of the heat exchanger.



Figure 2-15
Refrigeration System Set-up for Mock-up Cable Testing

Nitrogen was used as both the coolant and refrigerant for this system. At atmospheric pressure, the saturation temperature of LN_2 is 77K. By lowering the pressure, the temperature of the bath can be reduced to an absolute minimum of 63.2K. However, for practical systems, a minimum bath temperature of 65K can be realized due to the pressure/volume flow rate dependencies of the vacuum compressors. By increasing the pressure of the LN_2 in the loop, the saturation temperature can be higher than 100K. The bath pressure was controlled with a vacuum compressor that drew out the evaporated refrigerant and maintained the desired pressure. A pressurizing tank was connected to the loop to serve as a buffer volume and maintain the cable coolant pressure.

The refrigeration system was designed to operate with limited human involvement regardless of loading. The evaporative bath system is conceptually simple and requires little adjustment other than to maintain nitrogen refrigerant in the sub-cooler. A control system was included to monitor and adjust the parameters relevant to filling the sub-cooler bath.

2.6.3 Engineering and Test

The refrigeration system underwent several testing cycles. When it was originally received from the manufacturer, tests were conducted to establish its heat dissipation capabilities and the affect that variable loading had on the outlet temperature from the heat exchanger. A specially designed isolation loop was used that could introduce up to 2kW of heat directly to the flow. Figure 2-16 below shows the results of these tests. Also illustrated is the nominal temperature rise through the loaded circuit at varying power levels. These tests were repeated each time that the system was moved and set-up to verify that the system was not damaged.

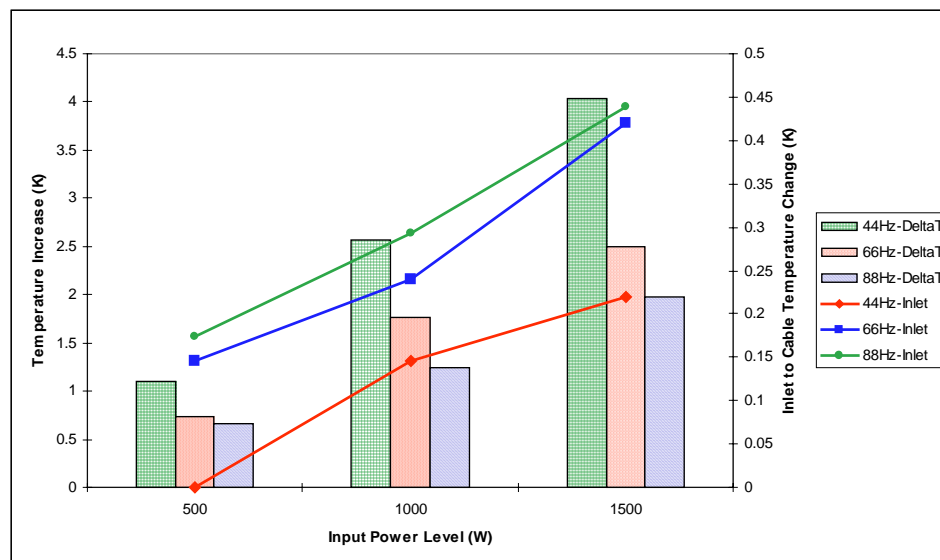


Figure 2-16
Refrigerator System Proof Tests at Various Power Levels and Flow Rates

The system allowed achieving, in full load conditions, average cable temperature in the range from 73 K up to 81 K. This temperature range was sufficient, as described later in section 3.2, to carry out the superconducting testing programs.

The refrigeration system operated reliably for a total duration of 27 weeks. The problems experienced were minimal, and related either to the quality of the air supply to the control valves or vacuum degradation of components.

2.6.4 Monitoring System

The properties of the LN₂ have a significant effect on the cable system's performance. Therefore, it is important to monitor the conditions within the system continually looking at the LN₂ pressure and temperature. Analyzing these variables can provide real-time information about the performance of the system.

The monitoring system has three primary functions:

- Experimental - to measure performance parameters for analysis,
- Diagnostic - to indicate a failure or abnormal operational condition,
- Control - to provide data for feedback control of the refrigeration system.

One of the greatest challenges to the monitoring system was that several of the most crucial parameters had to be measured at locations of high voltage. Obviously, measuring data at high voltages means that there cannot be signal, communication, or power supply wires passing between the sensing site and the ground. To solve this problem, a system was used where all of the signal conditioning occurred in the high voltage environment and the data was converted to digital signals and transmitted to ground via infrared (IR) communications (see Fig. 2-17). A data acquisition system on the ground received, stored, and displayed the data.



Figure 2-17
Monitoring System at High Voltage Potential.

The data acquisition and display system was designed to receive signals from the monitoring system and provide a real-time data display and alarm log. The data was also continually downloaded to a database program for storage on the hard drive. Figure 2-18, below, shows the data display window used for the testing program.

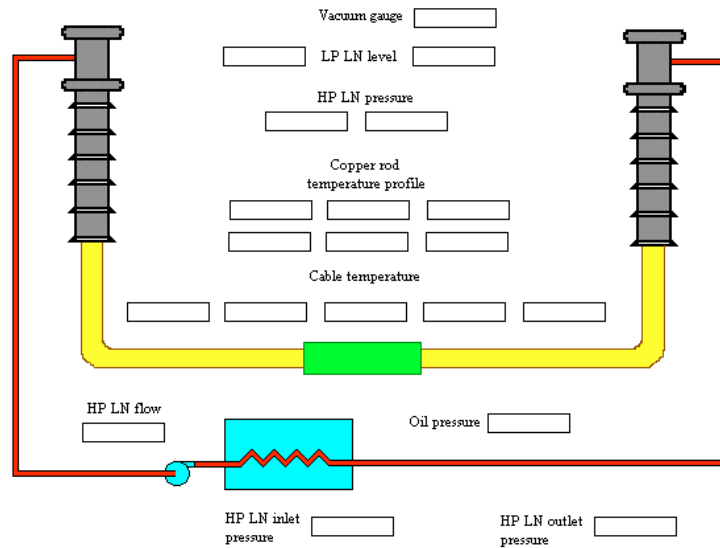


Figure 2-18
Data Display from Data Acquisition System

The parameters measured using the remote system included the temperature in the cable duct, the vacuum of the cable cryostat, the pressure of the flow in the cable, and the liquid level in the low pressure chamber. All of the instruments for these measurements were connected to the cable at the terminations using pass-thrus or cold-traps, depending on the measurement.

2.7 Oil Pumping Plant

Many high voltage dielectric systems must be maintained at a high pressure to minimize any voids in the insulation system. For the prototype system, a high-pressure fluid-filled (HPFF) system was selected, because it represents a large portion of the existing cable infrastructure in the US.

The necessary operating pressures are well defined by industry specifications. For a 115kV PPL insulated cable system, standard HPFF practice requires a pressure not below 190psig. To maintain this pressure on the cable system, an oil pumping plant was used. The pumping plant was fabricated by Pirelli Jerome, Inc. The plant used a 250-gallon reservoir tank and a 5hp pump to maintain pressure in the cable circuit. The plant was equipped with pressure gauges and automatic starters, to permit unattended operation.

3

EXPERIMENTAL RESULTS

The testing program implemented during this program was designed both to verify the success of the cable system design and manufacturing processes and to further the understanding of the mechanisms involved with high temperature superconductivity and their impact on cable technology. Three separate testing programs were implemented to achieve these goals:

- testing superconducting properties of tapes,
- testing performance of superconducting cable assemblies,
- HV testing and cable qualification testing.

The testing of superconducting tapes for this program was performed both to enhance the general understanding of superconducting phenomena and to provide necessary engineering data about the tapes' critical currents and critical strain behavior. These tests were invaluable to the success of this program, their methods and results are thoroughly covered in previously published literature [3.1, 2.5, 2.6, 2.7, 2.8]

3.1 Superconductor Testing Program

The performance of a HTS conductor for power transmission lines is determined by the amount of current that it can sustain and the power losses occurring in the alternating current transfer. The factors that directly affect these properties include the basic properties of the individual tapes, any tape degradation factors, and the geometry of the conductor assembly. One of the main goals of the experimental activity for this program was to measure I_c and AC losses in multi-layered HTS conductor assemblies. In order to isolate the impact of manufacturing and handling, incremental testing was conducted at each stage.

The direct current critical current (typically denoted as I_c) is the most widely quoted measure of superconducting performance. Because of the broad transition out of the superconducting state exhibited by the Type II superconductors, and in particular by the HTS materials, a common standard has been adopted to determine the critical current for a superconductor. For multi-tape conductor configurations, the accepted measure of I_c is defined as the cable current at which the conductor experiences a voltage loss of $1 \mu\text{V}/\text{cm}$ (or $0.1\text{mV}/\text{m}$) at 77K without the imposition of external magnetic fields. Though superconductors will carry a direct current (less than the critical current) without any significant penalty of energy loss, a conductor operating in alternating current will cause energy dissipation at any current level, as will be shown and discussed later on. Because power cables typically operate using alternating current, the AC dissipation of the conductor represents a significant factor in the design and operation of HTS devices for power applications.

The experimental program was set to address the following issues:

- verify the reliability and repeatability of the Pirelli developed experimental techniques to determine I_c and AC loss in HTS cable and cable conductors
- monitor how I_c and AC loss are affected during the various steps of a cable construction by mechanical stress, thermal cycling, electromagnetic interactions, etc
- set a basis of experimental observations from which move towards the modeling of AC losses in cable conductors.

3.1.1 Conductor Samples

In the experimental program conductor samples with different features were investigated. The tested samples can be divided into two classes – Prototype Multi-strand Conductors (PMCs) and Machine-stranded Conductor Assemblies (MCAs).

Table 3-1
Summary of Conductor and Cable Samples and Tests Performed

Task	Sample	Length(m)	Number of HTS layers	Ic (A) 77 K	Tests
1	MCA 2	1	8	3300 measured	PIRELLI Ic, electrical AC loss
2	MCA 2	3	8	3300 measured	PIRELLI Ic, electrical AC loss
3	MCA2	13	8	3300 measured	PIRELLI Ic, electrical AC loss at 40, 60, 90 Hz
4	MCA 2 with cryostat	13	8	3300 measured	PIRELLI Ic, electrical AC loss
5	MCA 2	1	8	3300 expected	LANL calorimetric AC loss x1-Ø - 76, 70 K
6	MCA 2	1	reduced from 8 to 4 layers	1800 expected	LANL calorimetric AC loss 1-Ø - 76, 70 K
7	MCA 2	1	reduced from 4 to 3 layers	1350 expected	LANL calorimetric AC loss 1-Ø - 76, 70 K
8	MCA 1	1.5	4	1800 measured	PIRELLI Ic, electrical AC loss 40, 52, 60 Hz ENEL Boil off calorimetric AC loss 50 Hz
9	PMC 1	1	2	1290 measured	PIRELLI Ic, electric AC loss LANL Calorimetric AC loss 1-Ø - 76 K 3-Ø - 76, 64 K 2-Ø - 76 K
10	PMC 2	1	2 layers electrically insulated	1250 measured	LANL calorimetric AC loss 1-Ø - 75, 69, 64 K 3-Ø - 75, 69, 64 K 3-Ø - 76, 70 K with 20 cm spacing
11	MCA2 Conductor only, straight configuration	50	8	3320 measured	PIRELLI Ic
12	MCA2 With cryostat and electrical insulation Straight configuration	50	8	3100 measured	PIRELLI Ic 73, 76, 81 K Electrical AC loss 50 Hz, 73, 76, 81 K
13	MCA 2 Set up for HV tests termination comprised U configuration	50	8	2860 measured	PIRELLI Ic

The PMCs are short, hand-made conductors carefully assembled to create the best possible object for the measurement. These samples have been manufactured by American Superconductor Corporation.

The MCA conductors, prepared by Pirelli, were intended to provide samples representative of cables which would be manufactured in a factory environment using industrial processes. The construction of the conductors was performed using a winding machine and the HTS tapes come from an industrial wire manufacturing campaign. As can be seen in Table 3-1 below, several MCA conductor samples were evaluated. The use of a winding machine created two long-length conductors from which all of the MCA samples were cut.

The PMC and MCA samples share two main features: the lay angle of tapes and the conductor former diameter (approximately 30-mm for the MCAs and 28.6 mm for the PMCs). Both PMCs were built into a two-layer configuration, while the MCA-1 and MCA-2 were 4- and 8-layer conductors respectively. All the samples were manufactured with the same generation tapes, so that the critical current per tape was almost the same.

When not specified, I_c and ac loss measurements are performed at 77 K and in single-phase configuration. “3-Ø” refers to measurements in which 3 conductors, one superconductor and two copper, are positioned on the vertices of an equilateral triangle and contemporarily energized. When not specified the distances among the centers of the three conductors is 10 cm. In “2-Ø” measurements the conductors are disposed in the same configuration than for “3-Ø”, but the superconducting phase is disconnected so that only the copper phases are energized. In both configuration the ac loss has been measured at 60 Hz.

3.2 AC loss tests on cable conductors

The evaluation of AC losses in HTS cables is necessary to adequately design commercial systems. Several factors have to be assessed, including the effect of cable length and the effect of the other conductors in the circuit. No single technique has been developed so far which permits all necessary evaluation to be conducted at the same time. Subsequently, the results obtained with different measurement techniques have been compared for this project. These techniques include an electrical method developed by Pirelli, a temperature measurement technique developed by Los Alamos National Lab (in conjunction with EPRI and the DOE Office of Energy Technology), and a boil-off calorimeter developed by ENEL, the national Italian electrical utility, in the framework of the SMT 4-CT95-2008 contract of the European Community.

Pirelli using a four contact method has performed electrical single-phase AC loss measurements. For this technique, the power lost during current transport is measured by the voltage drop along the conductor. Using a lock-in amplifier, the magnitude of the losses in phase with the applied current can be distinguished from the total voltage drop to provide the real losses in the cable. A detailed description of this technique is documented in the available literature [3.1], [3.2], and [3.3].

Among the features of this technique is that it can easily be adapted to conductors of different lengths. Measurements at different temperatures were possible for the 50m cable installation with the sub-cooled refrigeration system.

Los Alamos National Laboratory Superconductivity Research Department developed a device, which evaluates the power losses in a conductor using temperature difference calorimetry. This procedure creates a thermal system, which approaches a unidirectional thermal conduction system with insulated ends. Solving the differential heat equation yields a parabolic equation for the temperature profile along the conductor. By performing some normalization to reduce non-idealities of the experimental system, the total amount of heat generated in the conductor can be calculated.

This system offered the capability of measuring the sample with closely controlled end temperatures ranging between 64K and 77K. Also, this system provides the means to measure samples exposed to currents typical of a three-phase configuration and variable spacing between conductors. Tests were performed to evaluate the three-phase losses on the HTS conductor both with and without current flowing in the sample.

A second calorimetric method was used to measure the AC losses in the conductor assembly. This technique, developed by the R&D division of the Italian electrical utility ENEL, measures the AC loss using a boil-off calorimeter.

Using this technique, tests were conducted at 77K and 50Hz with the sample in a single-phase configuration, but the method is in principle suitable for 3-phase measurements at any temperature. Further details will be offered in the following test result section and in (ref [3.2] and [3.3])

A detailed description and comparison of these techniques can be found in [3.3].

In summary, the results achieved using the above testing programs are as follows:

1. The cabling processes (application of cryostat, dielectric, etc.), if properly performed, do not greatly affect conductor performance (task 4, 13,14)
2. Superconducting properties are not significantly affected by the strains imposed during manufacturing, handling, transport and installation (task 3, 11, 12, 13)
3. The critical current of the conductors varies with changing temperature following approximately the same empirical law followed by tapes (task 12)
4. The AC losses measured in cable conductors samples are independent of the length of the sample (tasks 1, 2, 3, 13)
5. Hysteretic losses provide the main contribution to AC losses in BSCCO tapes conductors in single phase configuration (task 3, 8)
6. The dependence of AC losses on temperature is mainly due to the variation of the critical current (task 5, 6, 7, 11, 12)

7. The AC loss for 2-layer conductors in trefoil configuration with 10 cm distance among the phases are from about 2 to 3 times higher than the same losses in single-phase(task 9, 10)
8. The AC losses for conductors in trefoil configuration are approximately inversely proportional to the square of the distance between the conductors (task 10)
9. The eddy losses produced in the stainless steel cryostat tubes are negligible provided the two corrugated tubes are electrically disconnected. Significant losses may arise in the cryostat if there is current circulating between the two corrugated cryostat tubes or between the conductor and the corrugated tubes.
10. The cross check of three different and independent measurement methods indicates that all of them are suitable to perform reliable AC loss measurement in the suitable current range (tasks 1- 5, 6 - 8, 9)
11. The presence of an insulating interlayer between superconducting layers doesn't affect the AC losses of the 2-layer conductor (task 9,10)

3.2.1 Electrical Measurement Technique (Pirelli)

The electrical method that has been used for measuring the AC losses in HTS tapes and in multistrand conductors is in principle exactly the same. In a four-probe configuration, an AC current of known amplitude, frequency and phase is passed into the sample. The voltage drop along the sample is measured by means of a Lock-In amplifier that provides suitable sensitivity for low AC voltages and the capability to directly produce a vectorial analysis of the measured signal. Losses are then directly calculated multiplying the rms. values of the current and of the voltage component that is in phase with the current.

Several modifications have been introduced into the experimental set up conceived for tapes in order to adapt the method to the new requirements related to the use of higher currents, and to the different geometric arrangement of samples.

Please note the main circuit modifications adopted for lock-in technique measurements on tapes:

- three power amplifiers have been used in order to provide high quality currents up to 2000 A (in the range of frequencies around 50 Hz) into a current circuit that exhibits an inductance far exceeding the resistance;
- a resonant circuit has been used to minimize the power employed in counteracting the reactive part of the load;
- a Rogowsky like variable mutual inductance has been introduced in order to generate a finely tunable, purely inductive, compensation signal;
- a symmetric disposition of the return current conductors has been adopted to minimize the magnetic field generated by the return currents and the induced field in the surrounding environment.

But the most critical aspect to be addressed to define a correct procedure to measure AC losses on a cable sample was undoubtedly the positioning and features of the voltage taps.

In principle, the measurement of an ideal conductor sample, that is a sample whose tapes have all exactly the same electrical properties, that are wound on the former with a perfectly symmetrical disposition and that have all a uniformly negligible contact resistance with the copper terminations, is straightforward. It should be simply required to solder a couple of voltage taps put in whatever point of the conductor surface at a certain distance between them, and then to join the wires so to minimize the flux linked to the pick-up loop. This is because each tape is a perfectly equivalent path for the current and then each cross section of the conductor is an equipotential surface.

In an actual cable each possible irregularity, either of geometric or material nature, produces a slight variation of the amplitude and of the phase of the current and, consequently, of the voltage drop along each tape. Whatever is the nature of these non-uniformities, they can have a considerable effect on the measurement's precision because the cross section of the conductor is no longer an equipotential, and the measured voltage becomes dependent on the azimuthal position of the voltage taps.

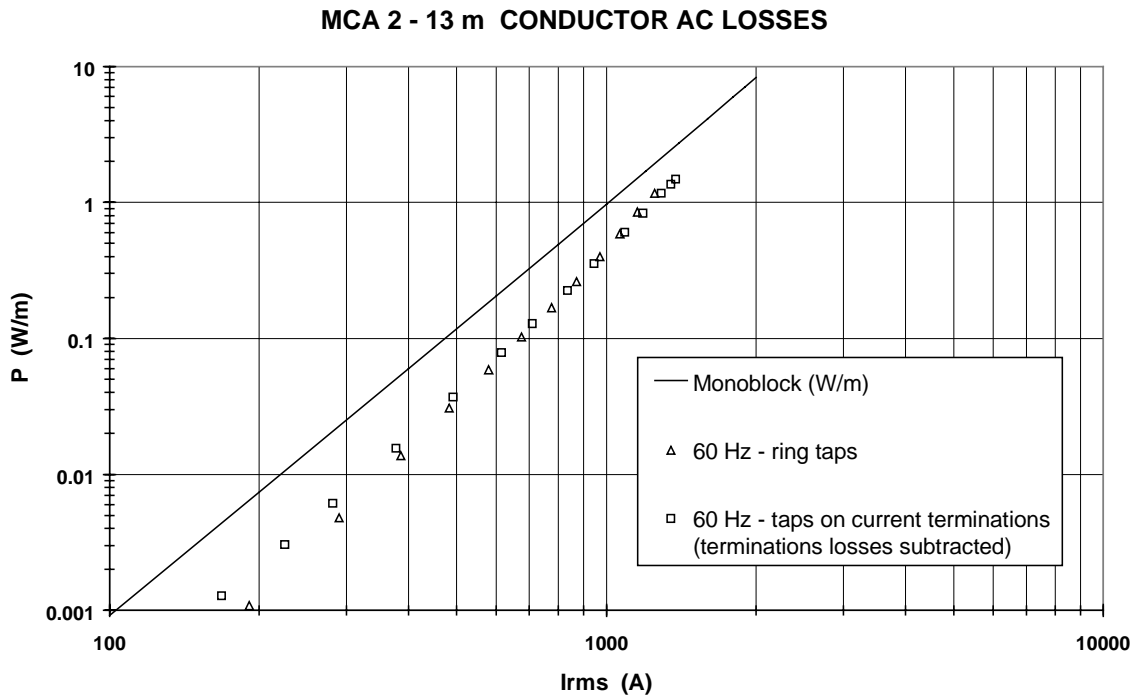
In practice, applying the technique described above to measure AC loss in actual cable conductors is not straightforward, and a suitable configuration for the voltage taps had to be designed in order to achieve reliable and reproducible AC loss measurements.

Two different kinds of voltage taps were selected.

A comparison between the results obtained with these two methods for the case of the 13 m conductor is shown in Figure 3-1 (see also [3.1]).

In all the graphs reporting the results of AC loss measurements, the losses predicted by the so called "monoblock" model will also be reported for comparing measured losses with those predicted by this simplified model. The "monoblock" model results represent the losses that would occur in a bulk hollow cylindrical superconductor with the same geometric characteristics and critical current of the sample (see also [3.4]).

The two methods give equivalent results for currents higher than roughly 500 A, i.e. in the range of practical interest for this specific application, while they differ for lower currents. The magnitude of the difference is representative of the scattering found when comparing measurements with different voltage taps in the current range well below 1000 A.



Electrical measurement at different frequencies

In the cable conductor arrangement the superconducting tapes suffer both the self-field due to the transport current and the external magnetic field caused by the current in adjacent tapes.

The different loss mechanisms that may take place in the conductors are

- hysteretic losses, intrinsic to II type superconductors in time-varying magnetic field;
- coupling-current losses, arising in multifilamentary superconductors in time-varying magnetic field;
- eddy current losses, i.e. dissipative phenomena in the metallic matrix.

As for tapes, a way for checking what is the prevalent mechanism is to measure AC losses Vs current for different frequencies. Peculiar of the hysteretic mechanism is that losses per cycle do not depend on the frequency of the current.

In Figures 3-2 and 3-3, the AC loss per cycle Vs Irms measured in the MCA2 13m sample at different frequencies is reported. The main component of the losses per cycle on a conductor in single-phase configuration is independent of frequency, at least in the spanned range, indicating that hysteresis losses remain the most important loss source in a cable conductor not subject to severe external magnetic fields.

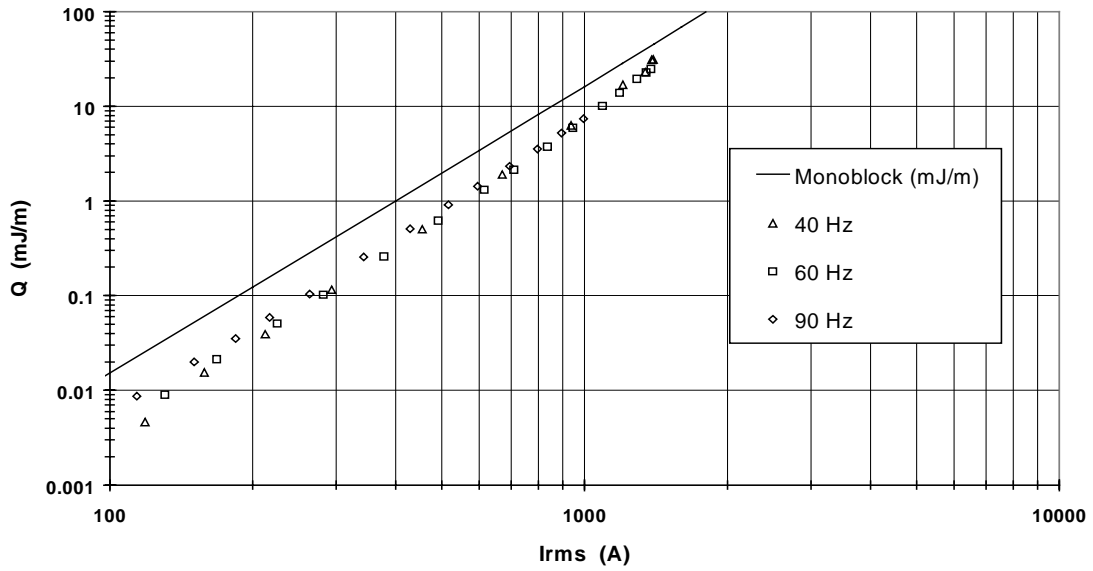


Figure 3-2
AC loss measurement at different frequencies: voltage taps on the current terminations.

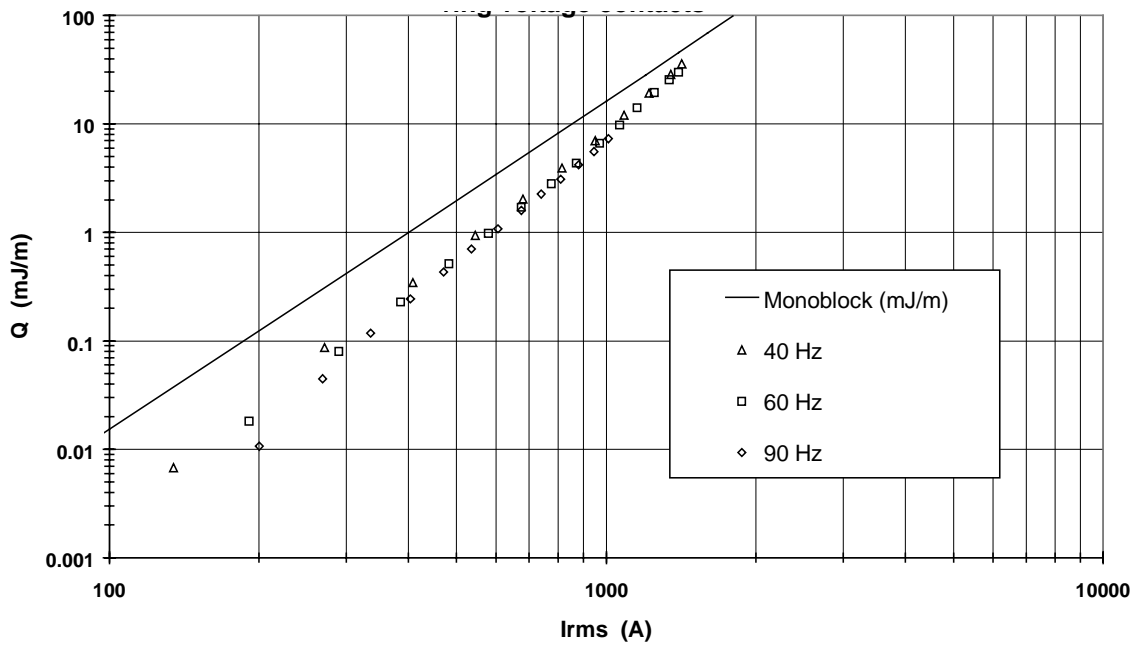


Figure 3-3
AC Loss Measurement at Different Frequencies: Low Resistance Ring Voltage Contacts.

Electrical measurement on samples of different length – MCA-2

One doubt that may arise when approaching the measurement of AC losses in cable conductors is if a 1 m or 3 m long sample is representative enough of a real 100 m or 1 Km cable section.

The doubt is connected to the problem of driving the current in a short sample so to get the same current distribution it would occur in a real cable section. In fact in a short sample, the contact resistance at the copper terminations may play a role in the current distribution among the layers and the tapes while in the long sample the current distribution is in principle dominated by the inductance of each current path.

To assess this point under an experimental point of view we measured the losses of three samples of different length but all coming from the same section of conductor MCA-2 (Figure 3-4).

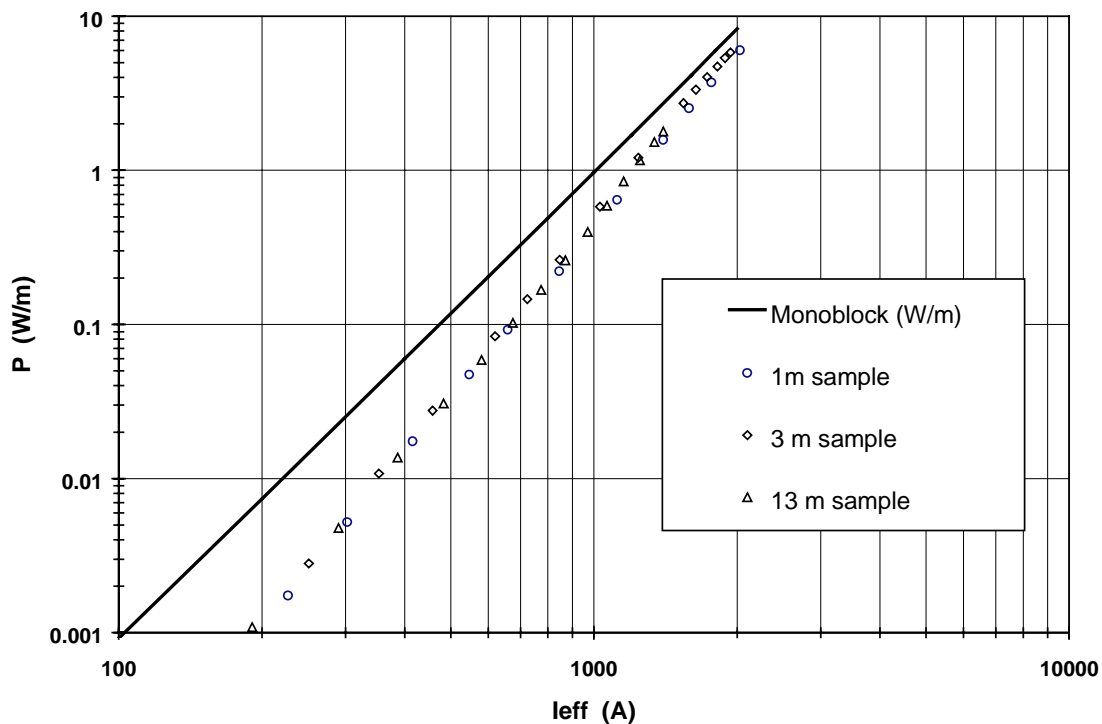


Figure 3-4
AC Loss Measurements on Samples of Different Length.

Although much more care has to be taken when dealing with very short samples (about 1m) the conclusion of the experimental work is that for this samples the AC loss is independent of the length. Further support of this conclusion is found in the following section.

3.2.2 Temperature Difference Calorimetric Technique (LANL)

To evaluate the power losses in short-length (about 1m) cable conductors Los Alamos National Laboratory Superconductivity Research Department developed a calorimetric system that has been extensively applied to measure PMC's and MCA's samples.

In this set-up the sample is thermally insulated and cooled only at the ends. The conductor then develops a parabolic temperature profile when carrying an ac current as long as the ac loss rate remains uniform along the conductor. This requirement is fulfilled as long as the temperature deviation is not large enough to affect appreciably the loss rate. In practice, the maximum temperature gradient between the center of the conductor and the terminations must be of the order of two degrees.

The parabolic temperature distribution arising in such a configuration with "internal" heat generation is easily calculated through the solution of the steady-state heat conduction differential equation (see [3.5]):

$$\frac{d^2T}{dx^2} = -\frac{q_L}{kA}$$

where x is the position along the conductor, k is the effective thermal conductivity of the conductor, A is the conductor cross-sectional area, q_L is the power dissipated in the conductor, and T is the temperature along the conductor.

The solution of the steady-state equation for an uniform rate of losses along the conductor allows correlating the dissipated power to the difference between the temperature at the center of the conductor and the average of the two end temperatures ΔT_m through the formula

$$q_L = \frac{8kA\Delta T_m}{L^2}$$

In situ calibration with a heater wound at the axial midpoint of the conductor gives the effective kA , and ΔT_m is determined from a curve fit to the temperatures registered by 14 platinum resistance thermometers positioned axially and azimuthally on the conductor. The maximum temperature sensitivity was about 5 mK.

Due to the fact that the losses produce an increase of the temperature along the conductor, the average temperature along the cable was slightly different for each loss rate. To have all the values of the loss Vs current characterization referred to the same temperature, the points were corrected scaling the losses using the I_c Vs temperature experimental results. (see [3.5])

For a deeper insight into the details of the temperature difference calorimetric technique it is possible to refer to [3.3], [3.5] and [3.6].

This technique was shown to have very good resolution, but has a fundamental restriction because it can be applied when the temperature profile in the conductor is parabolic, i.e. when the rate of losses along the conductor is sufficiently uniform to apply the calorimeter theory without relevant errors. Besides the rate of the produced losses can't exceed a maximum value above which steady state conditions are not reached any more. These two factors limit the maximum measured power to about 1 W. This system offered the capability of measuring the sample with closely controlled end temperatures that could range between 64K and 77K.

Also, this system provides the means by which to measure samples exposed to currents typical of a three-phase configuration and at different spacings between conductors. Tests were performed to evaluate the three-phase losses on the HTS conductor both with and without current flowing in the sample.

Comparison of Pirelli and LANL methods

Crosschecking the measurements carried out in the different laboratories is a good method to assess the accuracy of the different techniques.

For this purpose, a 1 m 8-layer MCA-2 sample was prepared and delivered to the LANL laboratories to measure its AC losses. These results will be compared with results from the Electrical Measurement technique described earlier in this section.

Figure 3-5 illustrates the comparison between the 13m sample measured in Pirelli and the 1 m sample measured in LANL. The calorimetric measurement confirms that for short samples the affect of variance between the contact resistances for the single tapes can be reduced through careful sample preparation, so that there is a minimal impact on the AC losses in the sample.

The PMC-1 conductor was also evaluated using the thermometric and electric measurement techniques. Again, good agreement between the two methods was shown, as can be seen in Figure 3-6.

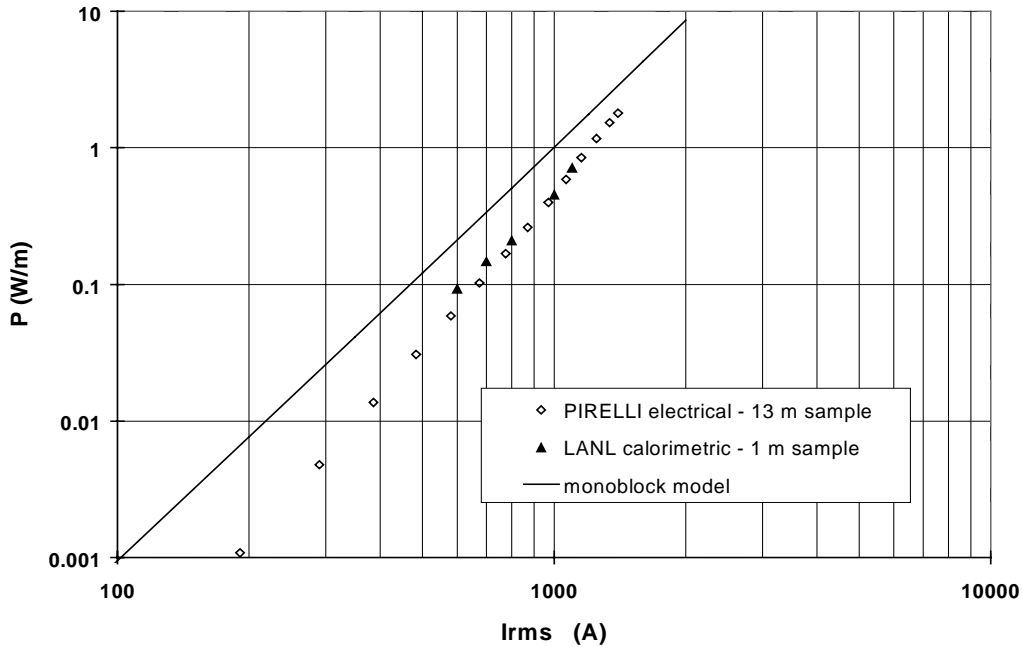


Figure 3-5
AC Losses on MCA -2 13 m Sample - Comparison of Electric and Calorimetric Techniques

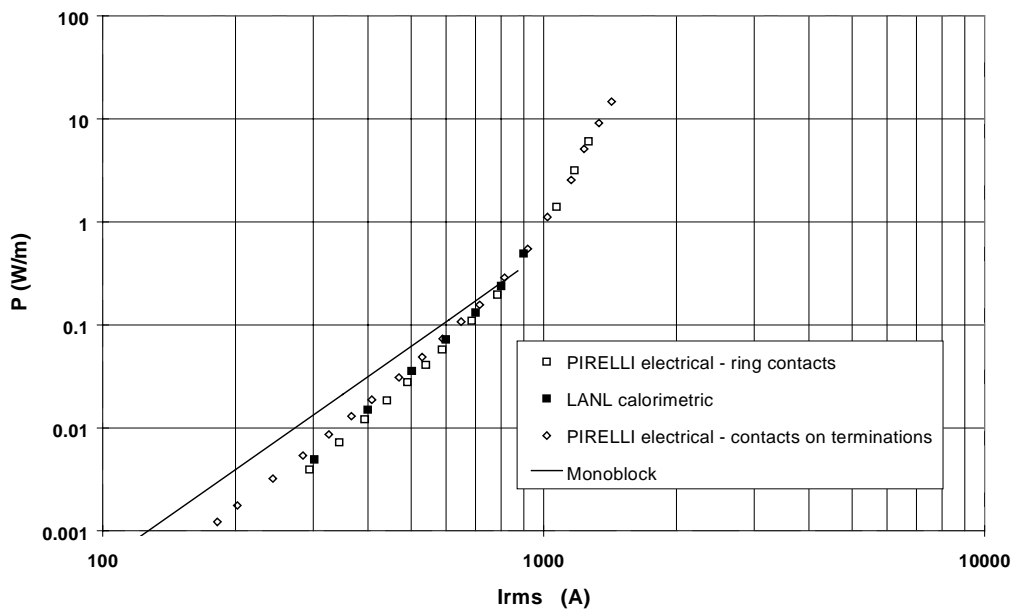


Figure 3-6
AC Losses on PMC-1 Sample - Comparison of Electric and Calorimetric Techniques

Due to the lower critical current of this sample ($I_c = 1230$ Amp DC) it was possible to test it well into the high current regime. The change in the slope of the loss curve that occurs when the peak current approaches the critical current ($I_{rms} = 870$ Amp) is perfectly visible.

3.2.3 Boil-off Calorimetric Technique (ENEL)

The 1.5 m, four layer MCA-1 conductor has been measured with three different measurement methods: the already described electrical and temperature difference methods and using a boil-off calorimetric technique developed at the ENEL research laboratories. ENEL and PIRELLI jointly developed the method in the framework of a European Community funded applied research program.

The principle of the nitrogen boil-off calorimetric method is the evaluation of the AC power losses, dissipated by the superconducting samples placed within the liquid nitrogen at boiling point, by measuring the gas evolution rate.

Heat generated within the liquid nitrogen bath, evaporates the liquid at a rate $(1/\lambda)(dQ/dt)$ where $\lambda=160.6 \text{ J/cm}^3$ is the latent heat of evaporation and Q is the dissipated energy. 1 W evaporates 22.4 ml/h of LN₂, and during evaporation each liter of LN₂ is transformed into 690 liters of nitrogen gas at ambient temperature and pressure. Hence, 1 W of dissipated power should in principle provide a gas flow rate of about 258 ml/min. In practice the actual relation between the dissipated power and the gas flow rate is determined by calibrating in situ the calorimeter supplying the cable conductor with known dc currents above the critical value I_c . The background flow rate with zero current must be evaluated separately and subtracted (see [3.2] and [3.3] for further information).

Pirelli, LANL and ENEL measurements comparison

Two different conductor specimens were measured during these tests. The conductor measured at LANL was a one meter section obtained from the 8-layer MCA-2 sample removing the external four layers. The sample measured by ENEL and PIRELLI was cut from the MCA-1 conductor (which was then used as the inner four layers of the MCA-2 conductor) and was 1.5 m long. Besides the difference in length, they both had the same geometric and electrical properties.

The experimental results, reported in Figure 3-7, shows a good agreement among the different methods. The lower current points of the boil off calorimetric characterization seem to draw away from the trend of the results obtained with the other two methods. This deviation can be ascribed to the low sensitivity of the boil off technique at that loss level.

Each measurement method has its limits and merits. If we consider the development of a measurement method not only as a tool but also as a result, it is worth to summarize here the main advantages and drawbacks of each of them.

The range of the electrical data is, as expected, much wider than that of the “calorimetric” ones. It must be noticed, however, that the sensitivity reached in the “temperature-difference” measurements was also remarkable, allowing to reliably detect a power dissipation of less than 20 mW. A peculiarity of this method, on the other hand, is that the current flowing along the cable must be not only large enough to produce detectable ΔT , but also not too large, so that the temperature along the cable can be considered “almost” constant. This limited the maximum

current to slightly below the critical current, and even in this case a temperature correction of losses due to the not uniform temperature in the cable is required. For exactly the same reason the sample must be not too long or too short, practically about one meter.

The “boil-off” system, although being the most penalized in term of sensitivity, being restricted to losses above about 200 mW, doesn’t suffer of any limitation in the direction of high currents.

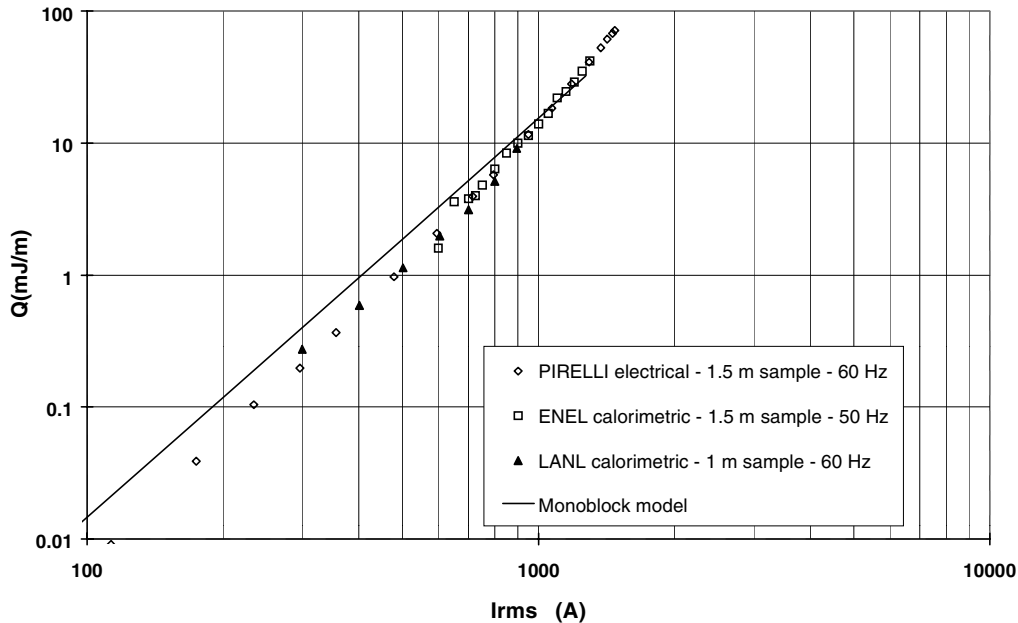


Figure 3-7
AC Loss on a MCA-1 Sample measured with Electric and Calorimetric Techniques

Both calorimetric methods have an advantage over the electrical method primarily because of their independence from the environmental electromagnetic condition. This makes them potentially advantageous in a wide range of applications (*e.g.* 3-phase cables) and useful as a reference for improving electrical measurements in complex configurations.

Both calorimetric methods suffer limitations concerning their range of applicability, both for current magnitude and sample length. While the electrical method does not suffer these limitations (except the challenge of providing a high quality signal at high currents), it is not currently appropriate for measurements having high levels of electromagnetic interference. Other elements that can be taken into account are:

- the time required to perform a measurement, which is quite long for the boil-off technique (at least 15 minutes for each point in the curve), and even longer for the temperature difference calorimetry (about one hour to reach steady state conditions). The measurement time for the electrical technique is very short.
- the complexity of the experimental assembly, which is certainly greater in the case of the temperature difference technique, due to the vacuum thermal insulation and the fine temperature control.

Regardless of the particular limit of each technique, it is remarkable that all of them had proved to be perfectly suitable to perform reliable measurements of AC losses on cable conductors.

3.3 Cryostat Effect on AC Losses

After the measurement program for conductor AC losses, the MCA-2 13 m long sample was used to test the effect of the cryostat construction on the conductor performance. After a few trials on dummy conductors containing 1 or 2 superconducting tapes to set the proper construction procedure, the inner and outer cryostat corrugated tubes were built on the 13 m sample (see Section 2.4.5). The critical current for this sample was measured before and after the cryostat assembly and the results indicated no change due to the cryostat construction.

The presence of the cryostat could, in principle, introduce additional AC loss in the cable and tests were performed to investigate this effect. Because the cryostat tubes in the warm dielectric cable concept are positioned very close to the cable conductor, they are subject to an intense magnetic field, which can induce losses. Two distinct loss mechanisms are responsible: eddy current losses in each cryostat corrugated tube; and losses due to currents circulating between the two tubes if they are electrically connected at the extremities of the cable. In the 13m sample the cryostat tubes were isolated at the ends, so only the eddy current effect was investigated.

An estimation of eddy current losses in the cryostat can be obtained through a simplified calculation. Essential features can be derived from the model case of losses due to eddy currents induced in a metallic tube with resistivity ρ due to alternating current flowing along the axis of the tube (Figure 3-8). System of cylindrical coordinates with z -axis identical with the tube axis is appropriate for this geometry. The physical quantities are referred to the length l .

Two assumptions are effective in simplifying the calculation. They can be accepted in the present case with good approximation:

1. Eddy currents in the metallic tube do not change considerably the local value of the magnetic field.
2. The tube is thin-walled, i.e. the wall thickness d is much smaller than the tube radius R .

On the basis of the two conditions given above one can reasonably approximate the value of the magnetic field in the tube section as:

$$B(r) = \frac{\mu_0 I_{ac}}{2\pi r} \approx \frac{\mu_0 I_{ac}}{2\pi R} \quad \text{for } |r - R| \leq d/2 \quad (1)$$

Here, $\mu_0 = 4\pi \times 10^{-7}$ Vs/Am. We are considering the harmonic alternating current of the form

$$I_{ac} = I_o \cos \omega t \quad (2)$$

where I_o is the peak value and ω the angle frequency $\omega = 2\pi f$. Azimuthal time-variable magnetic field will induce an electrical field parallel to the tube axis. In the metallic tube, this voltage will generate eddy currents that form a closed loop inside the tube, flowing in one direction near the outer surface and in the opposite direction near the inner surface. The so-called neutral line (where the density of induced currents is zero because of changing the sign) will coincide with the average radius of the tube, R , and it is opportune to express the electrical field as a function of a new coordinate $x = R - r$. It can be derived applying the 2nd Maxwell's equation to the closed contour depicted by dashed line in Figure 3-9. Because the electric field is zero on neutral line as well as along the rectangle sides perpendicular to the axis, we find

$$E(x) = E(R - r) = \frac{dB(R - r)}{dt} x \approx \frac{dB(R)}{dt} x = \frac{\mu_0}{2\pi R} \frac{dI_{ac}}{dt} x. \quad (3)$$

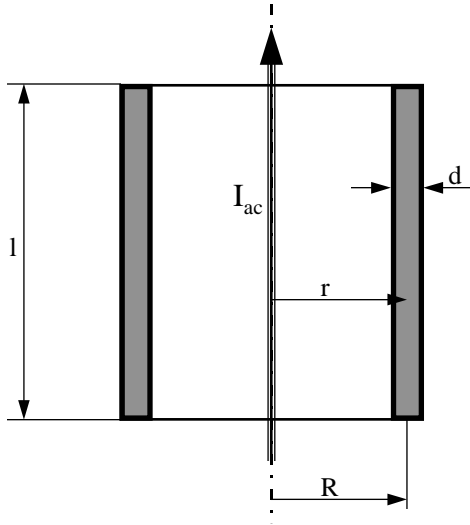


Figure 3-8
Alternating current I_{ac} flowing along the axis of a metallic tube, which is characterized by the radius R and the wall thickness d .

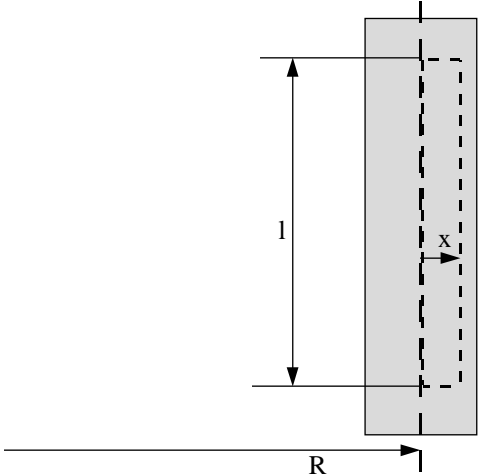


Figure 3-9
Contour used to derive the induced electrical field

The losses due to electrical current flow in a metallic material will be developed with the rate

$$w = \frac{E_{eff}^2}{\rho} \tag{4}$$

where E_{eff} is the effective value of AC electrical field that with the help of (3) can be expressed as

$$E_{eff}(x) = \frac{\mu_0}{2\pi R} \omega \frac{I_o}{\sqrt{2}} x. \quad (5)$$

The total loss power in the tube of length l is found integrating the loss rate (4) over the volume of the tube:

$$W = \int_{R-d/2}^{R+d/2} l 2\pi r w(r) dr \approx l 2\pi R \int_{-d/2}^{d/2} \frac{E_{eff}^2(x)}{\rho} dx = \frac{l \mu_0^2 \omega^2 I_{rms}^2 d^3}{\rho 2\pi R 12} \quad (6)$$

Inserting for μ_0 its value and gathering the numerical constants together we obtain the final expression for power losses in unit length of the tube:

$$\boxed{\frac{W}{l} = 8.3 \times 10^{-13} \frac{d^3}{R \rho} f^2 I_{rms}^2} \quad (\text{W/m}) \quad (7)$$

This cryostat consists of two corrugated tubes made in stainless steel with resistivity $\rho = 5.15 \times 10^{-7} \Omega m$ at 77K. The penetration depth of magnetic field at frequency $f=60$ Hz is then

$$\delta = \sqrt{\frac{2\rho}{\mu_0 \omega}} = 0.047 \quad (\text{m})$$

Wall thickness of both tubes is 0.6 mm. This implies that both conditions, under which the model in preceding paragraph was developed, are fulfilled and expression (7) can be used.

The tubes have external diameters 41.8 and 64.4 mm, respectively. The volume occupied by metal in corrugated tube is larger than for a straight tube of the same diameter by a factor of 1.02 for the inner tube and 1.07 for the outer one. So the effect of the increased effective length of the cryostat tubes can be reasonably neglected at a first approximation.

The total loss can be obtained calculating the eddy current loss in the inner and outer tubes according to (7), corrected for the corrugation effect.

Thus we find for the total losses in cryostat

$$\frac{W_{cryo}}{l} = \frac{W_i}{l} + \frac{W_o}{l} \approx (4.56 + 2.85) 10^{-10} I_{rms}^2 \quad (\text{W/m})$$

This estimation indicates that inserting the conductor into the cryostat should not cause any noticeable increase in the single-phase transport AC losses. This prediction is in agreement with the experimental data taken on a 13-meter sample of the cable (see Figure 3-10).

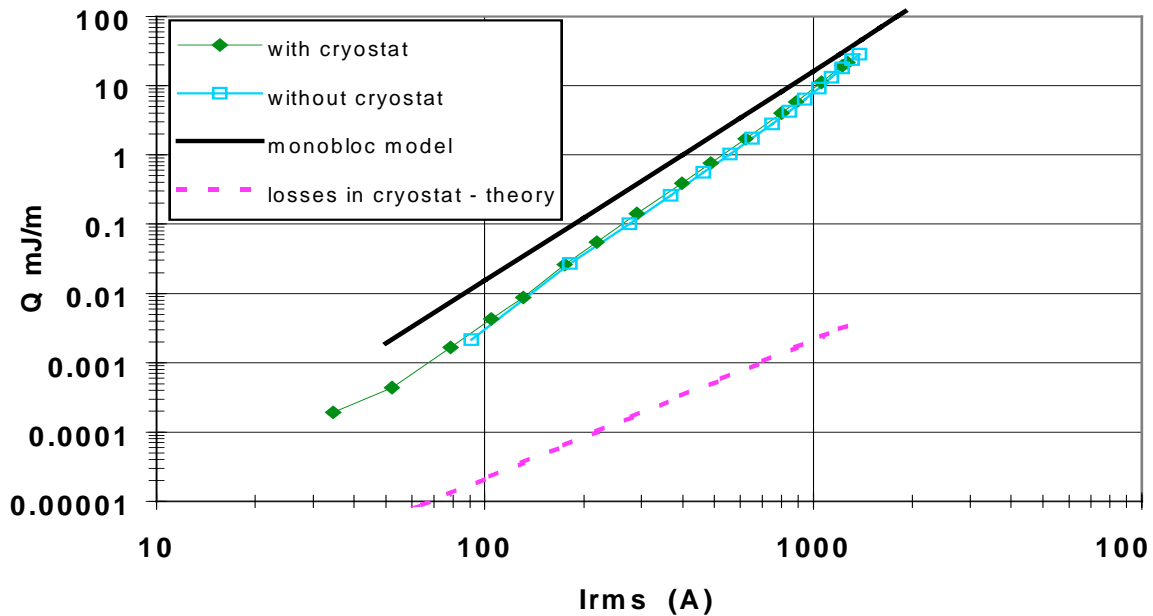


Figure 3-10
Comparison of losses determined experimentally on conductor with and without the cryostat.

3.4 Single phase AC Losses: Comparison with Theoretical Models

In this section, the AC loss measurement results obtained on different conductor samples will be reviewed and compared with the theoretical interpretations. The aim of this work is to provide reliable interpretations of the main factors determining the AC behavior of a HTS multistrand cable conductor in single-phase configuration.

One of the main results of the testing program undertaken for this project indicates that in the operating current range and in single-phase configuration, hysteresis is the dominant AC loss mechanism. Therefore the data will be analyzed in terms of the existing analytical models for hysteretic loss in HTS cable conductors. An overview of the models suitable for describing hysteretic AC losses in multi-strand cable conductor is reported in Appendix A.

The AC loss in multi-strand cable conductor strongly depends on the current distribution among the HTS layers and in this view a different behavior is expected for 2-layer and multi-layer cable conductor. The samples used for the AC tests consists of 2N (N=1,2,4) helically wound layers (one right-handed and the other left-handed). This winding pattern results in an almost uniform current sharing between the HTS layers in a 2-layer cable conductor. On the other hand the same

winding pattern in a 4-layer and 8-layer cable conductor creates a strongly non-uniform current distribution, with larger currents flowing in the outer layers.

Owing to this effect the 2-layer PMCs and the multi-layer MCAs are expected to have a different ac behavior. In both cases the results will be analyzed in terms of the model developed by J. Clem in collaboration with Pirelli and extensively described in Appendix A.

This model has been designed to describe a HTS conductor consisting of 2N helically wound layers, with the suitable winding pattern + - + - The tapes are assumed to be in electrical contact edge to edge such that any local radial magnetic fields are negligible, compared to the local longitudinal and azimuthal magnetic field. In this framework the current sharing among the HTS layers is determined by the inductive coupling and it can be calculated in all the cases of interest.

In particular in the 2-layer PMCs the selected winding angles result in an almost uniform current sharing between the two layers and then the AC loss can be calculated in the Clem model framework in the whole explored current range (See Appendix A).

Because the 2-layer PMC1 and PMC2 exhibited virtually identical AC behavior, as will be discussed in Sect. 3.6, the following discussion will consider the PMC2 as the reference for the 2-layer cable conductor.

In Figures 3-11 to 3-13, the experimental AC loss data versus the normalized current, $F = (I_o/I_c)$, at different temperatures, are reported and compared with the theoretical Clem model. In this model it has been assumed that the total energy dissipation occurs within the HTS layers, i.e. that the effective thickness for calculating ac loss is given by the HTS filaments bundle thickness. It is worth noting that the model shows a very good agreement with the experimental data at $T=76K$ up to $F \cong 0.6 - 0.7$ while for larger F values the experimental ac losses grow faster than predicted.

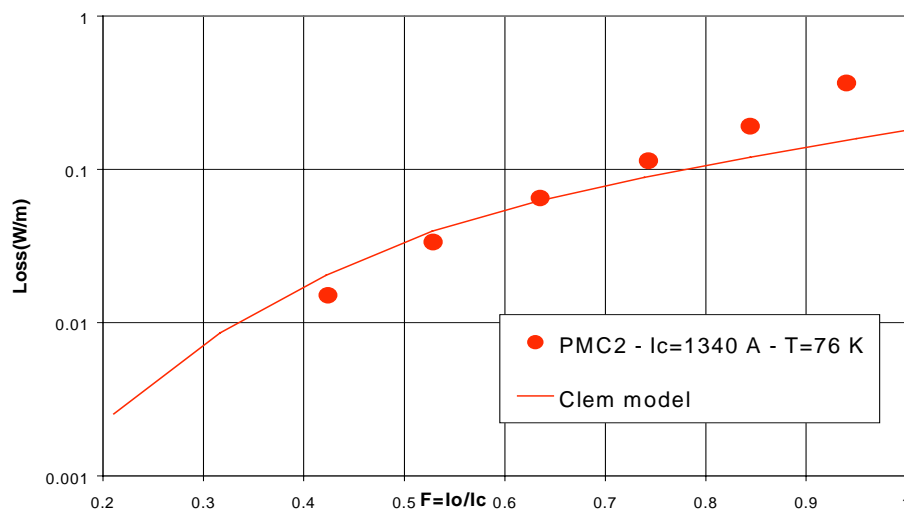


Figure 3-11
AC loss Vs F measured at 76 K in LANL with difference temperature calorimeter

The measurements at lower temperatures show a very good agreement with the model, but in these cases the high current range has not been explored. The experimental data can be represented through a power fit that in the 70K and 64K case is $\sim F^3$ while in the 76K case is $\sim F^{3.88}$, confirming that the loss increases at a more rapid rate than F^3 .

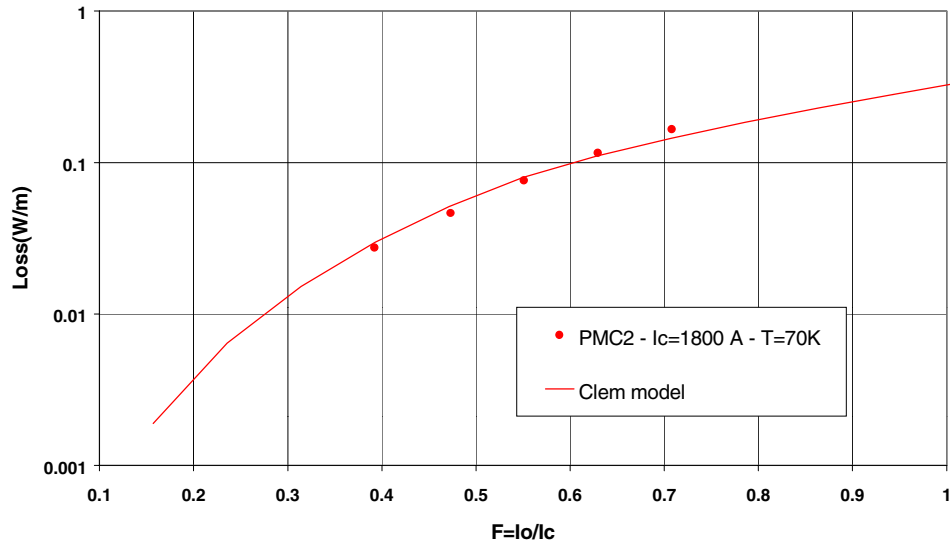


Figure 3-12
AC loss Vs F measured at 70 K in LANL with difference temperature calorimeter

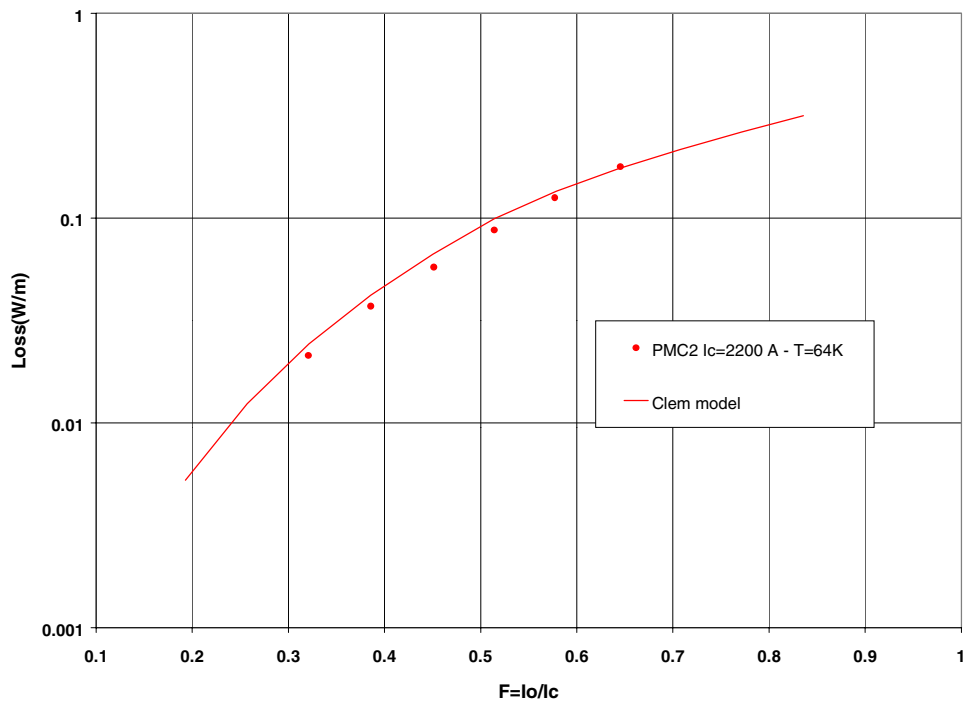


Figure 3-13
AC loss Vs F measured at 64 K in LANL with difference temperature calorimeter

The deviation between the model and the experimental data in the high current range can be ascribed to several factors, to be included in the theoretical model:

- in the high current regime the magnetic field originated by the transport current results in a reduction of the critical current density: this effect has to be calculated beyond the Bean model approximation, i.e. including the non-linear profile of the magnetic field penetrating the HTS layers. However the expected qualitative behavior is that the losses will increase faster, in the high current range, because of the reduction of the total critical current;
- in the Clem model the transport current is assumed to be uniformly distributed on the conductor surface, neglecting any effect of the radial field at the edge of the tapes due to the gap between tapes: no model has been developed so far that calculates the ac losses for tapes laid on a cylindrical surface including this “gap effect” then no quantitative estimation can be provided. However this effect has been calculated in an infinite array of tapes, in a flat arrangement, and the expected loss can be conveniently represented in the form $\alpha I^3 + \beta I^4$ with α and β depending on the geometrical configuration and on the critical current. A more reliable calculation has still to be developed for the actual conductor configuration;
- in the Clem model, a different behavior for losses is expected depending on the value of the current I compared with I_x , representing the current value where the two magnetic flux fronts, that are penetrating from both tape surfaces, meet in the HTS layer. In fact, as reported in Appendix A, in the low current range the HTS layers are supposed to be in the partial penetration regime of the magnetic field, while for high current the outer layer, affected by both its self-field and the magnetic field of the inner layer, reaches full penetration. In the picture of the Clem model the screening currents in the outer layer give no additional contribution to the losses. In the actual configuration this screening current is expected to reduce the effect of the magnetic field superimposed to the self-field in the outer layer. It would lead to a shift of the I_x value, extending the validity of the partial penetration model towards higher currents; in this case the ac loss $V_s F$ is expected to grow as F^3 even for currents higher than I_x ;
- the actual E Vs J DC characteristic of the HTS material is different from that adopted in the Clem model which is based on the critical state model. In fact in the critical state model the DC characteristic is supposed to be a step-like function, with a sharp transition for $J=J_c$. In the actual materials the DC characteristic is a broad curve, which is generally fitted, in the current density range around J_c , with a power law $E \sim J^n$, with n ranging typically from 10 to 20. This effect is expected to have an impact on the AC behavior of the conductor in the $F \sim 1$ region.

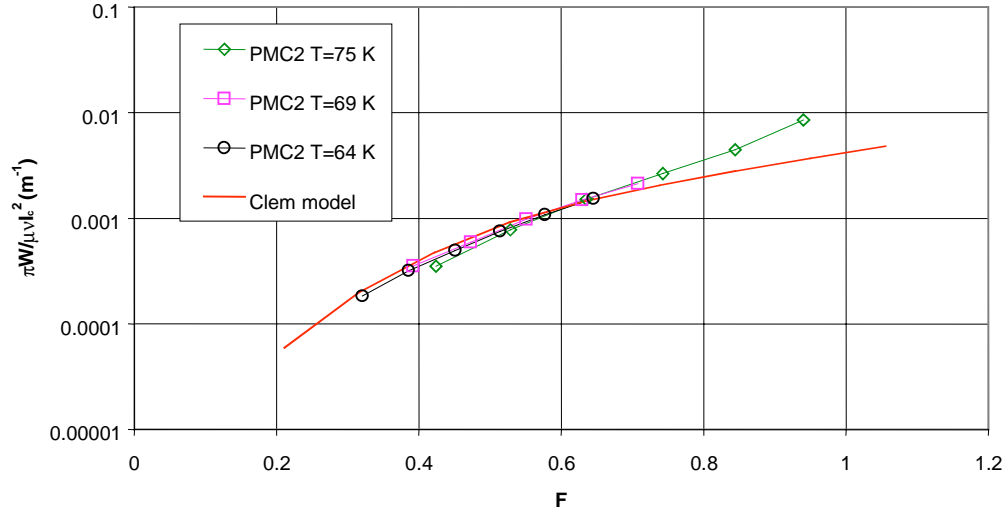


Figure 3-14
Reduced loss $\pi W/\mu\nu I_c^2$ Vs F for the PMC samples at different temperatures

Please note that according to this model the effect of the temperature on the AC loss is only due to the variation of the critical current: it gives a scaling with temperature that is in rather good agreement with the experimental data up to $F=0.6$. This is shown in Figure 3-14 where the reduced loss, defined as $\pi W/\mu\nu I_c^2$ (μ is the vacuum permeability, ν the current frequency), are reported.

In the MCAs, with 4 and 8 layers, the current distribution is strongly non-uniform. In this arrangement the current distribution has been calculated (see Appendix A) assuming that the thickness of the HTS layers doesn't influence the self-inductance and the mutual inductance of the helical layers.

The current mainly flows in the two most external layers. For an AC current amplitude above the critical current of the outer layer, there is a portion of the ac cycle for which the current in the outer layer is above the critical current for that layer. In this case, the current is forced to flow in the inner layers. The current in the layers is then non-harmonic and the current distribution among the layers depends on the transport current - which changes during the cycle.

In this case, the small-current expression for AC loss developed in the Clem model applies for peak currents lower than the critical current in each layer: $I_{rms} \leq I_c/(\sqrt{2} N 0.63) \sim 460$ A. For higher current values a more refined calculation is required, beyond the Bean model, taking into account the non-harmonic profile of the current in the layers.

However a simplified model can be drawn noting that in this cable design the current is almost equally shared between the layers with opposite chirality. In this model the 8-layer conductor can be described as a 2-layer cable conductor where all the right-handed (left handed) layers are fully coupled and then act as an unique layer whose thickness is 4 times the thickness of the actual HTS layer. In this "effective" 2-layer model the AC loss can then be calculated using the above described two-layer Clem model.

In Figure 3-15, the experimental ac loss per unit length Vs I at 76/77 K are reported and compared with the 2-layer effective Clem model. The reduced losses Vs F, measured at 76K and 70 K, are reported in Fig. 3-16 and compared with this model.

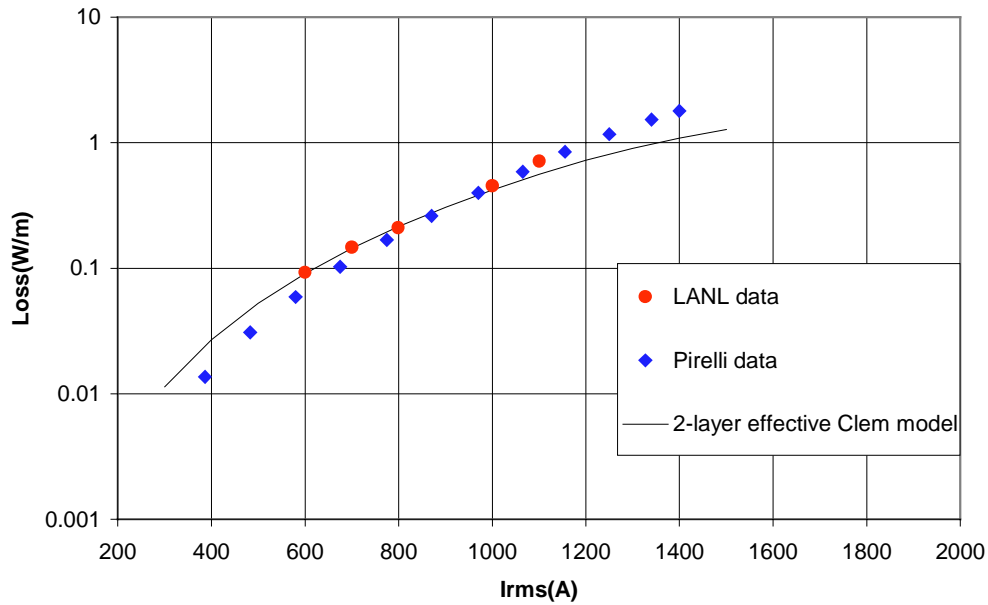


Figure 3-15
AC loss per unit length Vs I for the MCA2 sample at 76/77K compared with the theoretical model

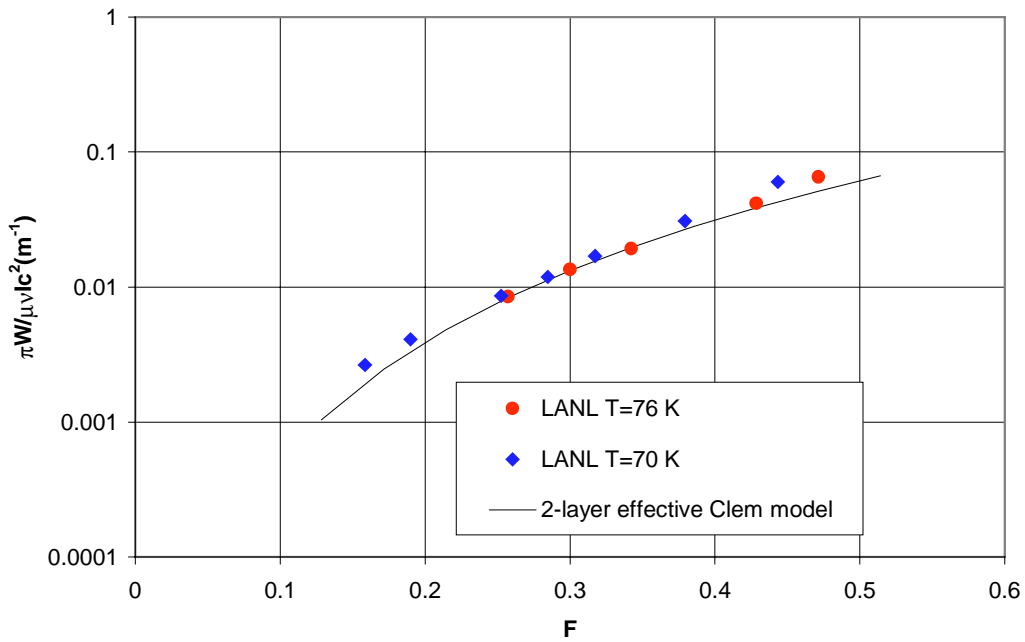


Figure 3-16
Reduced loss $\pi W / \mu \nu I_c^2$ Vs F for the MCA2 sample at different temperatures

In the MCA1 4-layer conductor the tapes are wound having layers with equal, but opposite lay angles and also in this case the AC losses can be calculated using the “effective” 2-layer Clem model. In Figure 3-17 the experimental ac loss per unit length Vs I at 76/77 K are reported and compared with the theoretical model.

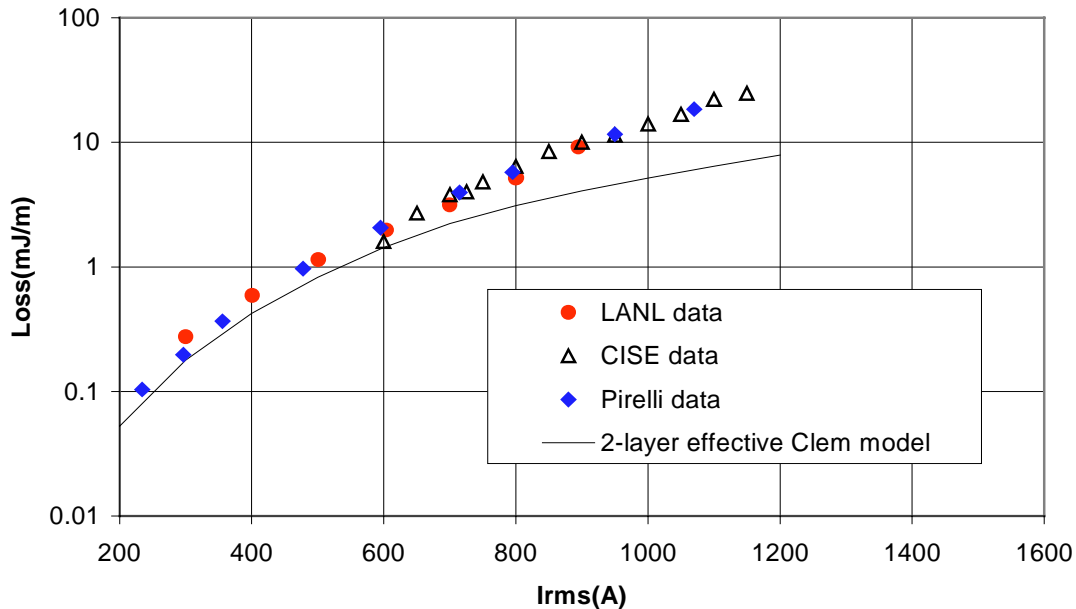


Figure 3-17
AC loss per unit length Vs I for the MCA-1 sample at 76K measured in different laboratories

3.5 LANL Three-Phase Measurements

The Los Alamos temperature difference calorimetric system was designed so to allow the measurement of losses for conductors arranged in both single and three-phase configuration. The single-phase configuration was obtained by putting the return current conductor 1 m away outside the calorimeter, to approximate the limiting case of very large spacing. For the three-phase arrangement the conductor’s centers were located at the corners of an equilateral triangle with 10 cm side, which is a typical distance between the conductors in a retrofit application in a pipe. The current distribution among the conductors was controlled so to realize a balanced, 120° shift, three-phase configuration. In this experimental set-up only the measured conductor was superconducting, the return ones were made of copper.

In Figure 3-18 the measurement results on the PMC1 sample in single-phase and multiphase configuration are reported. The curve indicated as “2 phase” represents the measured losses on the conductor with no current flowing in it (it is disconnected) but with current flowing in the two normal conductors.

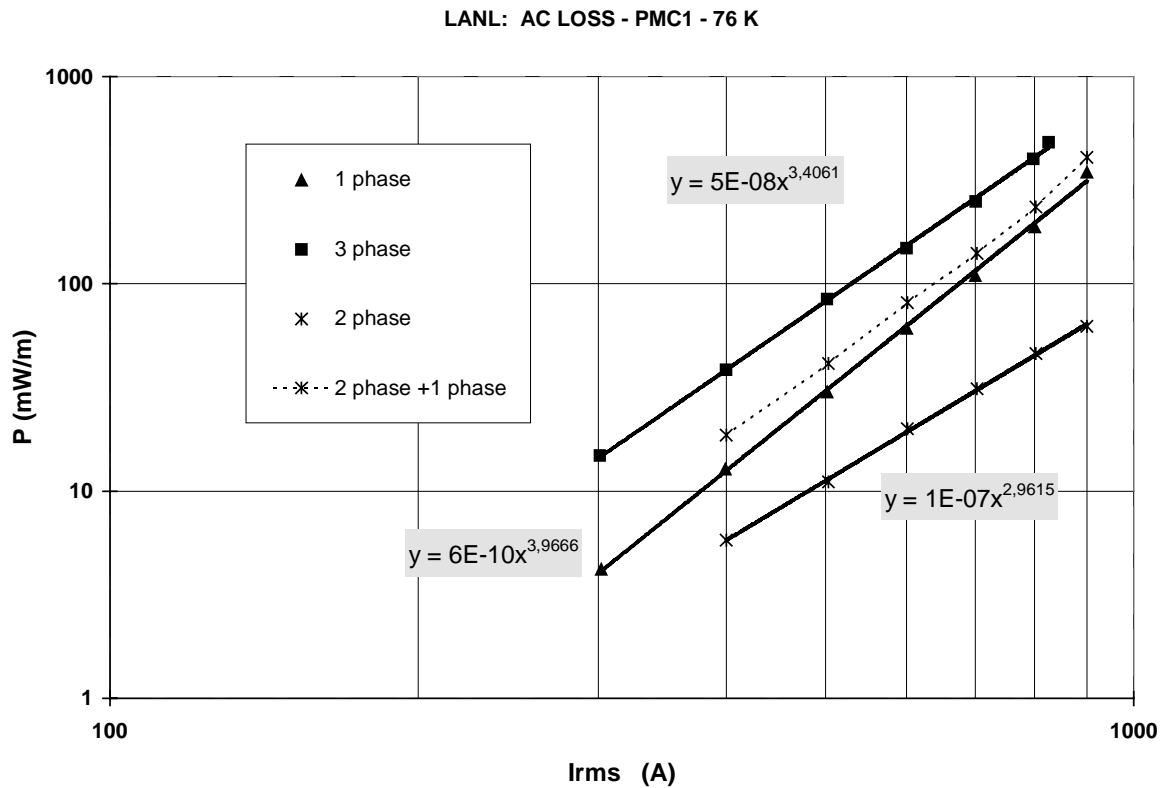


Figure 3-18
Comparison of 1 phase, 2-phase and 3-phase AC Losses on the PMC 1 Conductor.

As it is evident from the figure, the three-phase losses in such balanced equilateral configuration are 2-3 times higher than the single-phase losses, indicating a significant interaction among the three phases. Please note that the contribution due to the 2-phase losses is not sufficient to explain the increase in losses when passing from the single to the three-phase configuration. In other words, the three-phase losses are not simply the sum of the single and double phase losses (the sum is shown in the figure). Either the depression of the I_c of the conductor, due to the effect of the magnetic field of the other two phases, is not sufficient to explain the observed increase. This was seen energizing the PMC1 with an AC current and the two normal conductors with a DC current (see ref [3.3]), and then comparing the relative losses. For the case where the DC current in the normal conductors is equal to the AC current in the PMC, the increase in the losses was less than 5 %.

In the 3-phase configuration the AC loss has then to be described including the combined action of large transport currents and external AC magnetic fields perpendicular to the tape surface: a focused analysis is required to address this point that is still an open issue.

The 3-phase losses depend on the distance among the conductors: to address this point the PMC2 was measured in three phase configuration for two different distances, 10 and 20 cm at two temperatures 69K and 76K.

In Figure 3-19 the measurement results at 76 K are reported, together with the single-phase measurements. It is worthwhile to notice that is sufficient a distance of only 20 cm between the conductors to scale down the three phase loss almost to the single phase value.

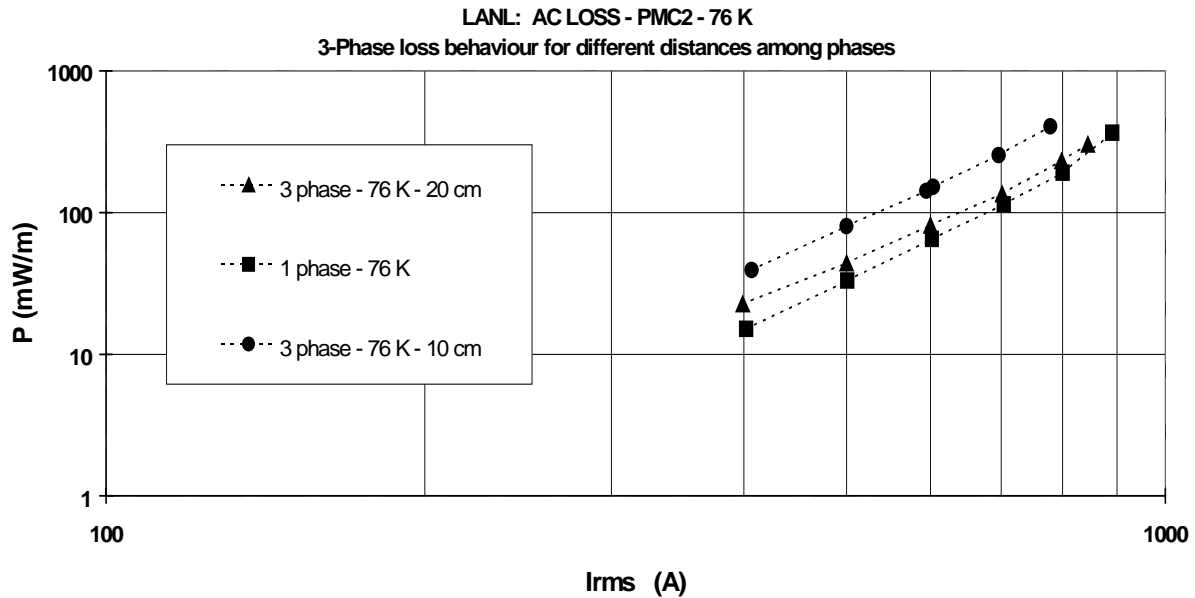


Figure 3-19
Three-Phase Loss for 10 and 20 cm distance between Phases Compared to Single-Phase Losses.

In Figure 3-20 the loss ratio (3-phase loss/1-phase loss) is plotted as a function of $1/(R)^2$, where R is the conductors spacing, for two different values of the transport current: the resulting curve is almost linear (except for the 69K 500 A curve), indicating a loss behavior roughly proportional to $1/(R)^2$.

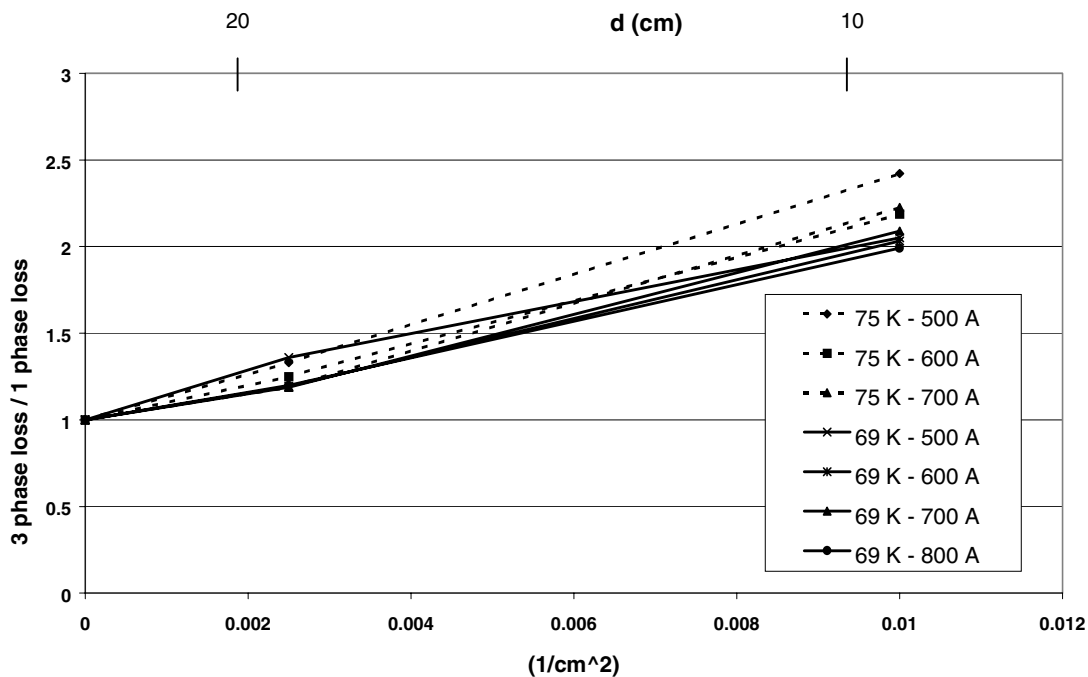


Figure 3-20
3-Phase / 1-Phase Loss Ratio Vs $1/d^2$

3.6 Interlayer Insulation

The previous literature contains some investigation of AC losses in multi-layer cables, which claim that a significant reduction in AC losses could be accomplished by electrically insulating the conductor tapes layers with a thin dielectric film [3.7]

In that study [3.7] two 2-layers conductors, differing only for the inter-layer electrical insulation, have been investigated by measuring AC loss in 1-phase configuration. In the conductor with no insulation between layers a quite large increase in AC losses, compared with the other conductor: this additional contribution to the losses showed a squared dependence on current. This behavior was attributed to the ohmic losses due to currents flowing between layers.

To investigate this effect two identical conductors (PMC1 and PMC2) were fabricated, with the only difference that in PMC2 a thin Kapton® film was allocated in between the two counter-wound layers of HTS tapes.

The following graph (Figure 3-21) compares the measurements on the two PMC's at 76 K in single and three-phase configuration made in LANL. The measurements nearly coincide, both in single and three-phase, indicating that at least for these two-layer cable conductors the dielectric layer has no significant effect on the AC losses. A similar loss coincidence for the two PMC's is seen at all the investigated temperatures (69K and 64 K).

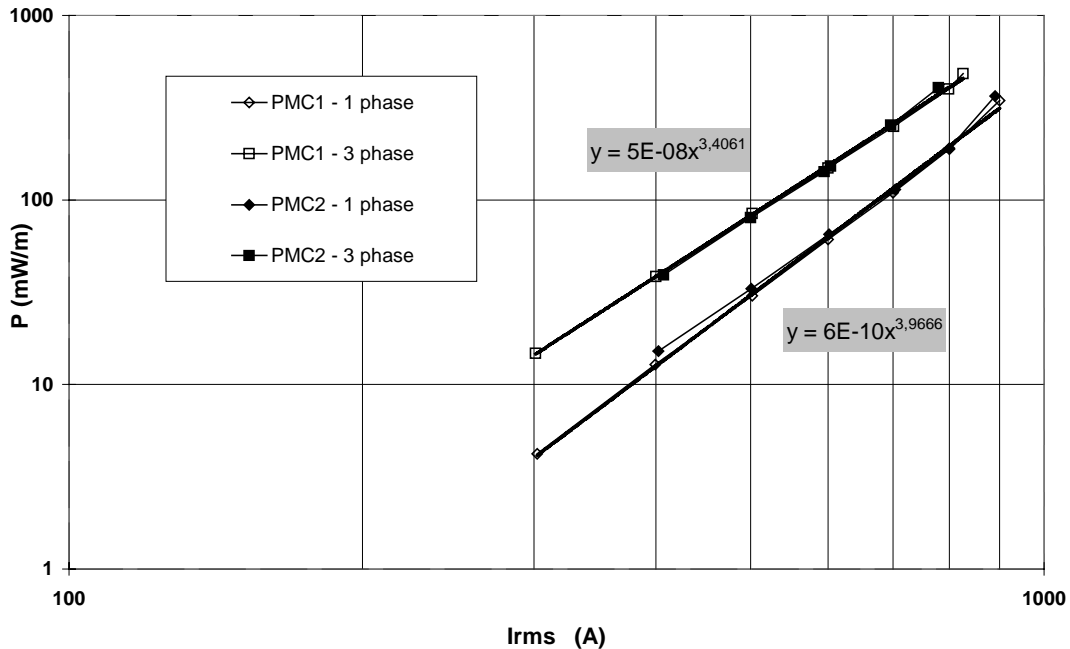


Figure 3-21
AC Losses on Samples with (PMC2) and without (PMC1) Electrical Insulation Between Layers.

The absence of any interlayer currents in these conductors is evident, since the power dependence on current in these PMC samples, is even higher than the cubic dependence predicted by the critical state models both for the single and the three-phase case.

3.7 8, 4, 3-Layer conductors: LANL AC loss Measurements

A further characterization addressed in the present test program concerns the dependence of losses upon the number of HTS layers. This was accomplished by measuring a 1m long sample of MCA-2 8-layer conductor with the LANL calorimetric technique, and then by peeling off the outer layers of the same sample and measuring it again. 8, 4 and 3-layer samples were obtained and characterized.

In Figures 3-22 and 3-23 single-phase loss measurements are reported, as obtained on these 8,4 and 3-layer conductors. Lower losses are expected for the cable with higher critical current. Please note that on these samples the critical current has not been directly measured, and the values we will refer to, are deduced from the data on longer samples.

In Figure 3-26 the reduced AC loss, defined as $W/\mu I_c^2$, at different temperatures are reported as a function of F . This representation allows comparing samples with different critical current. The results show that in the same sample measured at different temperatures, the reduced losses almost coincide, indicating that the only temperature dependence of the losses is due to the critical current. The reduced losses of different samples are instead different and in particular the 8-layer conductor has the greatest reduced losses in all the current range, while in the high current regime the 3-layer sample has the lowest losses.

This fact is not expected and it seems to indicate that the effect of unbalanced azimuthal currents, that is relevant in the 3-layer conductor, doesn't strongly affect the AC loss results.

In fact, for a conductor with an even number of layers the inductive coupling will tend to drive equal currents among clockwise and counterclockwise layers, with the result of approximating to zero the axial magnetic field inside the conductor. This isn't true for a sample with an odd number of layers, as is clearly stated by directly measuring the axial magnetic field inside the conductor by means of a calibrated pick-up coil put in the axial midpoint of the sample. The result of this measurements (see [3.6]) show that the axial field in the three layers sample was roughly an order of magnitude higher than in the 4 layer sample.

Moreover, as it has been seen in Sect 3.4, most of the current in the 4-layer and 8-layer MCA-s should be carried by the outer two layers, for transport current lower than about $I_c/(\sqrt{2} N 0.63)$, where N is the number of layers, i.e. for F less than 0.2. In this range the losses should in principle be almost insensitive to the number of layers and no considerable difference is expected between an 8 and a 4-layer sample. A general agreement with the described picture is found through experiment.

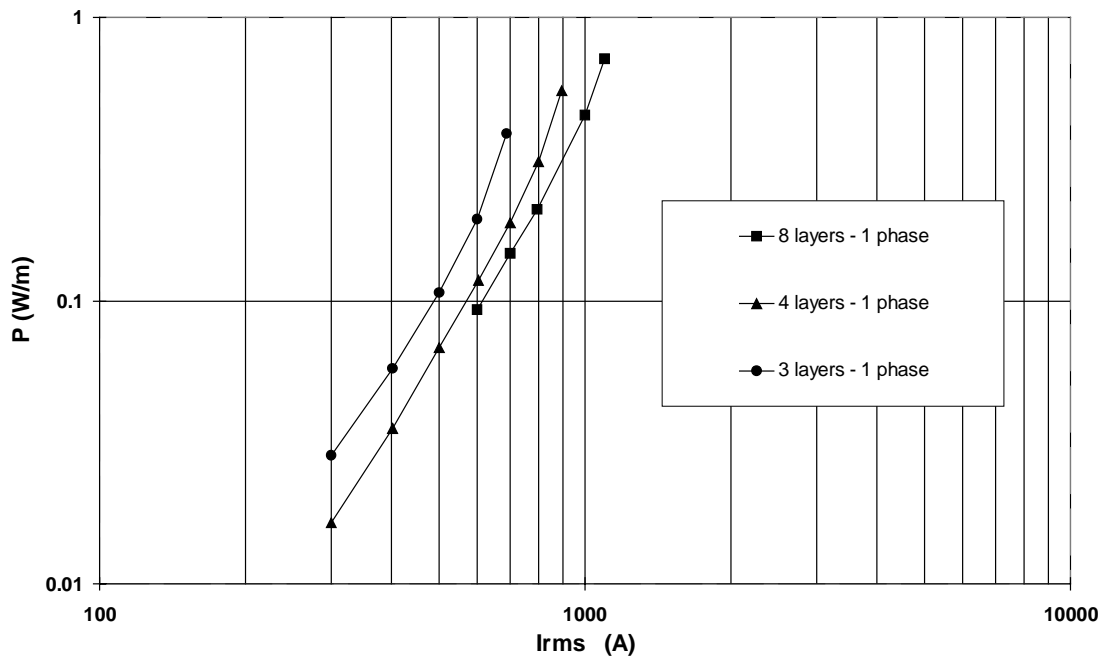


Figure 3-22
AC loss Vs Irms in 8,4 and 3-layer samples at 76K

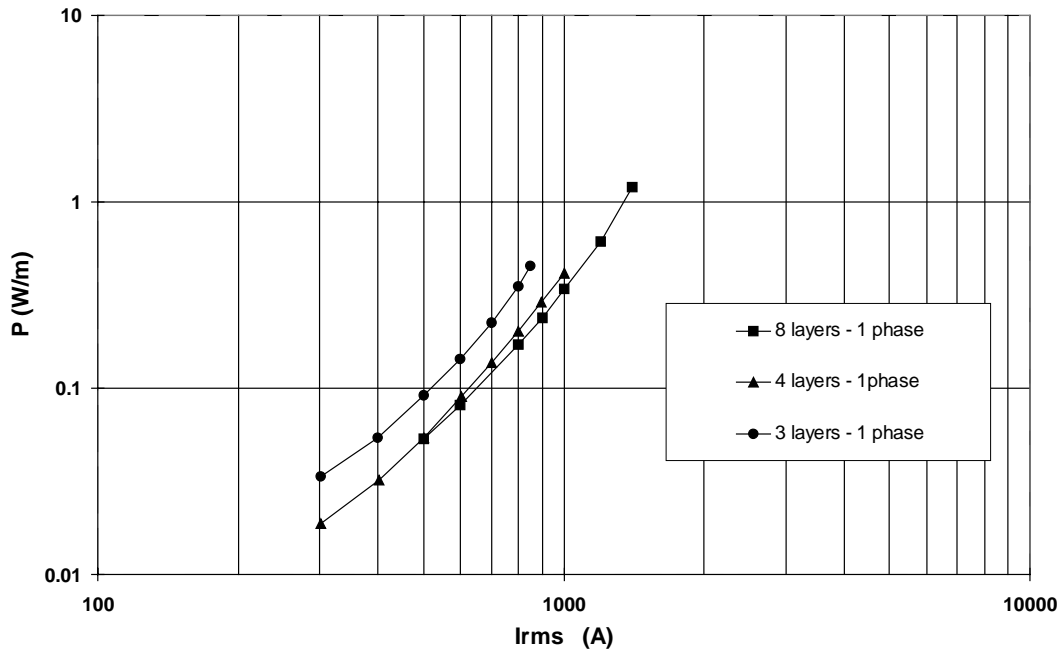


Figure 3-23
AC loss Vs Irms in 8,4 and 3-layer samples at 70K

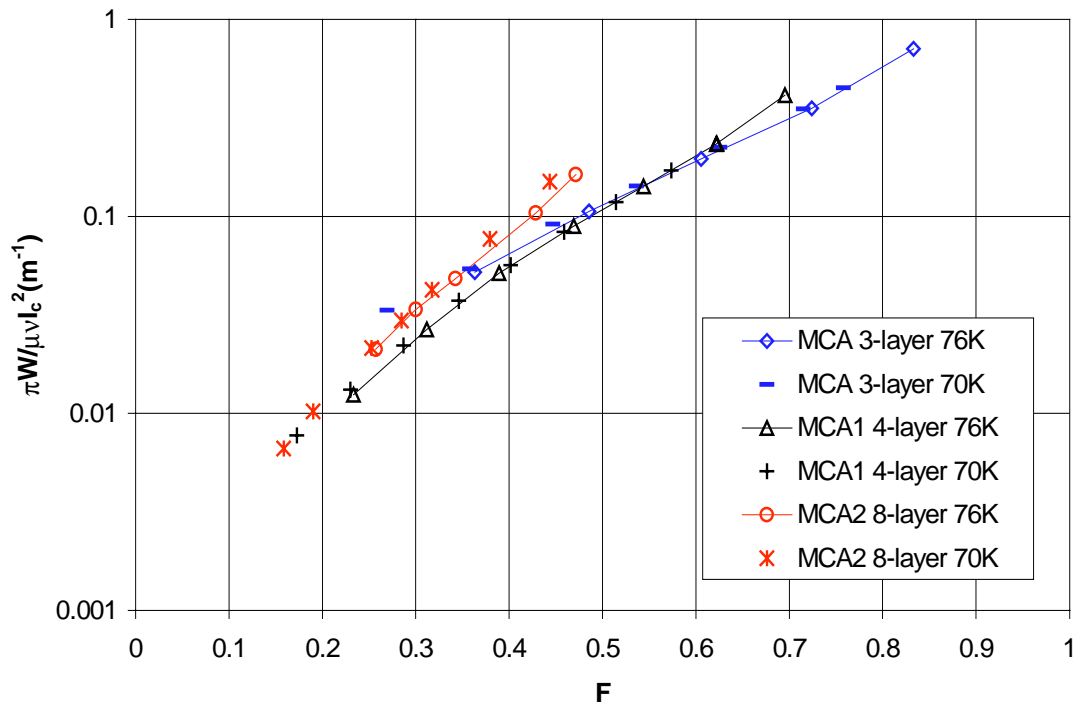


Figure 3-24
Reduced loss Vs F for 8,4 and 3-layer samples at 76K and 70 K.

3.8 Testing of the 50 m Prototype Cable

In the following section the electrical measurements concerning the superconducting properties of the prototype cable will be reviewed, following the cable manufacturing steps (conductor winding, cryostat fabrication, and dielectric application) and after its installation into a high voltage configuration. Once the superconducting properties were evaluated, the system was tested as a normal high voltage cable using tests specified from Association of Edison Illuminating Companies (AEIC) and the International Electrotechnical Commission (IEC).

3.8.1 Mechanical History of Prototype Cable: Cabling Processes

After the conductor construction and the immediately subsequent I_c -dc characterization (performed in Lexington in 1996 and described in Section 2.4.4) the conductor was wound on a reel and delivered for the cryostat construction and for insulation deposition.

To test the effect of the mechanical stresses due to the cryostat construction on the superconducting properties of the cable conductor, a 13-m long section of the conductor has been manufactured and electrical tests have been performed before and after the cryostat application. The results of these tests have been summarized in Section 2.4.5 and they have shown that cryostat manufacturing around the conductor should not cause any visible degradation in the superconducting properties. In the following Table 3-2 the mechanical stresses imposed upon the conductor due to the completion of the cryostat and thermal insulation, have been summarized:

Table 3-2
Mechanical history of EPRI 50 m before HV Installation

Actions	Manufacturing process stages
Winding and unwinding on reel/Pulling Through the line	Building of inner corrugated tube
Winding and unwinding on reel/Pulling Through the line	Mylar and spacer deposition
Winding and unwinding on reel/Pulling Through the line	Building of outer corrugated tube
Winding and unwinding on reel/Pulling Through the line	Dielectric deposition
Winding and unwinding on reel/Heating	Dielectric impregnation
Winding and unwinding on reel/Pulling Through the line	Lead sheath extrusion
Unwinding from reel and installation in straight configuration.	I_c and AC loss measurements at different temperatures

3.8.2 Superconducting Properties Testing: Straight Configuration

After the insulation deposition was successfully completed, the cable was installed in a straight configuration, suitable for measuring the superconducting properties separately from the high voltage arrangement. These tests were desirable to determine the critical current of the cable after the final cabling steps, as well as to measure the AC losses at different temperatures of a long conductor with electrically continuous cryostat terminations. In fact the effect of the circulating current through the cryostat can give additional losses in a configuration where the outer and inner pipes of the cryostat and the conductor are electrically connected, while it has been shown to be negligible where the ends are electrically disconnected (See Sect. 3.3).

The cable was laid in a straight configuration, laying on wood pallets above the ground to reduce the influence of any subterranean piping or conduit. To prevent any compressive deflection of the outer cryostat, due to the cool-down of the internal components, the ends were locked into position. This configuration creates the highest elongation requirement for the conductor assembly, since in a bent installation the axial contraction could produce a lateral shifting to reduce the realized path of the conductor assembly.

Critical Current

In this configuration DC measurements were carried out at three different average temperatures.

Voltage taps placed on the cable during conductor winding were used for measurement of the voltage drop. 16 voltage taps were attached to the cable – 10 of the I_c type and 6 of the AC loss type. In the following figure 3-25 the scheme of the location of the voltage taps is reported

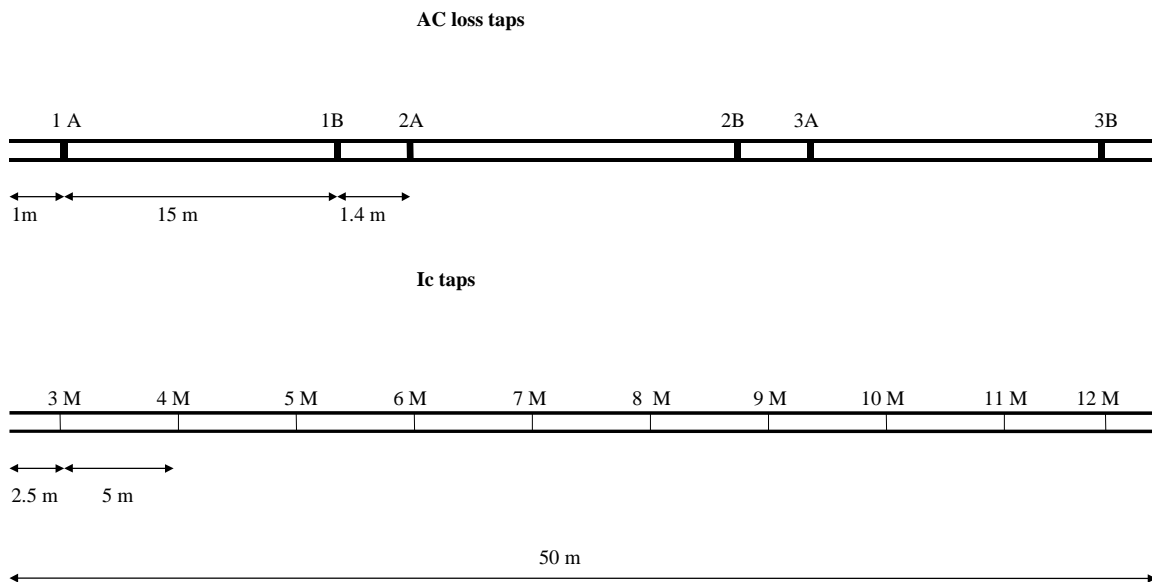


Figure 3-25
Scheme of the Voltage Taps Location along the Cable

In Figure 3-26, the DC curves measured at three different temperatures are reported: these values represent the measurements obtained with the M3-M11 voltage taps.

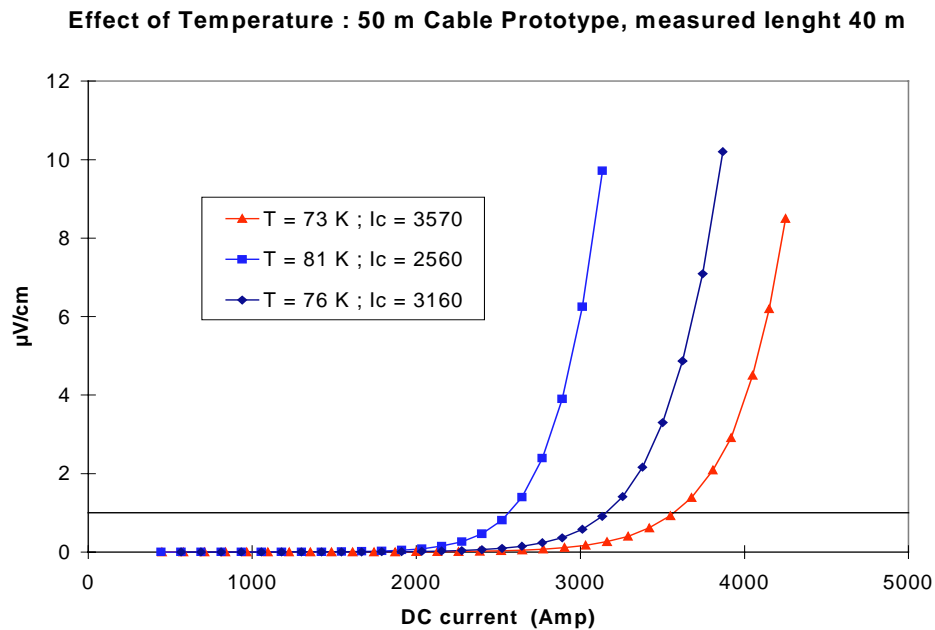


Figure 3-26
V-I Characteristics of the 50 m Prototype at Different Temperatures

The measurements on the cable conductor showed also that the conductor's critical current varies with temperature following approximately the same empirical law found for the single HTS tapes.

AC Losses

The cable's AC performance was tested in a suitably designed experimental installation, not requiring a cable joint or high voltage terminations. The cable was laid in straight configuration, using a couple of copper braids symmetrically disposed at about half a meter away from the cable for current return, as already experimented in the previous measurement on a 13 m cable conductor section (Sect. 3.2.1).

The voltage drop due to AC losses was measured using a lock-in amplifier for the measurement of the signal amplitude and an accurate phase meter for the phase angle with respect to a signal in phase with the current. The results of the AC loss measurements for the three different temperatures are reported in Figures 3-27–3-29 and compared to the prediction of the monoblock model.

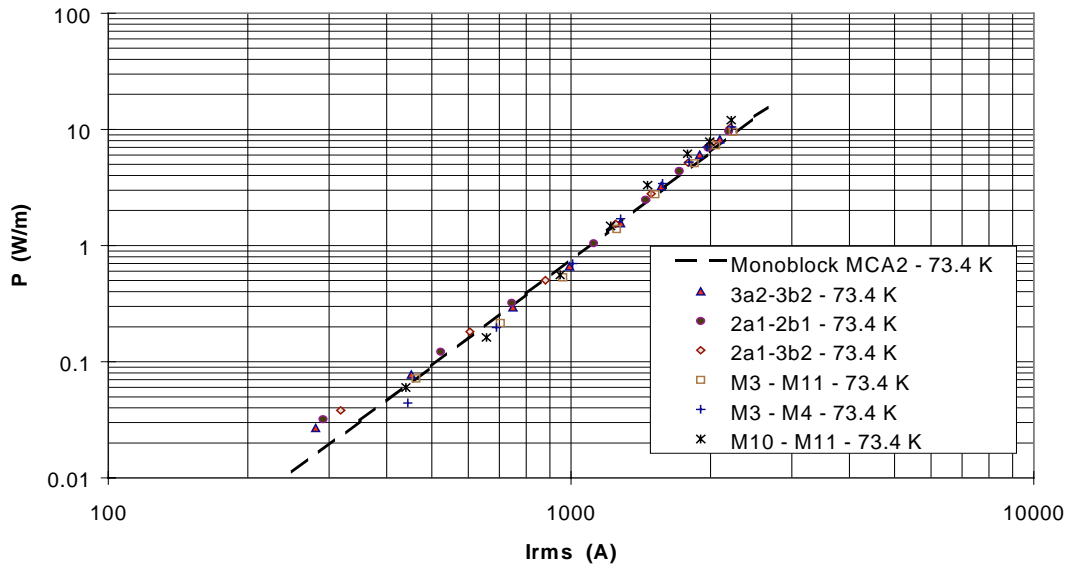


Figure 3-27
50 m cable AC Loss Measurements Vs I at 73.4K

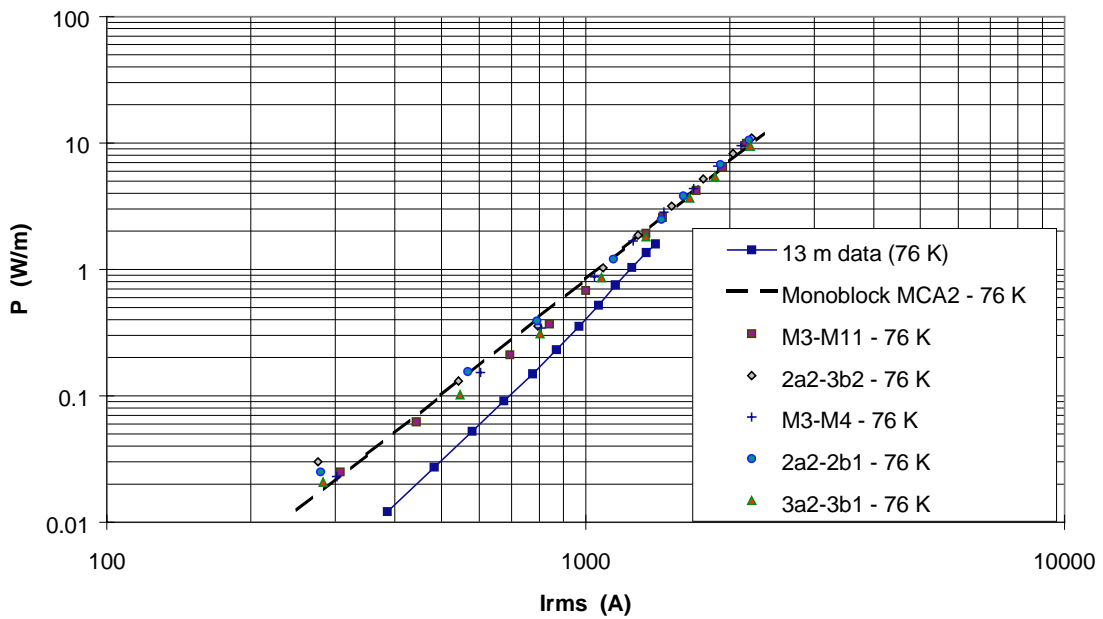


Figure 3-28
50 m Cable AC Loss Vs I at 76 K and the 13 m Sample AC Loss Vs I at 77 K

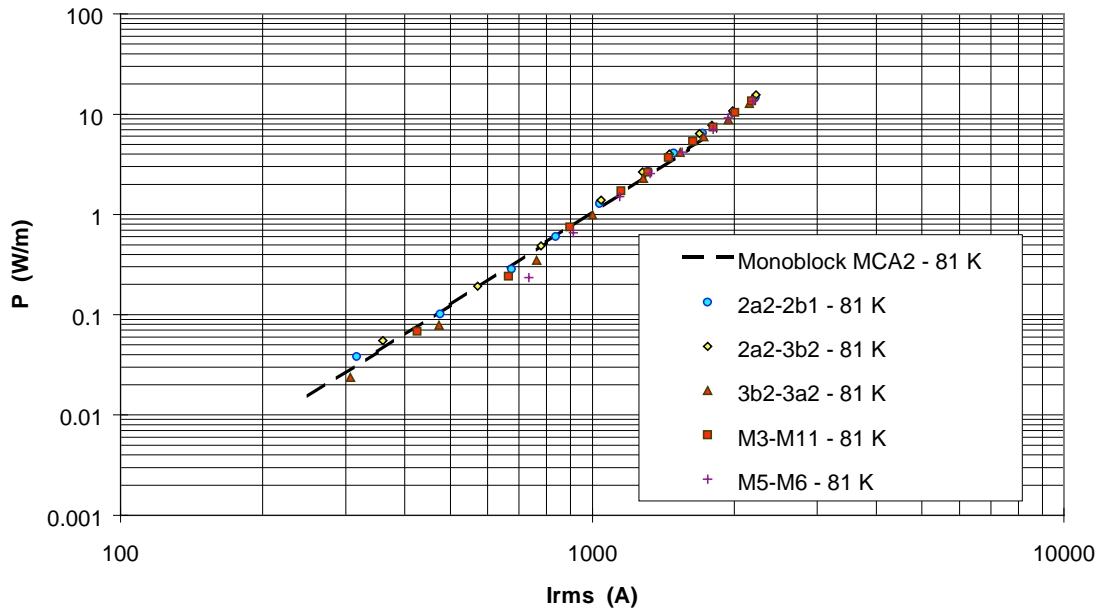


Figure 3-29
50 m Cable AC loss Vs I at 81 K

The resulting AC losses do not depend on the selected section of the cable and they are also independent of the distance between the voltage taps, indicating that the loss per unit length is correctly defined and that the 50 m cable has uniform performances.

Cryostat Effect

The AC losses measurements revealed two different contributions to the total dissipation: hysteretic losses, due to the intrinsic dissipation in the superconducting tapes, and ohmic losses, due to the current circulating in the cryostat. In fact, as can be seen in Figure 3-28, AC loss measurements on the 50 m and 13 m conductors show a considerable increase in the losses measured with the 50 m system.

The 13-m conductor showed only hysteretic losses, as it has been widely tested (See Sect. 3.2.1). An additional effect due to the presence of the cryostat was found in the 50 m cable installation because the stainless steel (SS) cryostat tubes were electrically connected between themselves and with the terminations at the cable ends. To estimate the increase in losses due to the presence of the cryostat a simplified circuit model can be used, where see Figure 3-30:

- the superconductor is assumed to be a pure inductance (with good approximation for $I < I_c$)
- the cryostat SS tube is considered a pure resistance and only the contribution of the outer tube will be included, as shown later.

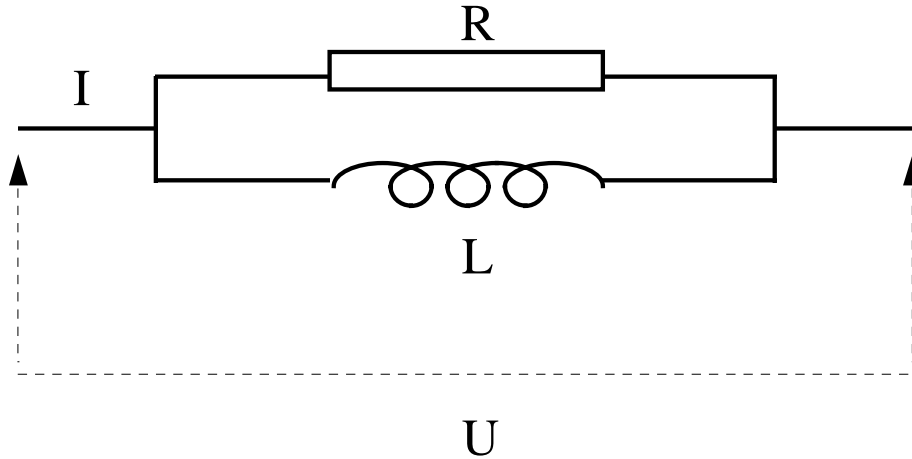


Figure 3-30
Scheme of the Circuit Model to Estimate the Additional Losses in the Cryostat

With the assumption of a purely inductive conductor, if we don't have the cryostat resistance in parallel, we would have 90° degrees phase angle between the voltage U and the current I and no losses ($\text{Re} |U| = 0$ with I real). With the cryostat in parallel instead:

$$U = Z \cdot I \tag{1}$$

where

$$Z = \frac{Z_c \cdot Z_s}{Z_c + Z_s} \tag{2}$$

$Z_c = R$	Cryostat impedance
$Z_s = i \cdot \omega \cdot L$	Conductor impedance

so

$$Z = \frac{\omega L R \cdot (\omega L + iR)}{R^2 + \omega^2 L^2} \tag{3}$$

and

$$\text{Re}|U| = \frac{\omega^2 L^2 R}{R^2 + \omega^2 L^2} \cdot I \tag{4}$$

The additional losses are then:

$$P = \text{Re}|U| \cdot I \tag{5}$$

The conductor inductance has been estimated using the following expression:

$$\frac{L}{l} = \frac{\mu_o}{2 \cdot \pi} \ln \frac{Rc}{Rs} \quad (6)$$

$Rc = \text{cryostat outer tube mean radius} \cong 30.5 \text{ mm}$
 $Rs = \text{superconductor mean radius} \cong 16.5 \text{ mm}$

so that we get:

- $R = 6 \cdot 10^{-3} \Omega/\text{m}$
- $\omega L = 3.9 \cdot 10^{-5} \Omega/\text{m}$

Due to the different order of magnitude of these quantities the inductive term can be neglected and we get the following expression for the losses:

$$\frac{P}{l} = \frac{\omega^2 L^2}{R} \cdot I^2 \quad (7)$$

The same expression holds for the inner cryostat wall, but, due to the smaller radius, losses in it would be approximately about 7% of those in the outer cryostat wall, so its contribution can be neglected in a first approximation.

In Figure 3-32, the ac loss at 76 K have been reported: the bold solid line has been obtained adding to the 13 m data the additional losses in the outer cryostat estimated above. The resulting curve is in good agreement with the experimental data on the 50m cable.

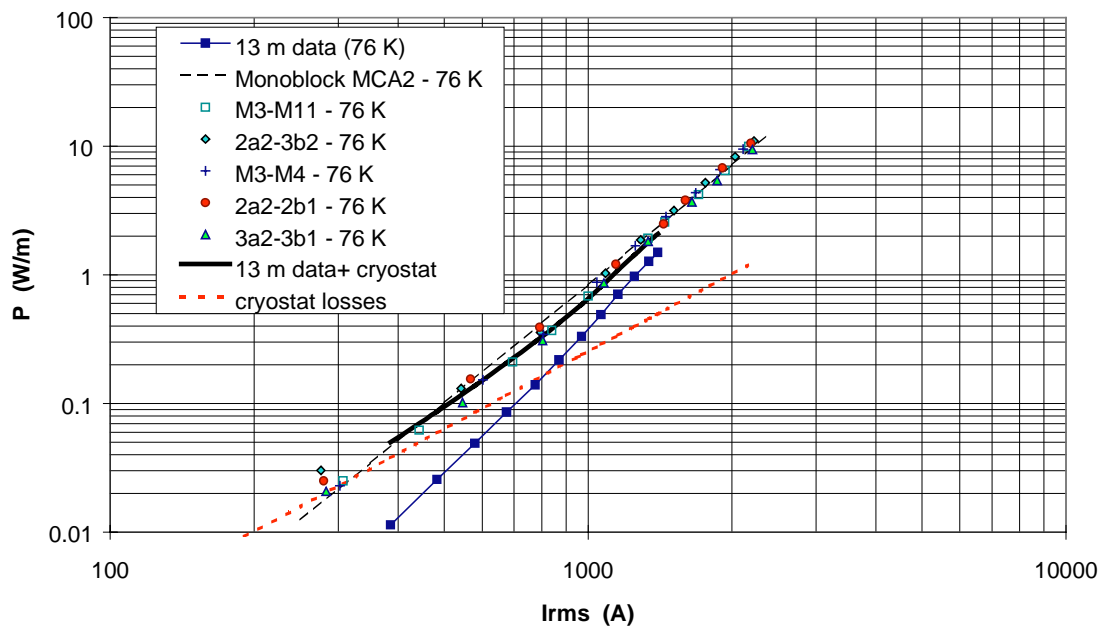


Figure 3-31
Estimation of the Additional Losses Due to Current Circulating in the Cryostat

3.8.3 Thermal and Mechanical History of the Prototype Cable: “Straight” Tests and High Voltage Installation

After the I_c and AC loss tests described above, the final preparations were made to the cable for HV installation. This process included removal of the protective lead sheath and application of moisture barrier and skid wires.

The cable was moved to the HV laboratory to be installed for HV electrical tests (as will be described in Section 3.9). In this second test installation, the cable was cut at about one third of its length and then jointed with a splice (See Section 2.5.2).

The additional mechanical and thermal history of the cable is summarized in Tables 3-3 and 3-4, below, including the straight configuration tests described earlier.

Table 3-3
Mechanical history of EPRI 50 m cable [Straight Tests → High Voltage Installation]

Actions	Manufacturing process stages
From straight measurement configuration to reel	Skid wires deposition
Unwinding from reel and installation in U configuration	HV tests installation

Table 3-4
Thermal history of EPRI 50 m cable [Straight Tests → High Voltage Installation]

Testing period	Temperature and pressure	Performed tests
July 1998 (3 weeks)	5 bar 73 - 80 K	I_c e AC loss measurements at different temperatures
14 - 15 November 1998	5 bar, 77 K	cooling tests
17 - 20 November 1998	5 bar , 77 K	I_c measurements

For the HV testing installation the cable was laid in an asymmetrical U shape, as depicted in Figure 3-32. The cable was contained in a stainless steel pipe filled with pressurized oil (the high voltage installation is detailed in Section 3.9). For the installation, it was necessary to remove some of the conductor for the fabrication of the terminations and joint. This created a different voltage taps location profile, which is illustrated in Figure 3-33.

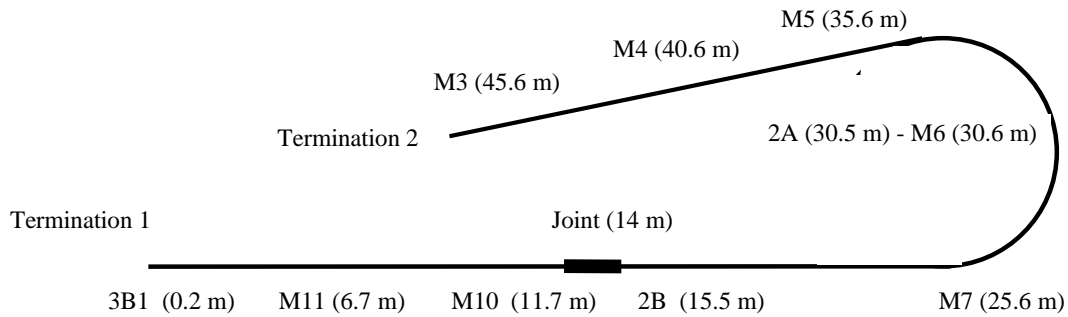


Figure 3-32
Asymmetrical U disposition for the HV test installation and voltage taps disposition. In parenthesis are reported the distances of each Vtap from termination 1.

3.8.4 Superconducting Property Testing: HV Installation Configuration

Critical Current

The critical current results at the different stages of the cable construction are reported in fig.3-33.

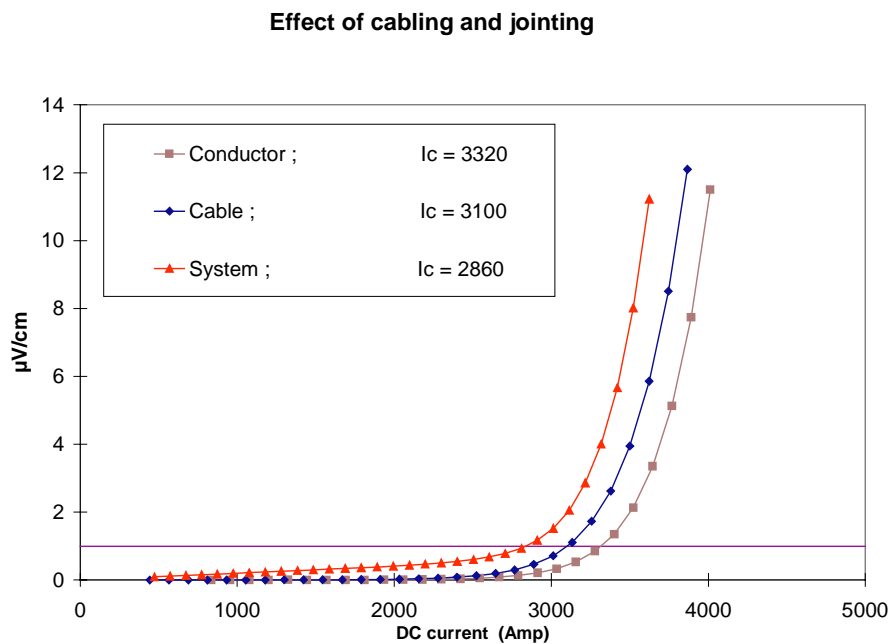


Figure 3-33
V-I Characteristic as Measured on the Conductor just After Construction, on the Cable during the AC Loss Measurement, and on the Final Complete System Comprising the Joint

In Figure 3-33, the V-I Characteristic is displayed as measured on the conductor just after construction, on the cable during the ac loss measurement, and on the final complete system

comprising the joint. It is clearly visible in Figure 3-33 that the presence of the joint introduces a small resistive voltage drop even for currents below I_c .

The V-I curve can be fitted by a power law of the form: $V \sim I^n$ as for the superconducting tapes. The value of n for the curve in Figure 3-33 has been reported in Figure 3-34.

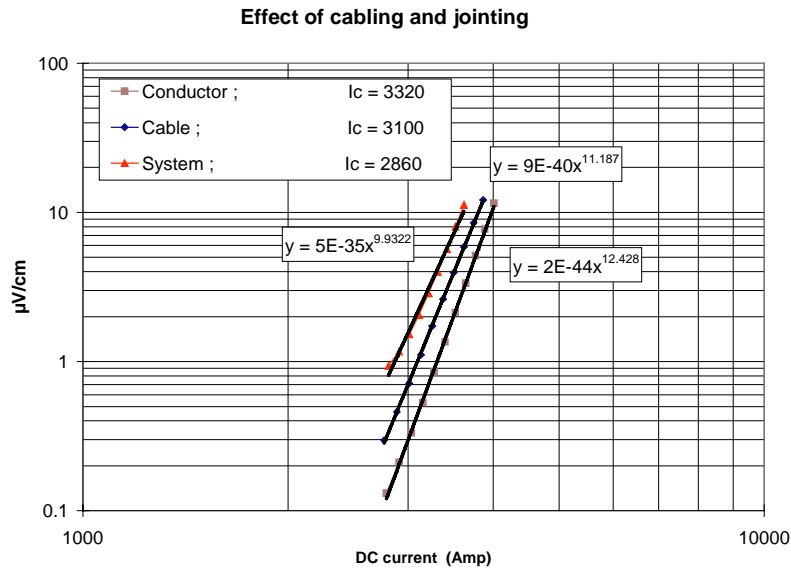


Figure 3-34
n-Value Determination for the Bare Conductor, Cable and System Configurations. Effect of cabling and jointing

3.9 High Voltage System Testing

To ensure the dielectric system design and application, four series of High Voltage tests were performed on the cable system and components. These tests included:

- Factory tests on both the mock-up and prototype cables (and component tests when applicable),
- Mock-up cable system testing (without cryogenic terminations, Feed Trough Bushing, or coolant),
- Mock-up cable system testing with the cryogenic components installed and the cable cooled,
- Final cable system tests using the 50 m prototype cable and all accessories with the cable cooled.

The results of the factory tests on the cable confirmed that the dielectric insulation had been properly applied, as shown by conformance with the applicable cable standards [3.8, 3.9, 3.10].

3.9.1 HV Testing on Mock-Up Cable without Liquid Nitrogen

The mock-up cable, see section 2.4.6, was installed with conventional terminations and joint. A series of tests based on AEIC CS2/97 were performed to verify all of the component designs and their implementation. These tests were performed prior to installation of the cryogenic components to isolate any affect that those additional accessories and the LN₂ coolant might create.

The tests performed and their conditions are summarized in Table 3-5.

Table 3-5
Mock-up Cable High Voltage Testing Summary (without LN₂)

Test	Test Parameter	Test Result
Ionization factor test	Voltage level: (8, 10, 20, 30, 40, 50, 60, 70, 80) kV r.m.s.	Satisfactory (1.16 – 1.18)X10E-3
Power factor measurement vs. temperature	Voltage level: 115 kV r.m.s. Oil temperature (pipe): 21 °C, 55 °C, 75 °C)	Satisfactory (1.21X10E-3, 1.14X10E-3, 1.33X10E-3)
HVAC test	Voltage level: 165 kV (r.m.s.) Voltage applied for: 24 hours	NO BREAKDOWN
HVAC test (sealing end investigation)	Voltage level: 205 kV (r.m.s.) Voltage applied for: 1 min.	NO BREAKDOWN
HVDC test (joint investigation)	Voltage level: 275 Kv Voltage applied for: 15 min.	NO BREAKDOWN
HOT LIGHTNING IMPULSE WITHSTAND TEST	Oil temperature (pipe): 75 °C Starting Voltage: 400 kV Final Voltage: 550 kV Step Voltage: 25 kV Shots per step: 10 shots both polarity Polarity sequence: +,-/+,+/-,+/-,-	NO BREAKDOWN
HVAC TEST AFTER LIGHTNING IMPULSE	Voltage level: 120 kV r.m.s. Voltage applied for 15 min.	NO BREAKDOWN

Test Assembly Description

The mock-up cable system was installed in such a way that it could be tested in the absence of the cryogenic-specific components (except the joint assembly). The cable was pulled into the pipe enclosure as a continuous element and the section to be jointed cut in situ. The two conventional terminations were installed with the cryostat sealing ends completed, but without the cryogenic terminations and Feed Through Bushing.

On each terminations the cable screen could be sectionalised from the terminations themselves to permit the measurement of tan delta for the cable only, excluding the contribution of terminations.

Cable connector NEMA pads were brazed to the pipe enclosure just below the termination assembly. To heat the cable system to the necessary test temperatures, current was passed through the length of the pipe enclosure. Jumper lines connected each pipe section to ensure electrical conductivity and avoid “hot spots” at the pipe connection locations. Thermal insulation was wrapped around the pipe.

Ionization Factor

The ionization factor for the cable was measured with the dielectric at ambient temperature. Measurements were taken at voltages ranging between 8 kV and 80 kV, as listed in Table 3-5, above. The results showed that the cable exhibits a satisfactory ionization factor.

Power Factor / Dielectric Power Factor

The power factor for the cable was measured at various temperatures and voltages, as listed above. The temperature was controlled using the heating tapes described earlier. The results showed that the cable exhibits satisfactory Power Factor levels.

HV AC Time Test

As soon as the power factor measurements were completed (with the cable at ambient temperature), the voltage was increased in order to reach the voltage level of 165 kV ($2.5 U_0$). The assembly has been kept at this voltage level for 24 hours with no breakdown or flash-over.

HV AC Termination Test

In order to test the termination assembly the voltage level was increased to 205 kV (and kept at this level for 1 minute) with no breakdown or flash-over.

HV DC Joint Test

The voltage was increased to 205 kV and kept at this value for 5 minutes. Immediately after the 5 minutes, the voltage was increased to 275 kV for 15 minutes. No breakdown or flash over occurred.

Lightning Impulse Test

The dielectric system was warmed to the test temperature (75 °C) and tested for impulse breakdown using the heating tapes and thermal insulation.

The waveform of the impulse used was as follows:

FRONT TIME:	1.78 μ s
TIME TO HALF VALUE:	58 μ s

The lightning impulse test was performed as follows:

Starting Voltage:	400 kV
Starting Polarity:	Positive
Step Voltage:	25 kV
Shots per Step:	10 (+) Polarity 10 (-) Polarity
Polarity Sequence:	+/-, +/-, +/-, ...
Final Voltage:	+/-550 kV

No breakdown or flash-over was detected during this test.

HV AC Proof Test

Following the Lightning Impulse test, the equipment was changed so that an AC Proof test could be conducted. This test verifies the integrity of the dielectric insulation to indicate if any puncture has occurred, but remained undetected.

Cable voltage was increased to 120 kV (1.67 U_0) for 15 minutes with no breakdown or flash-over.

3.9.2 High Voltage Mock-Up System Tests – with Liquid Nitrogen

After verifying the correct operation of the conventional insulation system, the cryogenic components unique to the WD cable system were assembled and the system cooled to operating temperatures

The same series of tests were performed, except the HVAC test after lightning impulse. The Hot Impulse Test has been extended to 625 kV, as detailed in Table 3-6 below.

**Table 3-6
Mock-up Cable High Voltage Testing Summary (with LN₂)**

Test	Test Parameter	Test Result
Ionization factor test	Voltage level: (8, 10, 20, 30, 40, 50, 60, 70, 80) kV r.m.s.	Satisfactory (1.16 – 1.18)X10E-3)
Power factor measurement vs. temperature	Voltage level: 115 kV r.m.s. Oil temperature (pipe): 21 °C, 55 °C, 75 °C)	Satisfactory (1.21X10E-3, 1.14X10E-3, 1.33X10E-3)
HVAC test	Voltage level: 165 kV (r.m.s.) Voltage applied for: 24 hours	NO BREAKDOWN
HVAC test (sealing end investigation)	Voltage level: 205 kV (r.m.s.) Voltage applied for: 1 min.	NO BREAKDOWN
HVDC test (joint investigation)	Voltage level: 275 kV Voltage applied for: 15 min.	NO BREAKDOWN
HOT LIGHTNING IMPULSE WITHSTAND TEST	Oil temperature (pipe): 75 °C Starting Voltage: 500 kV Final Voltage: 625 kV Step Voltage: 25 kV Shots per step: 10 shots both polarity Polarity sequence: +,-/+,+/-,+/-,+/-,-	NO BREAKDOWN
HVAC TEST AFTER LIGHTNING IMPULSE	Voltage level: 120 kV r.m.s. Voltage applied for 15 min.	NOT PERFORMED

Test Assembly Description

The cryogenic components were then added so that the complete mock-up cable system could be tested with the conductor, terminations, and FTB at nominal operating temperatures. The vacuum within the cable cryostat was created and sealed, as well.

To avoid stray currents through cryogenic transfer lines (made from stainless steel and in contact between the pipe enclosure and the ground), instead of heating the oil via Joule effect in the pipe, heating tapes were wrapped around the pipe to heat the cable system. Again, thermal insulation was wrapped around the pipe.

Ionization Factor

The ionization factor for the cable was measured with the dielectric at ambient temperature and the conductor assembly cooled to approximately 75 K. Measurements were taken at voltages ranging between 8 kV and 80 kV, as listed in Table 3-6, above. The results showed that the cable exhibits a satisfactory ionization factor.

Power Factor / Dielectric Power Factor

The power factor for the cable was measured at various temperatures and voltages, as listed above. The temperature was controlled using the heating tapes described earlier. The conductor assembly was cooled to approximately 75 K. The results showed that the cable exhibits satisfactory Power Factor levels.

HV AC Time Test

As soon as the power factor measurements were completed (with the cable at ambient temperature), the voltage was increased in order to reach the voltage level of 165 kV ($2.5 U_0$). The assembly has been kept at this voltage level for 24 hours with no breakdown or flash-over.

HV AC Termination Test

In order to verify the cryogenic terminations (including the FTB) the voltage level was increased to 205 kV (and kept at this level for 1 minute) with no breakdown or flash-over.

HV DC Joint Test

The voltage was increased to 205 kV and kept at this value for 5 minutes. Immediately after the 5 minutes, the voltage was increased to 275 kV for 15 minutes. No breakdown or flash over occurred.

Lightning Impulse Test

The dielectric system was warmed to the test temperature (75 °C) and tested for impulse breakdown using the heating tapes and thermal insulation, and the conductor assembly was cooled to approximately 80 K.

The waveform of the impulse used was as follows:

FRONT TIME: 1.78 μ s

TIME TO HALF VALUE: 58 μ s

The lightning impulse test was performed as follows:

Starting Voltage:	500 kV
Starting Polarity:	Positive
Step Voltage:	25 kV
Shots per Step:	10 (+) Polarity 10 (-) Polarity
Polarity Sequence:	+/-, +/-, +/-, ...
Final Voltage:	+625 kV

3.9.3 High Voltage Test of the 50 m Prototype Cable System

The dielectric system used for the Mock-up and Prototype cables was virtually identical. The only real differences between the two cables were the length and the presence of superconducting tapes rather than aluminum. Fundamentally, there should be no change with regards to dielectric performance.

As discussed in Section 3.8.3, the complete cable system (including HV terminations, joint, dielectric fluid pressurization system, and cryogenic accessories) was installed in a laboratory suited for High Voltage test and measurement. The cable installation is shown by the photograph in Figure 3-35.



Figure 3-35
50 m Prototype Cable Installation in High Voltage Testing Facility

The testing program implemented was based on the applicable cable standards [3.8, 3.9, 3.10] and was virtually identical to that used for the testing of the Mock-up cable. The only difference between the programs are that the Hot Impulse Test was completed at 550kV. The tests performed are described below in Table 3-7.

**Table 3-7
High Voltage Testing Summary on Prototype Cable**

Test	Test Parameter	Test Result
Ionization factor test	Voltage level: (8, 10, 20, 30, 40, 50, 60, 70, 80) kV r.m.s.	Satisfactory (1.37 – 1.64)X10E-3)
Power factor measurement vs. temperature	Voltage level: 115 kV r.m.s. Oil temperature (pipe): 16 °C, 55 °C, 75 °C)	Satisfactory (1.36X10E-3, 1.09X10E-3, 1.04X10E-3)
HVAC test	Voltage level: 165 kV (r.m.s.) Voltage applied for: 24 hours	NO BREAKDOWN
HVAC test (sealing end investigation)	Voltage level: 205 kV (r.m.s.) Voltage applied for: 1 min.	NO BREAKDOWN
HVDC test (joint investigation)	Voltage level: 275 kV Voltage applied for: 15 min.	NO BREAKDOWN
HOT LIGHTNING IMPULSE WITHSTAND TEST	Oil temperature (pipe): 75 °C Starting Voltage: 450 kV Final Voltage: 550 kV Step Voltage: 25 kV Shots per step: 10 shots both polarity Polarity sequence: +,-/+,+/-,+/-,+/-,-	NO BREAKDOWN
HVAC TEST AFTER LIGHTNING IMPULSE	Voltage level: 120 kV r.m.s. Voltage applied for 15 min.	NO BREAKDOWN

Test Assembly Description

Two cable samples (one approximately 15 m in length and the other approximately 35 m long) have been pulled inside in the pipe enclosure. A joint was installed (as described in Section 2.5.2) to continue the electrical conductivity and the dielectric and thermal insulation systems. On each cryogenic terminations the cable screen could be sectionalised from the terminations themselves (to permit the measurement of tan delta for the cable only, excluding the contribution of terminations).

In order to allow the cable feeding with High pressure Liquid Nitrogen (HPLN) and the cryogenic terminations feeding with Low Pressure Liquid Nitrogen (LPLN) the Feed Trough Bushing has been assembled and placed between the two cryogenic terminations. (As discussed in Section 2.5.3, the FTB breaks the electrical continuity of standard metallic liquid nitrogen transfer lines).

To heat the dielectric oil and insulation, electrical resistance heating tapes were wound around the pipe enclosure, and covered with thermally insulating tapes. By maintaining a constant outer temperature, with no internal heating, the temperature of the dielectric fluid and insulation can be accurately controlled to meet the temperatures specified in the testing standards.

Ionization Factor

The ionization factor for the cable was measured with the dielectric at ambient temperature and the conductor assembly cooled to approximately 75 K. Measurements were taken at voltages ranging between 8 kV and 80 kV, as listed in Table 3-7, above. The results showed that the cable exhibits a satisfactory ionization factor.

Power Factor / Dielectric Power Factor

The power factor for the cable was measured at various temperatures and voltages, as listed above. The temperature was controlled using the heating tapes described earlier. The conductor assembly was cooled to approximately 75 K. The results showed that the cable exhibits satisfactory Power Factor levels.

HV AC Time Test

As soon as the power factor measurements were completed (with the cable at ambient temperature), the voltage was increased in order to reach the voltage level of 165 kV (2.5 U₀). The assembly has been kept at this voltage level for 24 hours with no breakdown or flash-over.

HV AC Termination Test

In order to verify the cryogenic terminations (including the FTB) the voltage level has been increased again up to 205 kV (and kept at this level for 1 minute with no breakdown or flash-over).

HV DC Joint Test

The voltage was increased to 205 kV and kept at this value for 5 minutes. Immediately after the 5 minutes, the voltage was increased to 275 kV for 15 minutes. No breakdown or flash over occurred.

Lightning Impulse Test

The specified thermal conditions, 75 °C isothermal in the pipe, were reached with the same method used during the power factor measurement while the conductor was cooled to approximately 75 K.

The waveform of the impulse was as follows:

FRONT TIME: 3.40 us

TIME TO HALF VALUE: 44.90 us

The Lightning impulse test has been carried out as follows:

Starting Voltage: 450 kV

Starting polarity: POSITIVE

Step Voltage: 25 kV

Shots per step: 10 both polarity

Polarity sequence: POS - NEG / NEG – POS / POS – NEG / ...

Final Voltage: 550 kV (B.I.L.)

The assembly withstood, without any breakdown or flash over, 10 shots at 550 kV in positive polarity followed by 10 shots at 550 kV in negative polarity.

HV AC Proof Test

The assembly, after the lightning impulse test, was submitted to the HV AC Proof Test. This test applies an AC voltage of 120 kV ($1.67 U_0$) for 15 minutes with no breakdown or flash-over.

3.9.4 Impulse Testing of the Feed Through Bushing

The Feed Through Bushing represents the only component which must satisfy both thermal and dielectric functions simultaneously. Because its particular design is unique to the WD cable system, there was no previously available commercial operating experience on which to compare its performance. Consequently, tests were designed to determine its ultimate impulse breakdown resistance, as well as to determine its principal breakdown mechanism.

The FTB assembly was completed and LN₂ bypass loops made so that the channels which convey the sub-cooled LN₂ (no vapor bubbles present) were connected to make a closed-loop to and from the refrigeration plant. The other channels, which carry saturated and evaporated nitrogen into and out of the cable system, were filled with both saturated nitrogen (mostly liquid) and nitrogen gas.

The system was cooled for sufficient time for the thermal profile through the bushing to be reached and then impulse tested.

The waveform of the impulse was as follows:

FRONT TIME: 2.60 us

TIME TO HALF VALUE: 59.92 us

The Lightning impulse test has been carried out as follows:

Table 3-8
Hot lightning Impulse Test on FTB

Hot lightning impulse test up to breakdown	Starting Voltage: 450 kV Final Voltage: breakdown or flash over Step Voltage: 25 kV Shots per step: 10 shots both polarity Polarity sequence: +,-/-,+/-,-,+/-,-/.....	BREAKDOWN AT + 828 kV (withstood 10 shots at – 850 kV)
--	---	--

The FTB withstood as shown in Table 3-8, without any breakdown, 10 shots at 825 kV in positive polarity followed by 10 shots at 825 kV in negative polarity. Furthermore, the FTB passed 10 shots in negative polarity at 850 kV. Subsequently, during the depolarization, a breakdown occurred in the FTB at 828 kV in positive polarity. Therefore the 850 kV level was not reached in positive polarity. A second shot, performed with the same charging voltage on the Impulse Generator, has been applied to the FTB: the breakdown has been confirmed. This result indicates that the FTB under test has a 50% margin over the 550 kV BIL.

3.9.5 Conclusions

A dielectric system was designed and applied to a HTS cable that could provide the necessary level of mechanical and electrical resistance. Furthermore, the dielectric could be applied in a manner consistent with industrial practice, both in the factory and in the field.

The dielectric system (cable and accessories) was shown to perform beyond the criteria established for phase to phase or phase to ground voltages. Furthermore, the new system component (i.e. the FTB) was shown to exhibit at least an impulse breakdown strength that was 50% greater than the required design BIL.

3.10 Test of the cryogenic cooling system

Before connecting the cryogenic cooling plant to the cable system, tests were conducted to evaluate the performance of the system.

Because these tests were performed without the cable system, a test connection was introduced to close the flow loop. The function of this pipe was to permit controlled and measurable heat input to the system, while minimizing its effect on the other flow parameters.

Description of the test loop

The test setup consists of the refrigeration system connected with a test loop. The test loop is comprised of a pipe 6 ft (1.8 m) long which is connected to the refrigerator by two flexible transfer lines. The pipe serves as the resistive heating element of the test setup. Copper strips silver soldered to the pipe serve as electrical connection points. Electrically insulating flanges on each end prevent current from passing through the transfer lines to ground. The heater is powered by a current transformer and a variable voltage supply to supply current to the pipe.

Fiberglass blanket insulation was wrapped around the pipe to serve as thermal insulation (however all results are normalized against the zero current temperatures).

Cool down

The response of the refrigerator to lower operating temperatures is limited by the design of the refrigerator. This time also represents the time constant for system temperature change due to loading fluctuations. The time needed for changing the temperature of the cooling equipment was measured starting with the subcooler dewar filled with LN₂ at saturation at atmospheric pressure. The vacuum pump was activated (at t=0) and the temperature in the loop monitored.

Conditions in the test loop:
pressure 160 psig (12 bar absolute)
flow rate: 0.36 kg/s (100% nominal pump speed)

The loop temperature as a function of time is showed below in Figure 3-36:

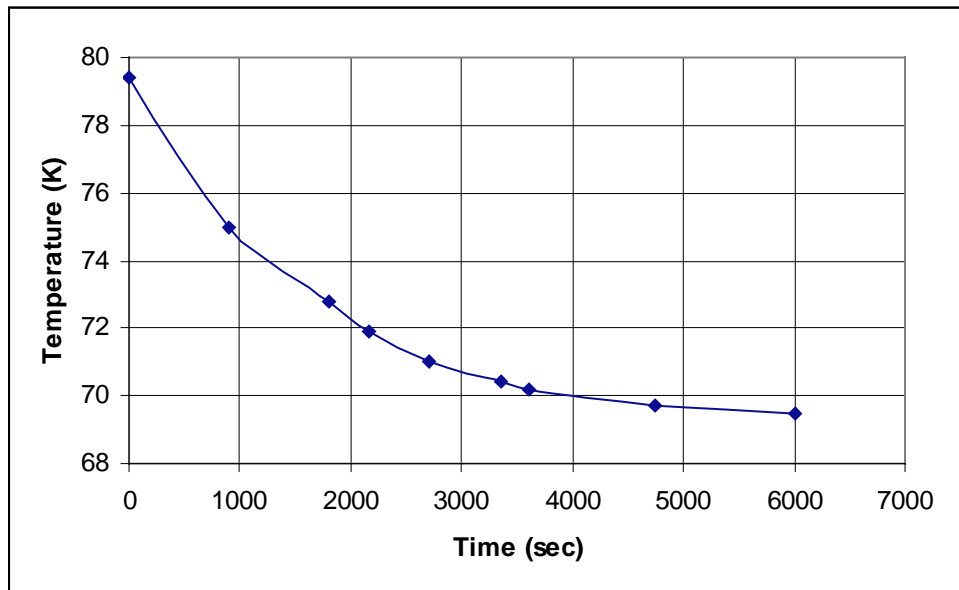


Figure 3-36
Cool-Down of Subcooler Bath

3.10.1 Functional evaluation

The refrigerator's performance has been verified for its ability to remove heat generated externally. Three different thermal loads have been applied via the test assembly. For each thermal load three different pump speeds were studied.

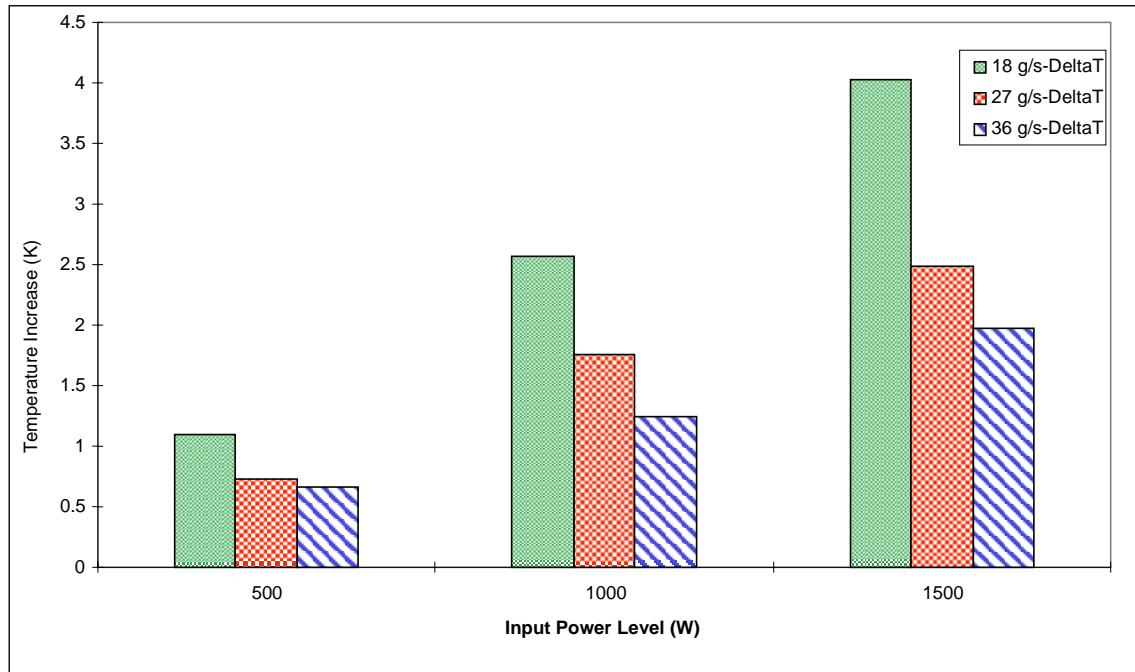


Figure 3-37
Temperature Rise through Test Loop at Different Powers and Flow Rates

In each case, temperature at the inlet and at the outlet of the pipe have been measured. The results obtained, are shown in the following figure 3-37.

Loss of Cooling

Because of the cable's high surface to volume ratio, it requires continuous removal of thermal energy. In the event that the cooling system is lost, the temperature in the cable will begin to increase and ultimately LN₂ will begin to boil in the circuit resulting in a pressure rise. To evaluate the effect of this condition on the cable, the worst possible conditions related to a loss of cooling were simulated.

The actual cable response is dependent upon the cable operating conditions, particularly the margin between saturation temperature and pressure. The conditions for the test were selected to represent a very severe test of the system response. The temperature at the inlet to the cable was approximately 75 K and the system operating pressure 50 psig. At the beginning of the test, the LN₂ circulating pump was stopped (which simulates a loss of cooling power), and the cable isolated from the pressure buffer tank.

The temperature in the cable increased immediately. As the volume of gas accumulates, it provides a buffer to the increase in nitrogen volume and the rate of pressure increase slows. After 780 sec (13 min) the pressure in the system had increased by 100 psi and the test was terminated. Almost immediately upon restarting the LN₂ circulation pump and opening the pressure buffer valve, the pressure returned to normal operating limits.

Had the LN₂ circulation pump been enabled during the test, the system response would have been slowed by an averaging of the system losses over the thermal mass of the circuit. This method provided a Loss of Pumping (therefore a Loss of Cooling too). The combination of these tests results in the most severe test of the system response.

The pressure response with time is shown in Figure 3-38.

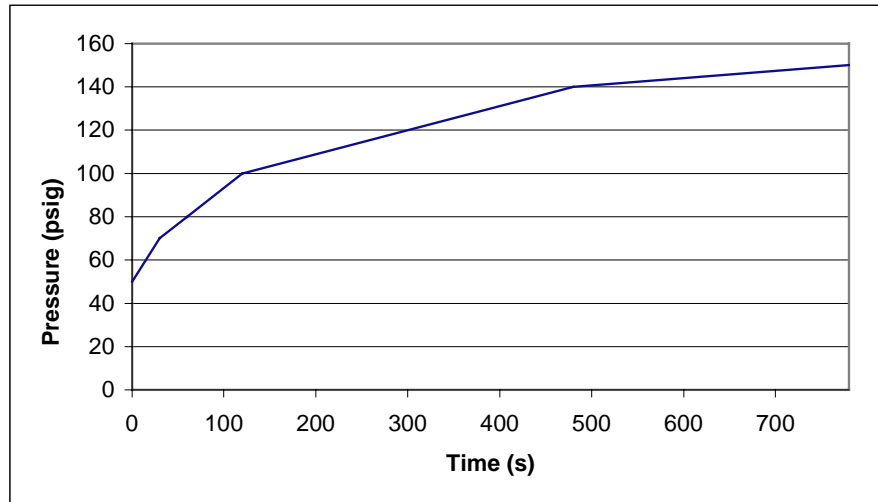


Figure 3-38
Pressure Response of Cable System to Loss of Cooling

Loss of Pumping

The Loss of Pumping to the cryogenic system means that the LN₂ circulation pump has failed. This condition could be caused by a number of problems, including component failure or loss of power. The circulation of LN₂ is the most critical factor for operation of the cable system. Without flow, the losses in the lower efficiency areas (terminations, FTB) cause a localized increase in temperature and possibly boiling of the LN₂. Loss of Pumping cause the LN₂ to stop. Thus there will be no more heat exchange with the sub-cooled bath, with consequently increase of coolant temperature and pressure.

As discussed earlier, this test was performed concurrently with the Loss of Cooling test, as they are inseparable in an evaporative cooling system.

Conclusions

The cooling plant, because of its design based on a sub-cooled bath of LN₂, has an ideal minimum operating temperature of 63. 2 K (triple point of nitrogen). Before its installation in the cable system, the cooling plant capacity to remove heat load up to 2 kW has been successfully verified. Loss of Cooling and Loss of Pumping tests have been performed. Resuming of cooling and pumping shown cooling plant capability to recovery normal operating limits in few minutes, without any damage.

3.11 Pipe Loss Verification

The primary advantage of HTS cable systems is that they can provide significant increases in cable ampacity without increasing cable diameter. Conventional cables suffer the obvious limitation in that the resistive losses in the conductor increase with the current squared. A less obvious, but no less important, loss component for pipe-type cable systems are the induced power losses of the steel pipe enclosure. The techno-economic evaluation of HTS cable systems depends upon all loss mechanisms, and the pipe losses at very high currents can become appreciable.

Existing standards for pipe-type cable systems [3.11] calculate the pipe loss contribution to the total system losses as described in the 1957 paper by Neher and McGrath. This seminal paper drew extensively from its references to compile a comprehensive treatment of the available body of empirical and theoretical studies [3.12]. Over the 40 years since this article was published, further experimental and practical activity has verified its methods and provided the basis for revisions that now are used as cable standards. As the empirical studies and practical experience have been focused on standard conventional cable systems, there is little published experience regarding the suitability of these techniques beyond the typical range of cable ampacities. The current cable construction and performance standards indicate that this range extends to a maximum ampacity of 1800 A. As the practical realities of a conventional cable system limit the current capacity, there has been little motivation to examine the suitability of the Neher-McGrath method to very high currents (over 3000 A).

To confirm the accuracy of the current pipe-loss calculation tools at very high current, a series of experiments was conducted to determine empirically the AC losses due to pipe-cable interaction in this current range.

There are several mechanisms that can be measured to reveal the magnitude of power loss due to the pipe enclosure. As the power loss is transferred from the conductors to the pipe, either the lost energy can be measured directly from the cables or the absorbed energy can be measured directly from the pipe.

Measuring the energy lost from the cables can be performed by evaluating the Watt-power (real) in the cable with and without the pipe enclosure. Comparing the magnitude of real power in the circuit yields the amount of power transferred to the pipe enclosure. A method, known as the Aron Method, based on this premise was used to measure electrically the losses in the system.

The alternative to measuring power lost by the cable circuit is to measure the power absorbed by the pipe enclosure. The simplest technique for measuring the power being transferred to the pipe is calorimetry. As energy accumulates in the pipe, its temperature will increase at a rate proportional to its power absorption. By taking the time derivative of the pipe temperature and comparing this with the thermal mass of the pipe, the power consumption can be calculated.

3.11.1 Experimental Installation

The experimental circuit installed consisted of a 75 m long feeders and the necessary equipment for supplying the power and for taking and recording measurements. A variable voltage (0 to 760 V) 100 kVA power supply and 12 transformers (four for each cable) were used. The maximum current rating for the setup was 3500 A. The feeder consisted of three XLPE unshielded insulated cables with approximately 750 kcmil (1600 mm²) Milliken copper conductors, having an outer diameter of 116 mm. Unshielded cables were used to avoid any induced currents.

The pipe, placed on ground over wood supports, was thermally isolated with a felt layer 16 mm thick, providing the same thermal resistance as a pipe buried in soil at a depth of 4.92 ft (1500 mm).

The feeder was connected by means of flexible copper conductors which could be easily disconnected to remove the metallic pipe. At the end of the feeder the three conductors are short-circuited by means of a copper connector, see Figure 3-39.

The three long cable were installed in a pipe enclosure made from carbon steel and with an outer diameter of 12 in. (298 mm), see figure 3.40. The thickness of the pipe was nominally 0.32 in. (8 mm). A typical HPFF cable system would use a carbon steel pipe with an outer diameter of 8.63 in. (219 mm) with a wall thickness of 0.32 in. (8mm).

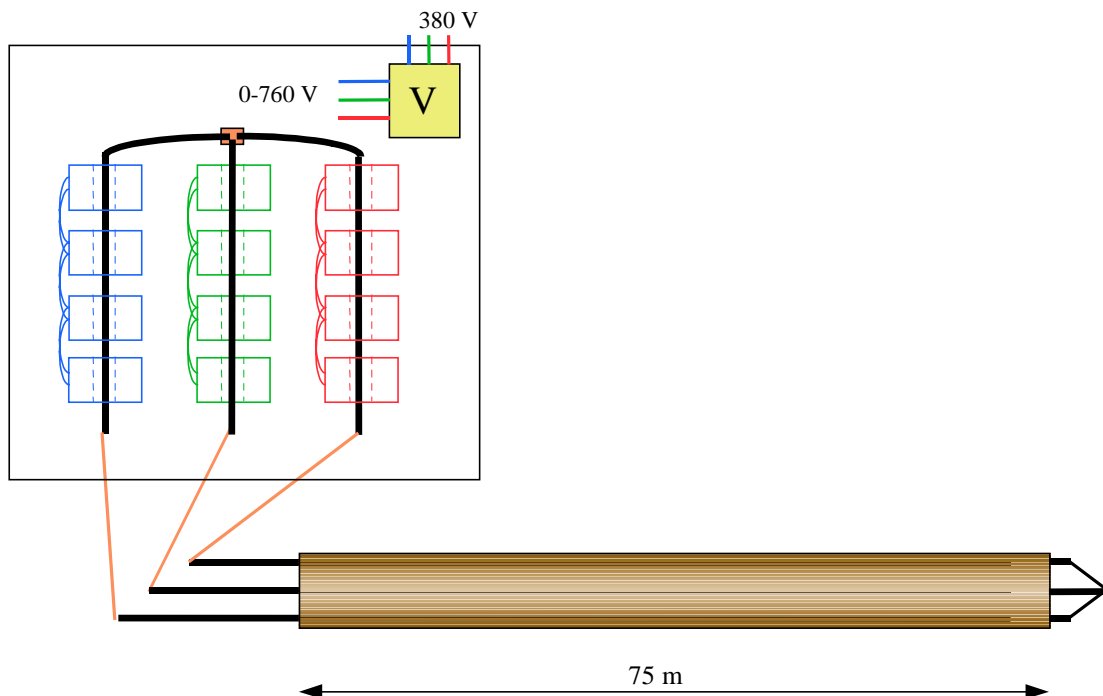


Figure 3-39
Experimental Setup

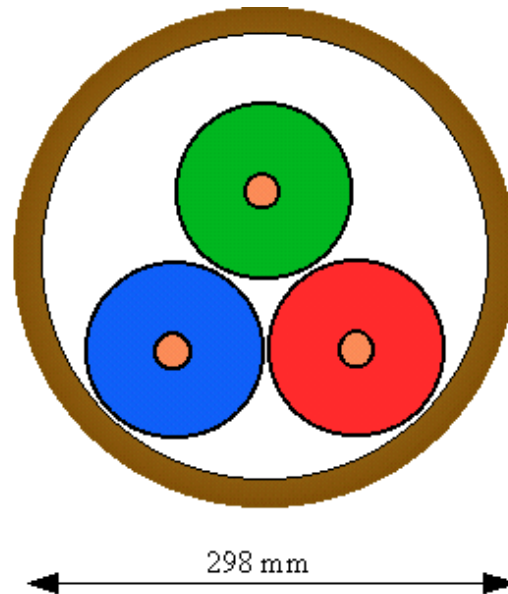


Figure 3-40
Cable Configuration Inside the Pipe

3.11.2 Measurement Methods

Aron Method

The measurement of the power dissipated by an isolated three-phase line (i.e. without neutral conductor or grounding cable) can be obtained using Aron method. This technique uses watt-meters on two phases and the voltage of the third phase, which is taken as a reference. The active power flowing in the two phases is measured and the power dissipated by the line calculated as the algebraic difference of the powers measured by the two watt-meters. The measurement of the dissipated power has been carried out both with and without the pipe. This technique suffers from pipe proximity effect, which add a loss contribution that cannot be separated from the pipe loss.

Calorimetric Technique

A calorimetric technique was the second technique used. The eddy currents and the hysteresis of the steel pipe causes heat generation, and consequently the pipe temperature increase. The loss (Q) can be calculated by comparing the rate of temperature rise (dT/dt) to the thermal capacity of the steel pipe (C) as shown in the formula:

$$Q = C \frac{dT}{dt}$$

where;

Q = Losses in the Pipe [W]

C = Thermal Capacity of the Pipe [kJ/kg-°C]

$\frac{dT}{dt}$ = Time rate of Change of the Temperature [°C/s]

Starting from time equals zero, the system is nearly isothermal and all of the temperature rise can be attributed to the pipe losses. Applying a current step, the steel pipe undergoes a temperature increase that is initially linear. Because no temperature gradients have developed, thermal coupling between the cable and the pipe and the pipe and the ambient will not occur. This measurement, however, considers the pipe enclosure at room temperature, so the temperature dependence of the pipe's resistance is not evaluated (a material resistance change of <10%).

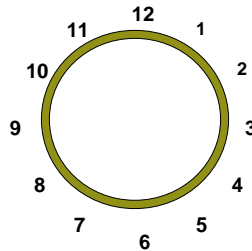


Figure 3-41
Position of Thermocouples around Pipe Enclosure

The pipe has been provided with 12 thermocouples placed as shown in Figure 3-41. The thermally insulating felt placed around the pipe created a system where the small temperature gradients (at time near zero) creates virtually no heat transfer to the ambient.

3.11.3 Experimental Description

A series of measurements were carried out to determine the pipe losses using different methods and different current levels. Two testing methods were used, because each compensates an experimental artifact of the other..

Aron Method

For the Aron measurement technique, see previous section, the system was permitted to operate for enough time to reach a thermal equilibrium similar to that that could be expected for an actual system. This reduces any error due to the temperature dependence of the pipe resistance. This technique, however, has a fundamental limitation in that the pipe losses are deduced from the conductor losses and must assume that the conductor losses are constant with and without the pipe enclosure. This is not an accurate assumption for the actual situation. There is a coupling of the magnetic fields of the cables and the pipe that causes an increase in losses in the cables.

Because this loss cannot be separated from the losses induced in the pipe, the total losses measured will be greater than the losses generated only in the pipe

The measurement of the dissipated power has been carried out with and without the pipe enclosure. The difference of the two values is reported in Figure 3-42. It can be noted that the losses depend on I^2 : particularly the pipe losses are 44.7 W/m at 1550 A and 187.7 W/m at 3090 A.

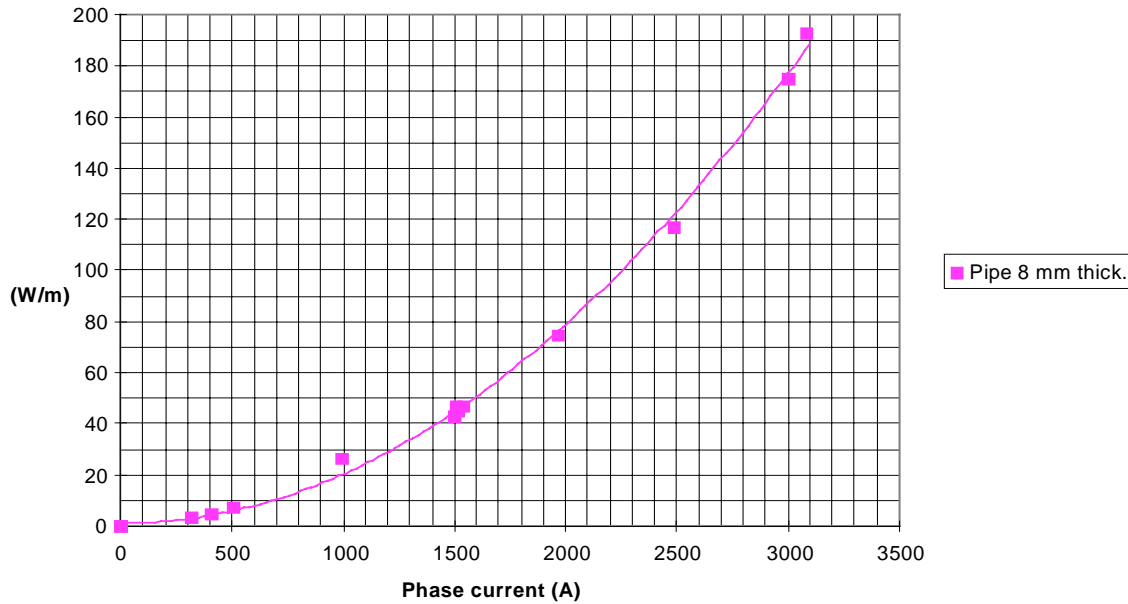


Figure 3-42
Mean Total Dissipated Power as a Function of Current

Calorimetric Method

Measurements using the calorimetric technique isolate the electromagnetic coupling effect and reveal only the pipe losses. To achieve this isolation, the temperature measurements are recorded at the beginning of the experiment. Measurements taken later will begin to include the effects of thermal coupling between the cables and the pipe and the pipe and the environment. After a sufficient amount of time, the time rate of change for the temperature will approximate to zero and the system will have reached its steady state. At this point, the total amount of energy being dissipated in the conductors and the pipe is transferred to the environment through the felt insulation.

Figure 3-43, below, shows the rate of change for the temperature increase for the initial time period, up to 5 minutes. Three peaks are present at positions 4, 7 and 12 in correspondence of contacts between the two lower cables and the pipe and in correspondence of max closeness between the pipe and the upper cable (reference Figure 3-41). The “flattening” of the profile as time increases is due to temperature variations around the pipe causing thermal transfer in the azimuthal direction (remember this figure illustrates the rate of change for the temperature, not the temperature itself). The averages of the temperature change rates for each time period are constant, indicating a constant heat generation rate.

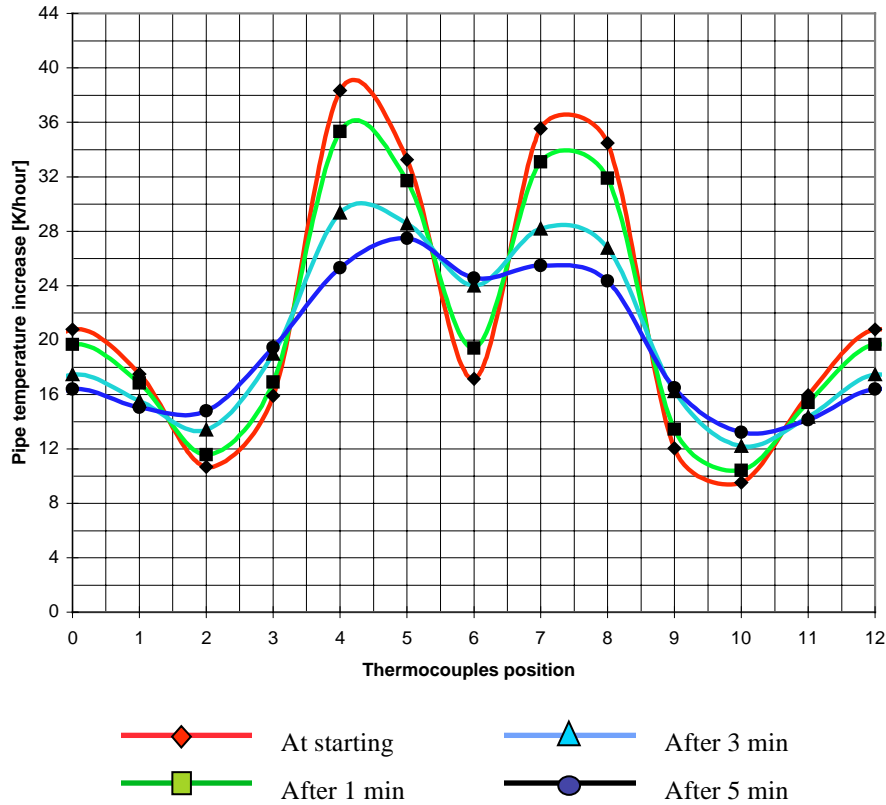


Figure 3-43
Pipe Temperature Increase with a Current of 3090 A

The characteristics of the pipe and the power measured with the calorimetric method at 3090 A are summarized in Table 3-9.

Table 3-9
Pipe Characteristics and Measured Power

Outer diameter	298 mm
Thickness	8 mm
Thermal capacity	26.2 kJ/m-K
Current	3090 A
Mean temperature increase	21.7 K/hour
Dissipated power	158.3 W/m

The dissipated power, measured with the Aron method (187.7 W/m), is greater than the value obtained with the calorimetric method (158.3 W/m). This is caused partially by the fact that the power is obtained as a difference between the losses measured with and without the pipe: therefore it includes the pipe proximity effect which influence the conductor losses. Cable losses without the pipe at 3090 A have a value of 460.6 W/m and increases to 490 W/m in presence of pipe. Therefore the calorimetric method allows to estimate the pipe loss only excluding the part of losses which is due to the mutual influence between pipe and cables.

Standard Equations

The most commonly used equations are based on the 1957 paper by J. H. Neher and M. H. McGrath entitled “The Calculation of the Temperature Rise and Load Capability of Cable Systems”. In particular the hereunder equations are those shown in “International Standard IEC 287-1-1, 1994; Calculation of the current rating”.

$$W_{pipe} = R_{eq} \cdot I^2 \quad (\text{W/m/phase})$$

R_{eq} = pipe equivalent resistance (Ω/m)

I = phase current (A)

$$R_{eq} = pt \cdot R_t + (1 - pt) \cdot R_c$$

$$pt = 5.33 \cdot \left(\frac{D_s}{D_p} \right) - 1.4$$

pt = triangular “percentage”

D_s = phase diameter (m)

D_p = pipe inner diameter (m)

being $D_s/D_p > 0.3$

$$R_t = 10^{-2} \cdot (0.0115 \cdot D_s - 0.001485 \cdot D_p)$$

R_t = “triangular” equivalent resistance

R_c = “cradle” equivalent resistance

$$R_c = 10^{-2} \cdot (0.00438 \cdot D_s + 0.00226 \cdot D_p)$$

The current standards represent the empirical and practical application of a body of work which includes over 40 years. Consequently, the focus of this work has been with pipe and cable characteristics encountered in actual cable systems. For example, most cable systems (with the exception of 345 kV and higher) use pipe enclosures with a nominal outer diameter of around 8.625 in. (~219 mm) and a thickness of 0.32 in. (8.0 mm) and have elevated operating temperatures. The pipe losses calculated using the standard equations are reported in Figure 3-44.

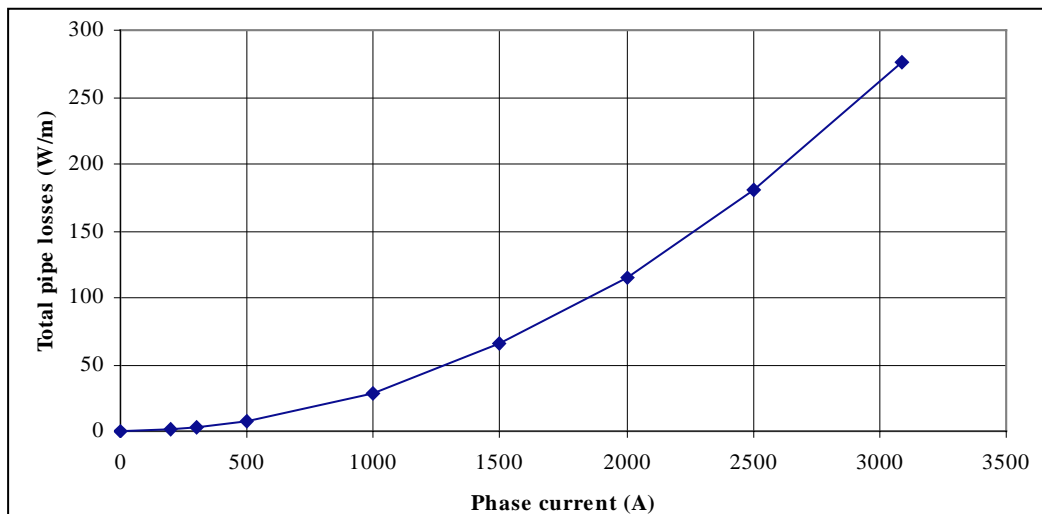


Figure 3-44
Calculated Pipe Losses using Standard Equations

3.11.4 Comparison of measured and calculated losses

In Figure 3-45, the measured losses (Aron method and calorimetric method) and the calculated losses (standard equations) are compared. The curve relevant to the calorimetric method has been extrapolated assuming an exponential trend ($W = K \times I^2$) and neglecting the pipe resistance variation due to the current losses and temperature. The results of this analysis could indicate that the standard equations present a conservative calculation of the pipe losses. However, these differences could be shown to be due to the difference in pipe diameter (between the pipes for which the standard equations were developed and the pipe used for the experimental activity) and the resultant reduction in magnetic field intensity at the pipe surface.

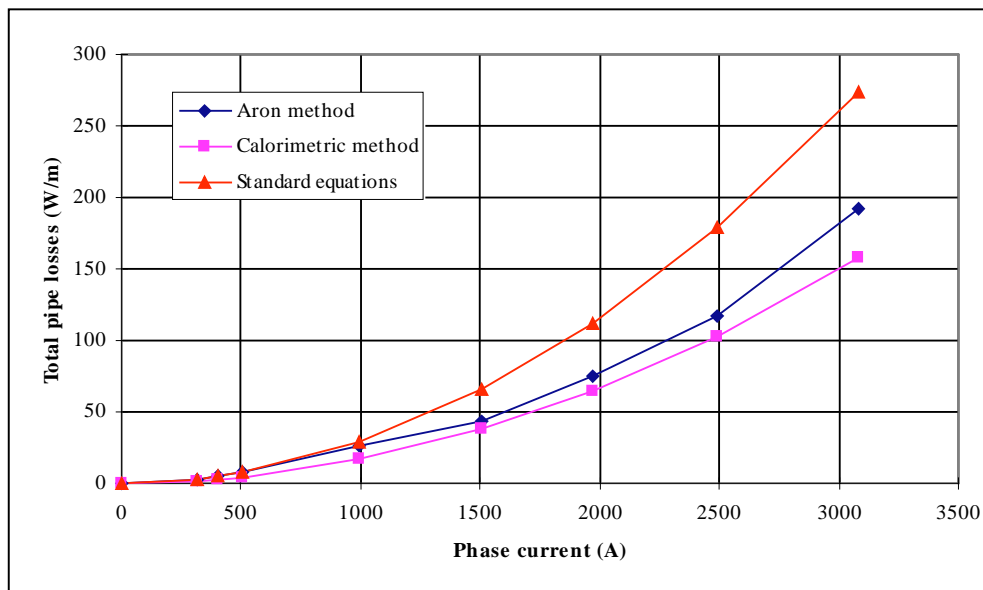


Figure 3-45
Comparison of Total Pipe Losses Determined with the Three Different Methods

To create a correlation between the losses found in the experimental configuration and those calculated using the cable standards, an equivalent resistance was found for a larger (12.0 in. or 300 mm outer diameter) pipe. It should be noted that this extrapolation assumes that the losses in the pipe scale linearly with the diameter of the pipe.

As the figure shows, the standard equations predict a higher loss than those measured with the experimental techniques under the specific experimental conditions. As all of the loss curves follow a $\alpha K \times I^2$ dependency, it is possible to create a linear scaling factor, shown as α , between the different methods.

Taking the losses at 3090 A, the standard equations predict losses of 275.8 W/m, while the Aron technique and the calorimetric technique measured 187.7 W/m and 158.3 W/m respectively. Therefore, the relative α coefficient for the different techniques can be determined as: 1.74, 1.19, and 1.

3.11.5 Results and Conclusions

The experimental system indicated that the current pipe loss calculation techniques over-state the pipe losses when applied to a 12 in. pipe enclosure operating at near ambient temperatures. Because the standard equations have been developed and refined using experimental studies and practical experience, the linear extrapolation of these models beyond the range (both for the pipe dimensions and the cable ampacity) from which they have been derived must be considered when analyzing the results.

Though these results do not provide conclusive evidence that the Neher-McGrath equations for pipe loss are not applicable to very high current levels, it does indicate that there are limits of applicability, i.e. larger pipe diameter and lower operation temperature. In order to develop a method for calculating pipe losses for conditions which deviate from the current practices, further empirical and analytical evaluation should be necessary.

A

THEORETICAL BASIS FOR AC LOSS CALCULATION

AC loss in Ag/2223 tapes

The self-field ac losses in a hard superconductor, as the BSCCO 2223, for a peak current I_0 lower than the critical current I_c , are mainly caused by the hysteretic penetration of the magnetic field in the critical state. This contribution is such that the loss per cycle results to be independent of the frequency of the transport current. The AC measurements performed on Ag/2223 tapes as a function of the frequency generally confirm this view in the frequency range 35-140 Hz; in some samples a small effect of the ohmic loss in the silver matrix has been detected in the low current region, i.e. far from the working regime, while the coupling-current loss does not affect the experimental results obtained so far on the Ag/2223 tapes in self-field.

The ac power losses per cycle in some MCA tapes, as a function of the reduced peak current $F=I_0/I_c$, where I_0 is the peak current, are presented: in Figure A-1 the ac loss Vs F , for different value of the frequency is reported.

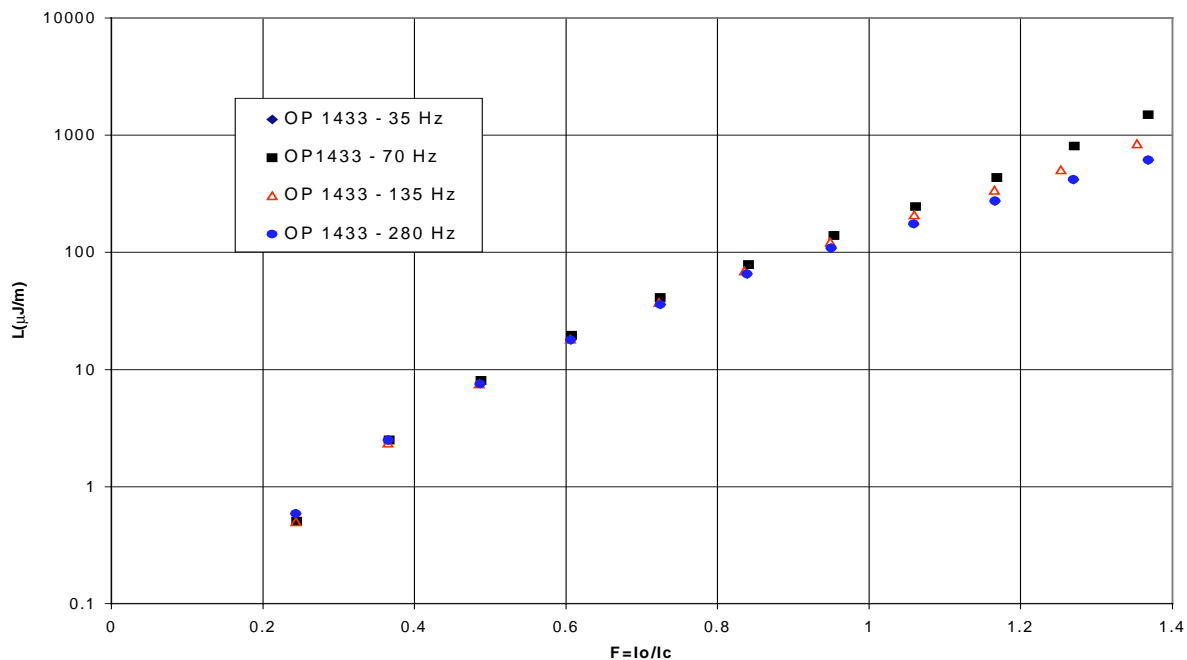


Figure A-1
AC loss Vs the reduced current F for the tape OP1433 at different values of frequency

In the spanned frequency range, and for $F < 1$, the ac power losses do not depend on frequency, confirming that the hysteretic losses are the most relevant contribution to the dissipation in these tapes, then in the following only this contribution will be analyzed in detail, neglecting the coupling-current losses, arising in multifilamentary superconductors in time-varying magnetic field, and the resistive losses, i.e. dissipative phenomena in the metallic matrix .

In a tape carrying AC a time-varying magnetic self-field is generated: this self-field penetrates the material, giving rise to the hysteresis phenomena which are characteristic of the hard superconductors. Due to this effect a net magnetic induction \mathbf{B} arises and, as a consequence, an induced electric field \mathbf{E} , according to the Faraday's law. The local rate of energy dissipation per unit volume is then given by $\mathbf{J} \cdot \mathbf{E}$, where \mathbf{J} is the macroscopic current density; the time average of $\mathbf{J} \cdot \mathbf{E}$ integrated over the volume V of the specimen yields the time averaged dissipated power P . Under alternating conditions, with a current $I = I_0 \sin \omega t$ where I_0 is the peak current and ω is the angular frequency, the energy lost in half a cycle L can be written as:

$$\frac{L}{2} = \int_{-I_0}^{I_0} \frac{d\phi}{dt} I dt = \int_{-I_0}^{I_0} I d\phi$$

where $\phi = \lim_{R \rightarrow \infty} \int_0^R \vec{B} \cdot d\vec{r}$ is the magnetic flux per unit length generated by the transport current.

The loss can be generally inferred from the electromagnetic theory, with only a little input from the microscopic theory of superconductivity, that describes the profile of the self-field, and of the screening current, in the superconductor. In the framework of the well known Bean model [A.1] the magnetic field penetrates the material generating a screening current on the surface of the material and the penetration length of the magnetic field inside the tape is a function of the peak magnetic field. The value of the current inside the superconductor is assumed to be J_c or $-J_c$, independently of the magnetic field intensity.

The correct modeling of the hysteretic losses in the anisotropic HTS tapes, even in the simplified framework of the critical state model, requires a good schematization of the superconducting core geometry, as it has been clearly stated by Norris [A.2]. In fact the hysteretic energy loss has been calculated in superconducting wires with elliptical and thin strip cross section, and each case results in a different behavior of the self-field losses $L(F, I_c)$, where F is the reduced peak current $F = I_0 / I_c$ and μ is the permeability of free space. In fact, for an elliptical cross section the energy loss is:

$$L(F, I_c) = \frac{\mu_0 I_c^2}{\pi} \left[(1 - F) \ln(1 - F) + \frac{(2 - F)F}{2} \right]; \quad (1)$$

while for a thin strip cross-section we get:

$$L(F, I_c) = \frac{\mu_0 I_c^2}{\pi} \left[(1 - F) \ln(1 - F) + (1 + F) \ln(1 + F) - F^2 \right]; \quad (2)$$

At low currents, where $F \ll 1$, the energy loss is given by:

$$L(F, I_c) \approx \frac{\mu_0 I_c^2}{6\pi} F^n, \quad (3)$$

with $n=3$ for elliptical and $n=4$ for thin strip core. Note that at low current the behavior is quite different and that in the whole current range up to $F=1$ the elliptical approximation gives losses higher than the thin strip losses.

In the actual multifilamentary tapes the filaments are strongly coupled, so that their core can be treated as homogeneous: the cross-section is different from either geometry however both geometries are in principle suitable for approximating the superconducting core of a tape [A.3].

In these tapes losses are anyway generally lower than predicted by the “ellipse” curve, and have a current dependence closer to the F^4 predicted by the “thin strip” behavior. In homogeneous samples with a well identified core geometry the ac loss are well described by this model.

In Figure A-2, we report the loss data for a MCA like multifilamentary tape sample with a well defined core geometry: as it may be observed from the cross section micrograph (2a) this tape seems to show a strip cross section, and the reported ac losses are quite close to the strip core geometry.

This simple application of the Norris model supports the correlation between losses and the geometrical features of different tapes, but cannot account for the quantitative difference in the measured losses appearing in samples with similar core geometry [A.3].

A more refined analysis is required on this subject, for explaining the particular features of the ac loss Vs F curve: for this purpose the assumption of constant J_c through the whole cross-section of the wire, which is equivalent to considering a macroscopically homogeneous material, seems to be too simplistic. In fact both longitudinal (j_c changing along the wire length) and transversal (j_c depending on the distance from the wire axis) inhomogeneities are probable to be found in real wires.

In Ref. [A.4] it has been presented a model for analyzing how the transversal inhomogeneity of the sample, resulting of nonuniform j_c , could affect the transport loss.

In this model a simple circular geometry for the wire cross-section with stepwise change of j_c at certain radius has been assumed: thus the superconducting wire has a cross-section consisting of the inner cylinder of material with a radius a_i and a critical current density, j_{ci} , and the outer shell, with radii a_i and a_o having a different critical current density, j_{co} . The results will apply also to concentric elliptical structures.

The total critical current of the tape is

$$I_c = I_{co} + I_{ci} \quad (4)$$

given by the sum of the outer-shell critical current, I_{co} , and the inner-cylinder critical current, I_{ci} .



Figure A-2a
Cross section micrograph of the multifilamentary sample

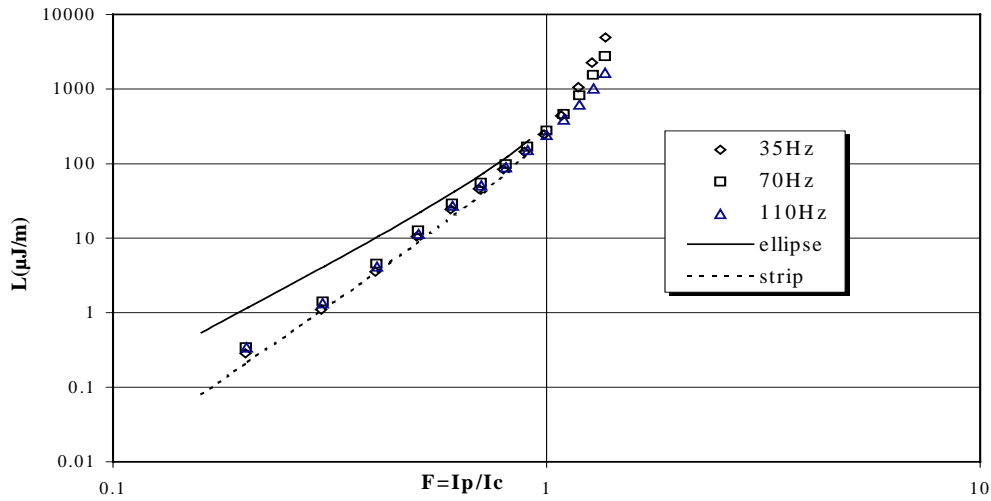


Figure A-2b
Measured loss per cycle and per unit length as a function of the peak reduced current i compared with the theoretical curves for the ellipse and thin strip core geometry.

These are given by the j_c 's of two shells as

$$\begin{aligned} I_{co} &= \pi(a_o^2 - a_i^2)j_{co} \\ I_{ci} &= \pi a_i^2 j_{ci} \end{aligned} \quad (5)$$

In the loss calculation we follow the procedure outlined in [A.2]. The total loss per AC cycle, W , is obtained integrating the loss per cycle density, $w(V) = l2\pi r w(r)$, over the whole wire volume:

$$W = \int_0^{a_o} l2\pi r w(r) dr \quad (6)$$

Here, the loss per cycle density is defined as

$$w(r) = \int_0^T j(r,t)E(r,t)dt \quad (7)$$

where T is the period of the AC cycle and

$$E(r,t) = -\frac{1}{l} \frac{\partial \phi(r,t)}{\partial t} \quad (8)$$

with the flux density determined by the magnetic field profile:

$$\phi(r,t) = \int_0^r B(r',t)dr' \quad (9)$$

In this calculation two parameters have been introduced:

$$\alpha = \frac{a_i}{a_0} \quad \text{and} \quad \eta = \frac{j_{ci}}{j_{co}}.$$

that depend on the microscopic structure of the materials and that are generally unknown, so in the following they will be fixed by fitting the experimental data.

The losses are then expressed as a function of the relative amplitude of the AC current, F , and the condition $I_t = I_{co}$ transforms to $F = F_x$ where

$$F_x = \frac{1 - \alpha^2}{1 + \alpha^2(\eta - 1)}. \quad (10)$$

Introducing the two functions of F :

$$\begin{aligned} g(F) &= F[1 + \alpha^2(\eta - 1)] \\ h(F) &= \frac{F - 1 + \alpha^2(1 - F + \eta F)}{\eta \alpha^2} \end{aligned} \quad (11)$$

the final form of the expression for transport loss per cycle and unit length is

$$\frac{W}{l} \Big|_{F \leq F_x} = \frac{\mu_0 I_c^2}{\pi [1 + \alpha^2 (\eta - 1)]^2} \left[g(F) \left(1 - \frac{g(F)}{2} \right) + (1 - g(F)) \ln(1 - g(F)) \right]$$

$$\frac{W}{l} \Big|_{F \geq F_x} = \frac{\mu_0 I_c^2}{\pi [1 + \alpha^2 (\eta - 1)]^2} \left[\frac{1 - \alpha^4}{2} + \eta^2 \alpha^4 h(F) \left(1 - \frac{h(F)}{2} \right) + 2(1 - \eta) \alpha^2 \ln \alpha + \right. \\ \left. + \alpha^4 \eta (\eta - 1) (1 - h(F)) \ln(1 - h(F)) + \right. \\ \left. + \eta \alpha^2 (1 - h(F)) \ln(\alpha^2 (1 - h(F))) \right] \quad (12)$$

Norris [A.2] has shown that the elliptical geometry is equivalent to that circular one when the purpose is to calculate the transport AC loss. Also in our case, considering the wire made of two elliptic shells with different j_c but the same eccentricity, will lead to the same end result. This is because the current distribution follows the same elliptical form. The parameter α in this case is the ratio of the large semi-axes of two elliptical shells. However, this result is no more valid if a shape different from the outer shell characterizes the cross-section of the inner one.

Correctness of the derived expression (12) was tested in two limiting cases when the solution is already known. Setting $\eta = 1$ (i.e. the current densities in both outer and inner part are equal) we found it simplifies to the result derived for a homogeneous round (or elliptical) wire (A.5). Similarly, putting $\eta = 0$ we found the formula for a hollow conductor identical to that derived in [A.6]:

$$\frac{W}{l} = \frac{\mu_0 I_c^2}{\pi h^2} [Fh(1 - Fh/2) + (1 - Fh) \ln(1 - Fh)] \quad (13)$$

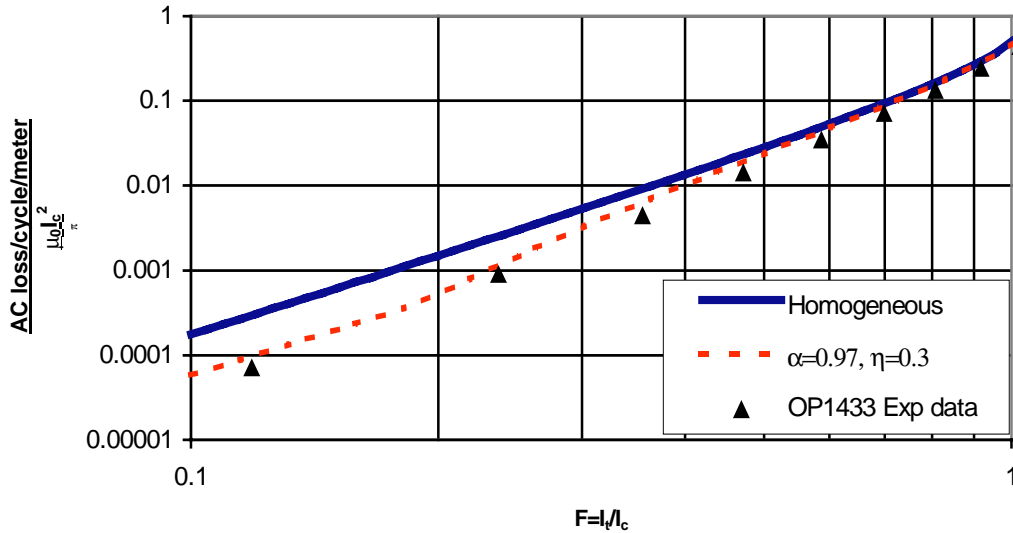


Figure A-3
Reduced loss per cycle and per unit length as a function of F

In Figure A-3, the reduced ac loss measurement results obtained on the sample OP1433 have been reported: the loss per cycle per unit length has been normalized by $\mu I_c^2/\pi$ and plotted Vs F. They have been compared with the theoretical prediction arising from the two-shell model and from the Norris elliptical model: in the low current region the two-shell model gives an adequate description of the change in slope that is a typical behavior in the reduced loss Vs F curve for these tapes. This behavior has been observed in several samples.

This approach provides us an analytical expression for transport AC losses in a round wire consisting of two concentric shells made of materials with different current carrying capability. This expression implies that the loss dependence on transport current can exhibit behavior differing in both the shape and the loss level from that expected for a homogeneous wire. The transition between different exponents of the loss curve has been found for the inhomogeneous wire. This feature, together with the loss level disagreeing with the model for a homogeneous wire on the basis of experimentally determined critical current, is a strong indication of the wire inhomogeneity. In this approach the loss strongly depends on the model parameters α and η representing the inhomogeneity of the sample and that have to be fitted on the experimental data.

The expression was derived for the cylindrical geometry, but it is also valid for the wire composed of two elliptical shells.

In summary the hysteretic ac losses for an isolated tape in self-field have been analyzed and compared with experimental data obtained on MCA tapes: the main features of the ac losses can be well described in the framework of the Bean model, including the geometrical characteristics of the superconducting core. A more refined analysis has been performed including the nonuniform J_c profile in the HTS tape and this gives an improved description of the ac loss behavior Vs I: This representation depends on two free parameters and it is in good agreement with experimental data. A microscopic definition of these parameters can be obtained only beyond the Bean model approximation.

AC loss in HTS cable conductors

The dissipative phenomena in HTS cable conductors in a.c. transport regime can be approached as in the Ag/2223BSCCO tapes. The ac losses can be due to the hysteretic losses, intrinsic to II type superconductors, to the eddy-current losses, arising in superconductors in time varying magnetic field, and to the resistive losses, i.e. the dissipation phenomena in the metallic matrix. Both the non-hysteretic losses per cycle result in a linear dependence on the frequency that can be easily distinguished from the hysteretic contribution.

In the current range up to the critical current I_c the resistive contribution to the losses can be neglected, and the current is assumed to flow only in the superconducting region.

The eddy current losses arise when there is a time-varying magnetic field within a conducting media because of the voltage gradient resulting from the changing flux through closed loops in the material. This contribution can be calculated according to the standard procedure currently in use for multi-layer helically wound tapes [A.6]: however for cable conductors in single-phase configuration this contribution is expected to be negligible.

This view is strongly supported by the results obtained in this project [see Sect. 3.2.1].

The dominant AC loss mechanism in the operating current range and in single-phase configuration is represented by the hysteretic losses, and to this subject the present section will be devoted to.

The rate of energy dissipation per unit volume in half a cycle L in the AC transport regime, with a current $I=I_0\sin\omega t$ where I_0 is the peak current and ω is the angular frequency, is given by:

$$\frac{L}{2} = \int_{-I_0}^{I_0} \frac{d\phi}{dt} I dt = \int_{-I_0}^{I_0} I d\phi$$

where $\phi = \lim_{R \rightarrow \infty} \int_0^R \vec{B} \cdot d\vec{r}$ is the magnetic flux per unit length. The theory for calculating ac losses is

generally based on the Bean model, where it is assumed that the resistivity of the superconductor jumps sharply from zero to large values at the critical current density.

To develop this procedure for calculating the ac losses of a generic cable conductor, even in the simplified framework of the Bean model, is still an open issue, unlike in the Ag/2223BSCCO tapes. In the following an overview of the most suitable models will be provided and the main approximations will be discussed. These models will then be exploited to analyze the experimental data (see Sect. 3.4).

Monoblock model

The correct modeling of the hysteretic losses in the single phase HTS cable conductor requires a schematization of the superconducting core geometry: the actual system to be considered is formed by n HTS layers wound around a cylindrical former. In a simplified model this conductor can be described as a superconducting tube carrying the transport current I and producing a purely tangential field B at the surface. This is the so-called monoblock model [A.6]: and in this case neither the details of the winding scheme nor the discontinuity in the HTS region, introduced by the tape structure, are taken into account. The transport current penetrates from the surface towards the interior of the tube, following the Bean model that is, the surface current density is always at a critical value j_c .

In this case the ac loss can be calculated as follows: the ac loss of the superconducting elliptical wire, as in Eq.(1), does not depend on the aspect ratio, i.e. it is the same as for a round wire. In a superconducting tube the ac loss is the same as the round wire provided the correct scaling of the critical current I_c . In conductors with the same outer radius R_{out} and same j_c we get $I_c^{tube} = I_c^{round} \cdot h$ where $h = (R_{out}^2 - R_{in}^2) / R_{out}^2$ and R_{in} is the inner radius of the tube. By substituting $I_c^{round} = I_c^{tube} / h$ in (1) the self-field loss per cycle per unit length is obtained:

$$L(F, I_c, h) = \frac{\mu I_c^2}{\pi h^2} \left[(1 - Fh) \ln(1 - Fh) + \frac{(2 - Fh)Fh}{2} \right]; \quad (14)$$

where I_c is the critical current of the conductor, F is the reduced peak current $F=I_0/I_c$ and μ is the permeability of free space.

In the limit of small value of $(F h)$ the eq. (14) becomes:

$$W = \frac{\mu F^3 I_c^2}{6\pi} \cdot \frac{R_{out}^2 - R_{in}^2}{R_{out}^2} \approx \frac{\mu F^3 I_c^2}{6\pi} \cdot \frac{2d}{R}. \quad (15)$$

Note that in the actual cases $h \ll 1$, thus the monoblock model and its limit for small current are almost coincident in the whole current range.

It is generally known that the monoblock model generally overestimates the actual ac loss in cable conductors: it depends on the assumption that the current penetrates from the surface, with a profile based on the Bean model. In a multilayer structure this is not true: the inductive coupling determines the current distribution among the layers and the penetration profile of the current has to be included in the calculation of the ac losses. However if no particular arrangement is realized, such that the current is forced to flow in the internal layers, the current starts to penetrate from the surface and the full penetration of the most internal layer is reached only when the peak current approaches the critical current. In the internal layers the penetration is strongly dependent on the conductor design and generally it is not well represented by the monoblock picture.

Uniform Current Distribution (UCD) model

The n -layer conductor with equal current distribution among the HTS layers represents a very interesting case, described in the so-called uniform current distribution (UCD) model [A.7].

In this model the conductor is viewed as a multilayer concentric structure with tapes parallel to the conductor axis and current uniformly distributed among the HTS layers.

The hysteretic AC loss per cycle is calculated assuming that each layer is represented as a superconducting slab in external parallel field and adding the contribution of each layer. The magnetic field has to be considered on the inside and outside of each layer as produced by the enclosed current flowing in the internal layers. The current in each layer is comprised from the transport current and the shielding current induced by the magnetic field H_m generated by the other layers. The penetration field H_p for each layer is $H_p = 2H_m + I_m = dJ_c$: herein H_m is the magnetic field produced by the enclosed layers, I_m is the rms transport current in the layer normalized to length, J_c its critical current density and d the thickness of the layer. For $H_m < H_p$ the loss per cycle per unit of external surface is given by:

$$L = \sum_m \frac{2}{3} \mu_0 \frac{H_m^3}{J_c} + \frac{2}{3} \mu_0 \frac{(H_m + I_m)^3}{J_c} \quad (16)$$

where μ_0 is the permeability of the free space and m the index of the layer. The first term represents the loss caused by the enclosed field on the inside of the layer and the second term expresses the loss of the field on the outside. The losses in this field range vary with the third power of the transport current, as in the monoblock model. For magnetic field larger than H_p , i.e. $2H_m + I_m > dJ_c$, the loss has the following form:

$$L = \sum_m 2\mu_0 t_1^2 J_c (H_m - \frac{2}{3} J_c t_1) + 2\mu_0 t_2^2 J_c (H_m + I_m - \frac{2}{3} J_c t_2); \quad (17)$$

t_i are the distances of the minimum field line in each layer measured from the inside and from the outside of the layer. The losses in this field range increase with the transport current more slowly than in the low current regime.

The main limit of this description is the assumption that the ac loss of the cable conductor can be adequately represented by the dissipation of a superconducting slab in parallel magnetic field. In fact while this approximation is completely justified in the small penetration regime, and in particular for structures such that $d \ll R$, where R is the external radius of the conductor, the high penetration limit would require a more detailed analysis. However this model gives a clear indication that the ac loss in a multilayer conductor with uniform current distribution among the HTS layer is reduced compared to the monoblock case, characterized by a strongly non-uniform current distribution.

Clem model

To analyze more deeply the hysteretic AC loss in a HTS cable conductor a model has been developed by John R. Clem (Iowa State University) in collaboration with Pirelli.

In the framework of the critical state model, a HTS conductor consisting of $2n$ ($n=1,2,3,4$) helically wound layers (one right-handed and the other left-handed), has been described, with a critical current density uniformly distributed within the layer. The tapes are assumed to be in electrical contact with each other, edge to edge, such that any local radial magnetic fields are negligible relative to the local longitudinal and azimuthal magnetic fields. Each tape is modeled as consisting of a uniformly distributed superconducting material, neglecting the effect of the silver matrix.

In this framework, a complete analysis of the 2-layer cable conductor has been performed. The analysis assumed a system described in cylindrical coordinates: $\rho = (x^2 + y^2)^{1/2}$, $\phi = \tan^{-1}(y/x)$, z , where the z -direction coincides with the axis of the cylinder, with corresponding unit vectors $\underline{\rho}$, $\underline{\phi}$, \underline{z} . Assuming that the pitch length L_p of the both inner and outer layer is the same, the winding angle $\theta(\rho)$ in a point depends on the radial coordinate and it is $\tan\theta(\rho) = 2\pi\rho/L_p$, for the outer, right-handed helical layer, and $\tan\theta(\rho) = -2\pi\rho/L_p$ for the inner, left-handed helical layer.

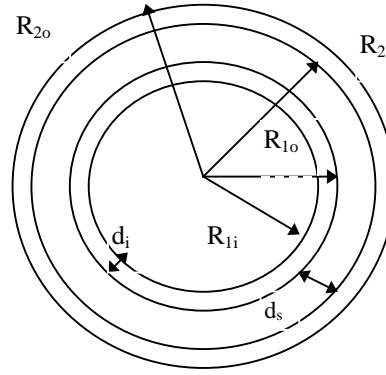


Figure A-4
Sketch of the cross section of the two layers conductor: 1- inner layer; 2 - outer layer.

The inner and outer radii of the inner layer are R_{1i} and R_{1o} , respectively, and the inner and outer radii of the outer layer are R_{2i} and R_{2o} ; d_i , $i=1,2$ represent the thickness of the superconducting layers, while d_s is the thickness of the separating layer.

The current sharing between the two layers can be calculated assuming an inductive coupling between the layers and $I(t)=I_1(t)+I_2(t)$, where $I(t)=I_0\sin\omega t$ is the total transport current and I_1 (I_2) is the current in the inner (outer) layer. The ratio of I_1/I_2 has been calculated ignoring the wall thickness and setting $R_j=(R_{ji}+R_{jo})/2$ $j=1,2$,

$$\frac{I_1}{I_2} = \frac{R_1^2 + R_2^2}{2R_1^2 + (L_p^2 / 2\pi^2) \ln(R_2 / R_1)}$$

Note that in the limit of infinite pitch length $I_1/I_2 \rightarrow 0$ and all AC current flows in the outer layer; for finite pitch length when $R_2 \rightarrow R_1$ we see that $I_1/I_2 \rightarrow 1$, such that the total current divides equally between the inner and the outer layer. In particular for a typical cable conductor configuration with $25^\circ < \theta < 45^\circ$ this ratio ranges between 1.05 and 1.1, then an equal current distribution between the two layers can be assumed.

To calculate the ac loss two main current regimes can be identified, separated by the crossover peak current I_x representing the value where the flux fronts of the magnetic field meeting in the middle of each layer. The crossover peak value I_x is given by

$$I_x = \frac{I_c}{2\chi + 1}$$

with $\chi = \cos 2\theta$.

For small current amplitude the hysteretic a.c. loss per cycle can be calculated in the same approximation used in the UCD model, i.e. assuming that each layer is represented as a superconducting slab in external parallel field.

The hysteretic loss per cycle per unit surface area can be computed using the expression:

$$W=2\mu H_o(\rho)^3 /3J_e \quad (18)$$

where H_o is the ac self field amplitude perpendicular to the current evaluated at the surface, J_e is the critical current density of the HTS layer ($I_c/2\pi R d \cos\theta$) and μ is the permeability of free space. Adding the contributions obtained at the three surfaces, i.e. for $\rho= R_{1i}, R_{1o}, R_{2i}$ and R_{2o} , we get the following expression for the ac losses per cycle per unit length:

$$W = \frac{\sqrt{2}}{6\pi} \frac{(2+3\chi+3\chi^2+2\chi^3)}{\cos^2\vartheta} \frac{\mu_0 d}{R} \frac{I^3}{I_c} \quad I \leq I_c/\sqrt{2} \quad (19)$$

with the same layer thickness $d=d_1=d_2$, $R=(R_{1i}+R_{2o})/2$ and I representing the rms value of the transport current.

This expression is obtained under the hypothesis: $I_1=I_2=I/2$, justified for $\theta \gg 0$; in the limit of zero winding angle this would be no longer valid, and the hysteretic ac loss should be calculated with the assumption that $I_1=0$ and $I_2=I$. This condition cannot be obtained as the limit for $\theta =0$ in the Eq.(19). The ac loss for this case can be obtained by the general expression (18), defining H_o , the magnetic field at the surface, as $H_o=I/2\pi R$ and $I_c=(2\pi R d) J_c$. The loss per cycle per unit surface area becomes:

$$W = \frac{\mu F^3 I_c^2 2d}{6\pi(2\pi R^2)}; \quad (20)$$

please note that the loss per cycle per unit length in this case is:

$$W = \frac{\mu F^3 I_c^2}{6\pi} \cdot \frac{2d}{R}. \quad (21)$$

that is the low current limit of the monoblock model (Eq. (15)).

In the high current regime a detailed analysis of the dissipation in the outer layer must be carried out: the ac loss can be calculated in a general form using the Poynting's theorem:

$$W = \int_0^T E_z(R_{2o}, t) H_\phi(R_{2o}, t) dt$$

E and H represent the electrical and magnetic field to be integrated in a period T .

The resulting ac loss per cycle per unit length is then given by:

$$W = \frac{\mu_o}{48\pi} \frac{d}{R} \frac{I_c^2}{\cos^2 \vartheta} \left[2F(3+F^2)\chi - 2 + 3F + 7F^3 + 3F \frac{(1-F)^2}{\chi} - \frac{(1-F)^3}{\chi^2} \right] I \geq I_x / \sqrt{2} \quad (22)$$

The expressions in (19, 22) have been compared with experimental data obtained on the 2-layer PMC samples in Sect. 3.4.

In the n-layer conductor, with $n > 2$, the current distribution among the HTS layers plays an important role in determining the AC loss.

The low amplitude current regime can be approached in the same way developed for the 2-layer case. The distribution of low-amplitude ac currents among the various helical layers is determined primarily by the self-inductances of the layers and the interlayer mutual inductances and it is independent of the transport current. If the layers alternate in helicity, from layer to layer (e.g. a right-handed outer layer, a left-handed layer in the second layer down, another right-handed layer in the third layer down, etc.) most of the current is carried in the outer two layers, and the third layer down carries a small ac current in the “wrong” direction. The remaining inner layer carries very little current. For instance for the MCA-2 8-layer cable conductor the resulting values are:

$$i_1 = 0.000171762 \quad i_2 = -0.000687049$$

$$i_3 = 0.00240467 \quad i_4 = -0.00893164$$

$$i_5 = 0.0333219, \quad i_6 = -0.124356$$

$$i_7 = 0.464102 \quad i_8 = 0.633975.$$

where i_j $j=1, \dots, 8$ is the fraction of the total current flowing in each layer. The current flows mainly in the two external layer and a reverse current is also found.

The hysteretic ac losses for small ac amplitude are then calculated using an approach similar to that used to derive Eq. (19). The hysteretic loss per cycle per unit of surface area at any surface can be computed using the familiar result $W_A = 2\mu h_0^3 / 3J_c$, where h_0 is the ac field amplitude at the surface and J_c is the critical current density of the HTS layer. The relevant amplitude of h_0 to use at each surface is the amplitude of the field perpendicular to the current at that surface. To determine the behavior of the total loss per cycle per unit of external surface area, we add all the contributions of the form $2\mu h_0(\rho)^3 / 3J_c$, at each of the surfaces, i.e. $\rho = R_{1i}, R_{1o}, \dots, R_{Ni}, R_{No}$. We have, for $N = 2, 4, 6, 8, \dots$,

$$W_A(\theta) = \frac{2\mu_0 I_0^3}{3(2\pi R)^3 J_c} S_N(\theta). \quad (23)$$

The behavior of $S_N(\theta)$ as a function of θ is reported in Figure A-5 for $N=2,4,6,8$

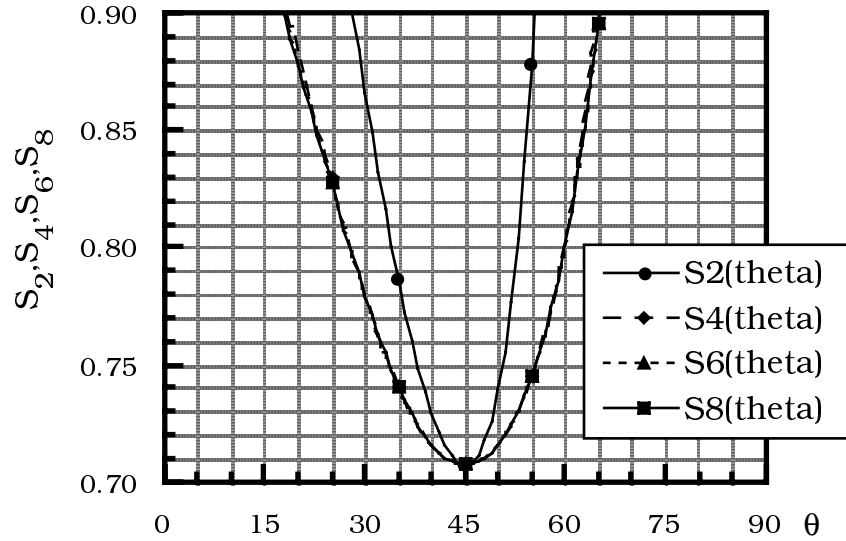


Figure A-5
Plots of S_2 , S_4 , S_6 , and S_8 versus the pitch angle θ (in degrees).

Here, S_N describes the effect on the low current AC loss per cycle per unit of external surface area when the number N of helical layers increases. The saturation effect (S_N tending to the same value as N increases) arises because for low-amplitude AC currents nearly all the hysteretic losses are localized in the outer two or three layers.

The current limit for the validity of the low-current I_0^3 loss expressions [Eq. (23)] is reached at the ac amplitude, $I_{OX} = I_C / (0.87 N)$ [i.e., $0.29 I_C$, $0.19 I_C$, and $0.14 I_C$ for $N = 4, 6$, and 8 , respectively]. This is the current amplitude when the flux fronts from the inner and outer surfaces of the outer layer first meet each other.

Please note that in this case the expression for AC loss calculated in the Clem model applies for peak current lower than the critical current in each layer: $I_{rms} \leq I_C / (\sqrt{2} N 0.63) \sim 460$ A. For higher current values a more refined calculation is required, beyond the Bean model, taking into account the non-harmonic profile of the current in the layers. In fact for ac current amplitude above the critical current of the outer layer, there is a portion of the ac cycle for which the current in the outer layer is above the critical current for that layer. Since the current density is slightly above J_C over this portion of the cycle, there will be a nonzero electric field component along the length of each tape in the outer layer, and it gives a non-negligible resistive contribution to the voltages along each layer.

As soon as the critical current is overcome in the outer layer, the resistance of the layer begin to compete with the so far inductively dominated current distribution, with the final effect of pushing more and more current into the inner layers. For part of the cycle (low current) the current distribution is dominated by the relative inductance of the layers, while for the other part (above the outer layer saturation current) both inductance and resistance determine the distribution. The resulting effect is that the current in the layers is non-harmonic, the current distribution among the layers depending on the magnitude of current and varying during the cycle.

In the above-discussed high current regime the ac losses have not been calculated in detail for multi-layer (more than two) conductors. For such high amplitude current regime a careful description of the ac loss behavior has been provided only in 2-layer cable conductor, where the current is always uniformly distributed between the layers. We can, however, make an estimate of the losses near the critical current for multi-layer conductors noting that for the discussed cable design the current is almost equally shared between the layers with opposite chirality.

The n-layer conductor can be described as a 2-layer cable conductor where all the right-handed (left handed) layers are fully coupled and then act as an unique layer whose thickness is $n/2$ times the thickness of the actual HTS layer. In this “effective” 2-layer model the AC loss can then be calculated using the above-described two-layer Clem model (see Sect. 3.4).

In conclusion the hysteretic ac losses for the HTS multi-layer cable conductor have been discussed in the framework of the Bean model. In particular the main results of the Clem model have been briefed because it represents so far the best description for the HTS multi-layer cable conductors. In this analysis two main regimes have been identified, depending on the value of the transport current compared to the crossover value I_x representing the value where the flux fronts of the magnetic field meet at the middle of each layer. In this range the current distribution among the HTS layers is mainly determined by the self-inductances of the layers and the interlayer mutual inductances. The dissipative behavior of each HTS layer can be assimilated to a slab in parallel magnetic field, with the losses proportional to the third power of the operating current.

The main limit of this model picture, even for the low current regime, remain the geometrical description of the superconducting structure: in fact each layer is viewed as consisting of an uniformly distributed superconducting material, neglecting the local radial magnetic field at the edge of each tape. The effect of this radial field has never been estimated and there is no evidence that it can be neglected compared to the local longitudinal and azimuthal magnetic fields. Moreover a more refined analysis would require going beyond the Bean model approximation for including the non-uniform J_c profile due to the effect of the local magnetic field acting on the HTS tapes in the cable conductor.

B

REFERENCES

Section 1

- [1.1] "Energy Applications of High Temperature Superconductors"
EPRI Progress Report
July 1992
- [1.2] "Design Concept of a Room Temperature Dielectric HTS Cable"
D.Von Dollen, P.Metra, M.Rahman
American Power Conference, Chicago
April 1993
- [1.3] "Wu M K, Ashburn J R, Torng C J, Hor P H, Meng R L, Gao L, Huang Z J, Wang Y Z, Chu C W, 1987 Phys. Rev. Lett. **58** 908
- [1.4] "Performance Summary of the Brookhaven Superconducting Power Transmission System"
Cryogenics 26 599-614

Section 2

- [2.1] "Recent Advances in Long Length Bi-2223 HTS Multifilamentary Composite Wire Development," M. Minot, D. Buczek, J. Gannon, P. Miles, D. Parker, P. Metra,
Applied Superconductivity Conference, Boston October 1994
- [2.2] "Manufacturing of HTS Composite Wire for a Superconducting Power Transmission Cable Demonstration"
D.M.Buczek, L.J.Masur, P.K.Miles, F.Sivo, D.Marlowe,
R.Podtburg,D.R.Parker,J.D.Scudiere (ASC) - P. Metra, M. Nassi, M. Rahman (Pirelli) -
D.W. Von Dollen (EPRI)
Applied Superconductivity Conference
Aug. 1996 - Pittsburgh, USA
- [2.3] C.P.Bean - Phys. Rev. Lett. 8, 250, (1962)
- [2.4] "Stresses and Strains in Multifilament HTS Tapes"; Skov-Hansen P., Han Z. and Bech J.I. 1998 "1998 ASC Conference MUA-02

References

- [2.5] "Mechanical properties of Bi-2223 Tapes"
Gherardi, L.; Caracino, P.; Coletta, G. Cryogenics ICEC supplement (1994) vol.34, p.781-4
- [2.6] "Critical current versus field behaviour in Ag / BSCCO-2223 tapes with different critical currents."
Gherardi, L.; Caracino, P. Coletta, G.; Spreafico, S.
Materials Science & Engineering B (Solid-State Materials for Advanced Technology) (May 1996) vol.B39, no.1, p.66-70
- [2.7] "Measurement of the ac power loss of $(\text{Bi,Pb})_2\text{Sr}_2\text{Ca}_2\text{Cu}_3\text{O}_x$ composite tapes using the transport technique"
G. Vellego, P. Metra, S. Fleshler, L.T. Cronis, G.E. Conway. A.P. Malozemoff, T. Pe, J. McDonald, J.R. Clem, Applied Physics Letters 67(21) November 1995
- [2.8] "Critical state and AC losses in multifilamentary BiSrCaCuO-2223 / Ag tapes studied by transport and magnetic measurements."
Goemory, F.; Gherardi, L.; Mele, R.; Morin, D.; Crotti, G.
Physica C (15 May 1997) vol.279, no.1-2, p.39-46

Section 3

- [3.1] "AC losses in Bi-2223 tapes for power applications"
Gherardi, L., Gomory, F. Mele, R. : Coletta, G. |
Superconductor Science & Technology , V.10 (1997) 909-913
- [3.2] "Comparison between self-field AC losses of a single-phase Bi-2223 cable measured by electric and calorimetric methods"
E.Cereda, G. Coletta, G.Crotti, L. Gherardi, G. Ottoboni, S. Zannella
Physica C 310 (1998) 231-235
- [3.3] "Application of electrical and calorimetric methods to the AC loss characterization of cable conductors"
G.Coletta, L.Gherardi, F.Gomory, E. Cereda, V. Ottoboni, D. Daney, M. Maley, S. Zannella
Applied Superconductivity Conf., Palm Desert, CA, 14-18 Sept 1998
Published in IEEE trans. Appl. Supercond. Vol.), NO. 2 June 1999, 1053-1056
- [3.4] "An analysis of the transport losses measured on HTSC single-phase conductor prototypes"
G.Vellego, P.Metra
Superconductor Science Technology, V.8(1995) 476-483
Feb 1995

- [3.5] “Single and three-phase AC losses in HTS superconducting power transmission line prototype cables”
 D.E. Daney, H.J. Boenig, M.P. Maley, J.Y. Coulter, S.Fleshler
 Advances in Cryogenic Engineering (materials), Vol. 44
 Edited by Balachandran et al., Plenum press, New York, 1988
- [3.6] “Single phase AC losses in Prototype HTS conductors for superconducting power transmission lines”
 D.E. Daney, M.P. Maley, H.J. Boenig, J.O. Willis, J.Y. Coulter, L. Gherardi, G. Coletta
 Physica C 310 (1998) 236-239
- [3.7] (Effective reduction of AC loss in HTSC cable conductor
 J. Fujikami N. Shibuta K. Sato H. Ishii T. Hara
 ISS 94 proceedings ed. K. Yamafuji T. Morishita , pag 1195
 Springer Verlag Tokyo 1995
- [3.8] AEIC CS2-90
- [3.9] IEC 60
- [3.10] IEC 230
- [3.11] IEC 287-1-1, 1994
- [3.12] “The Calculation of the Temperature Raise and Load Capability of Cable System”
 Neher, McGrath
 October 1957

Appendix A

- [A.1] C.P.Bean - Phys. Rev. Lett. 8, 250, (1962)
- [A.2] W.T.Norris - Jour. of Phys. 3, 489, (1970)
- [A.3] R. Mele et al. IEEE Trans. on App. Supercond. 7 , 1335,(1997)
- [A.4] Gomory et al. - Physica C 280 , 151, (1997)
- [A.5] Hancox, Proc.IEE **113** (1966) 1221
- [A.6] D.R Salmon and J. A. Catterall, j. Phys. D: Appl. Phys. **3** (1970) 1023
- [A.7] S. Mukoyama et al., IEEE Trans. on App. Supercond. 7 , 1069, (1997)
- [A.8] J. Rieger et al. , Supercond. Sci. Technol. **11** (1998) 902

About EPRI

EPRI creates science and technology solutions for the global energy and energy services industry. U.S. electric utilities established the Electric Power Research Institute in 1973 as a nonprofit research consortium for the benefit of utility members, their customers, and society. Now known simply as EPRI, the company provides a wide range of innovative products and services to more than 1000 energy-related organizations in 40 countries. EPRI's multidisciplinary team of scientists and engineers draws on a worldwide network of technical and business expertise to help solve today's toughest energy and environmental problems.

EPRI. Electrify the World

© 2000 Electric Power Research Institute (EPRI), Inc. All rights reserved. Electric Power Research Institute and EPRI are registered service marks of the Electric Power Research Institute, Inc. EPRI. ELECTRIFY THE WORLD is a service mark of the Electric Power Research Institute, Inc.

 Printed on recycled paper in the United States of America

1000160